Helium Assisted Sand Casting of Aluminum Alloys

by

Muhammad Qaiser Saleem

A dissertation submitted to the faculty of

WORCESTER POLYTECHNIC INSTITUTE

in partial fulfillment of the requirements for the degree of
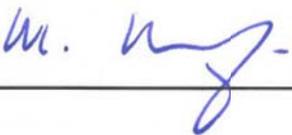
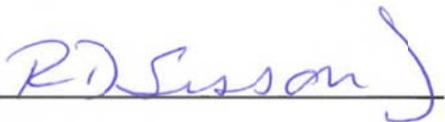**Doctor of Philosophy**

in

Manufacturing Engineering

April 2011

APPROVED:

Professor Makhlouf M. Makhlouf, Ph.D.

Advisor

Professor Richard D. Sisson Jr., Ph.D.

Director of Manufacturing and Materials Engineering

Abstract

Sand casting is the most widely used casting process for both ferrous and non-ferrous alloys; however, the process is marred by large grain size structures and long solidification times. The coarser microstructure has a negative effect on the mechanical properties of the cast components and the long processing time affects the overall productivity of the process. The research reported herein addresses these problems for aluminum sand castings by enhancing the rate of heat extraction from the casting by replacing air, which is typically present in the pores of the sand mold and has a relatively low thermal conductivity by helium which has a thermal conductivity that is at least five times that of air in the temperature range of interest. The effect of (1) the flow rate of helium, (2) the way in which it is introduced into the mold, and (3) the mold design on (a) the average grain size, (b) the secondary dendrite arm spacing, and (c) the room temperature tensile properties of castings is investigated and compared to their counterparts produced in a typical sand casting process. In addition, a cost analysis of the helium-assisted sand casting process is performed and an optimum set of parameters are identified. It is found that when the helium-assisted sand casting process is performed with close to the optimum parameters it produces castings that exhibit a 22 percent increase in ultimate tensile strength and a 34 percent increase in yield strength with no significant loss of ductility, no degradation in the quality of the as-cast surfaces, and no significant increase in the overall cost.

Acknowledgements

Table of Contents

List of Figures

List of Tables

1. Motivation and Objective

1.1 Motivation

Aluminum is the second most plentiful metallic element on earth [1]. It has been estimated that 8% of the earth's crust is composed of aluminum [1, 2]. Production of aluminum comes next to iron [2] and it is the most heavily consumed non ferrous metal in the world [1]. Aluminum's low density, resistance to corrosion, non toxic nature, non magnetic behavior, high thermal and electrical conductivity, ease of fabrication, ease of recyclability and appearance are its attractive features [3-5, 6].

As per 2008, the supply of aluminum in North America alone totaled 24.5 billion pounds whereas the total demand was 22.2 billion pounds [7]. Table 1 shows the breakup of this demand into different market sectors [7]

Table 1 Apparent consumption of aluminum by market (figures in millions of pounds) [7].

Major market	2008	% of total
Building & construction	2,595	11.7
Transportation	6,228	28.1
Consumer durables	1,338	6.0
Electrical	1,544	7.0
Machinery & equipment	1,516	6.8
Containers & packaging	4,918	22.2
Other	737	3.3
Domestic, total	18,876	85.2
Exports	3,274	14.0
Total shipments	22,150	100.0

From the Table 1 it is clear that the largest single market consumer for aluminum is the transportation sector; the primary reason for which is the high specific strength of aluminum in comparison to steels [4] and thus its potential to replace heavy steel automotive parts and contribute to the overall fuel efficiency of the vehicle. Current

projections show that the growth in aluminum usage in vehicles will continue at approximately 4 to 5 pounds per vehicle per year and approach 300 pounds per vehicle worldwide by the year 2020 [8]. For North American light vehicles this forecast is even higher (376 pounds per vehicle) by the year 2020. In 2002, the actual value of aluminum in a North American light vehicle was 274 pounds per vehicle [6]. So the trend & forecast indicate that the consumption of aluminum in this sector is still on the rise. The importance of aluminum in other industrial sectors can't be neglected owing to the range of favorable properties already mentioned. As demand for more technologically complex and ecologically sustainable products increases, opportunities for aluminum will continue to increase [1]. The extensive range of applications of aluminum can be attributed to; its significant capability to create many alloys with different metals and to obtain diversified properties in these alloys [9]. Currently more than 100 alloy compositions are registered with the Aluminum Association and more than 300 alloys are in international use [6]. Some of the properties that are displayed by these alloys (without considering the expanded capabilities of metal matrix and other composite structures) are presented in Table 2 [6].

Table 2 Range of properties obtained with aluminum alloys [6].

Tensile strength, ksi (MPa)	10-72 (70-505)
Yield strength, ksi (MPa)	3-65 (20-455)
Elongation, %	<1-30
Thermal conductivity, Btu.in./hr.ft^2.^{o}F at 77°F (W/m.K at 25°C)	660-1155 (85-175)
Modulus of elasticity, 10^6 psi (GPa)	9.5-11.2 (65-80)

Metal Casting accounts for about 33% of the available methods for processing aluminum and aluminum alloys [10]. Although there are a number of metal casting processes currently in use such as sand casting, shell molding, lost foam, vacuum casting, investment casting, ceramic molding, plaster casting, permanent mold casting, die casting, centrifugal casting and squeeze casting [6, 11]; sand casting is the most widely used process for both

2

ferrous and non-ferrous metals as it accounts for approximately 90% of the castings produced worldwide [12].

In principle the sand casting process makes use of expandable molds [13]. Typically, a sand mold consists of two parts: the upper part, which is known as the cope, and the lower part, which is known as the drag. A non-expandable pattern with an imprint of the desired shape (to be cast) along with risers, gating systems and pouring basin is used for packing the sand around it. Once the sand is packed around the pattern; the pattern is removed to produce a cavity in which molten metal is poured and allowed to solidify. Upon solidification, the mold is broken and the cast part is taken out for further finishing operations [11, 13]. Depending on the design; sometimes some additional components such as cores and chills are introduced during the molding process [11, 13]. Fig. 1 is a schematic representation of a typical sand casting process [14].

Despite the apparent simplicity in its principle and some of the great characteristics that it offers; there are many intricate issues that influence the sand casting process, its economics, and the properties of the cast part. One of the main adverse issues associated with the sand casting process is the inherently slow cooling rate.
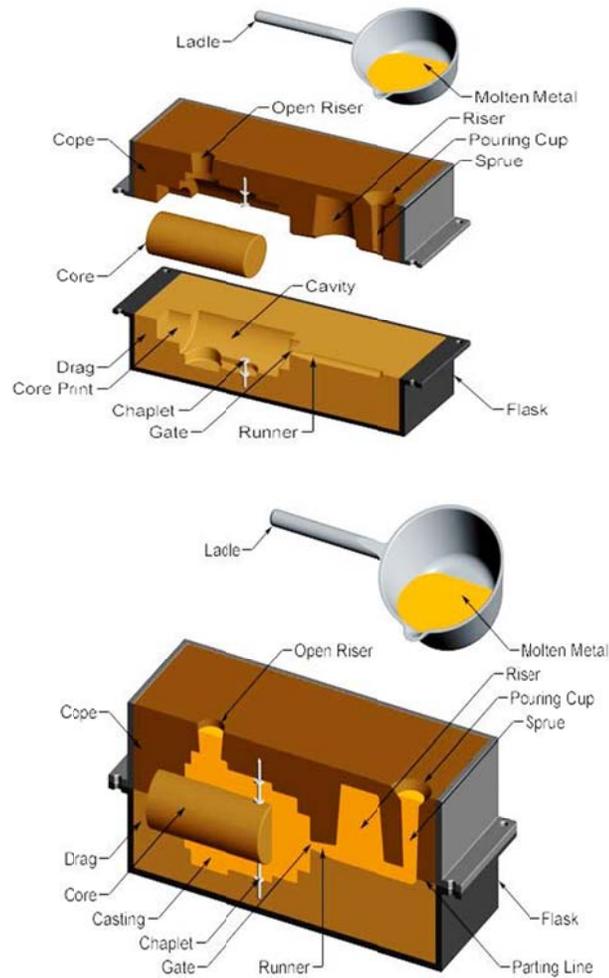
Fig. 1 Illustration of the typical sand casting process [14].

Although different types of sands e.g., silica (SiO_2), zircon ($ZrSiO_4$), olivine (Mg_2SiO_4), iron silicate (Fe_2SiO_4), etc. are available for use as molding material [13], the fact remains that sand molds composed have a relatively low thermal conductivity; (for this reason sand molds are often referred to as "insulating molds"). Table 3 lists some typical values for the thermal conductivity of materials used to make these insulating molds [15].

Table 3 Typical values of thermal conductivity of insulating molds [15].

Mold material	Thermal conductivity (W/m K)
Silica sand	0.52
Mullite	0.38
Plaster	0.35
Zircon sand	1.04

It is worthwhile to note that silica sand is the most widely used material in sand molds [13] mainly because it is the least expensive and it has acceptable properties for molding [16].The thermal conductivity values presented in Table 3 when compared to those of metals that are typically used in permanent molds (see Table 4 [17]), highlight the extent of insulation that sand molds present.

Table 4 Typical values of thermal conductivity of conducting molds [17].

Mold material	Thermal conductivity (W/m K)
Copper	399
Stainless steel	52
Cast iron	36

It goes without saying that the smaller magnitude of thermal conductivity of molding sand is one of the main reasons behind the slow cooling rate typical of sand casting operations.

The importance of cooling rate in the metal casting process is highlighted by the results of various studies that establish a reverse relationship between cooling rate and the microstructure of the cast component [18, 19]: In general a slow cooling rate results in a coarse microstructure.

Dendrite arm spacing and grain size are two of the many microstructure features that become refined with an increased cooling rate [19-21] and the quantitative

characterization of these two can thus be used to gauge the coarseness or fineness of microstructure.

Fig. 2 shows the inverse correlation between dendrite arm spacing and cooling rate for A356 alloy [18].
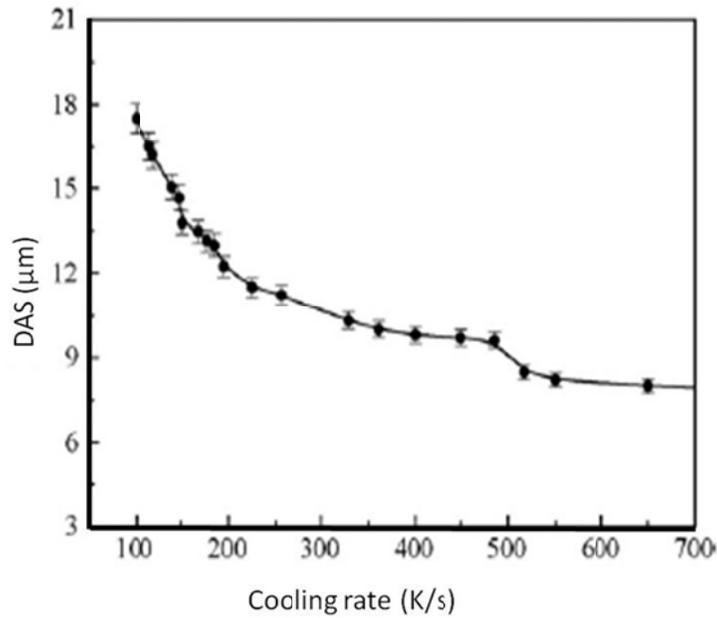
Fig. 2 Relationship between DAS and cooling rate [18].

The secondary dendrite arm spacing ($SDAS$) is related to the mean cooling rate, during solidification (R) by [22]

$$SDAS = CR^m \tag{1}$$

Where C is a constant, R is the cooling rate in °C/sec and $SDAS$ is in µm.

For A356/A357 alloy it has been reported that the relationship between the secondary dendrite arm spacing ($SDAS$) and the mean cooling rate of the primary aluminum dendrite cell fits well with the following empirical relation [23, 24]

$$SDAS = 39.4(R)^{-0.317} \tag{2}$$

Extensive studies have been done to investigate the effect of *SDAS* on the mechanical properties of aluminum alloys, especially their tensile properties [18, 19, 23, 25]. It is an accepted conclusion that other things being constant; a smaller *SDAS* results in better tensile properties [18, 19, 23, 25, 26].

As mentioned earlier; a fast cooling rate also refines the as cast grains [21]. The increase in yield strength by Hall-Petch strengthening demonstrates the benefits of a smaller grain size [27]. Other beneficial effects of grain refinement include less tendency to hot tearing, increased pressure tightness, improved feeding characteristics, consistent properties after heat treatment and finer distribution of secondary phases and porosity [21].

Fig. 3 for AlSi9Cu alloy shows that as the cooling rate increases, both the *SDAS* and grain size become finer and correspondingly there is improvement in ultimate tensile strength of the casting [19].
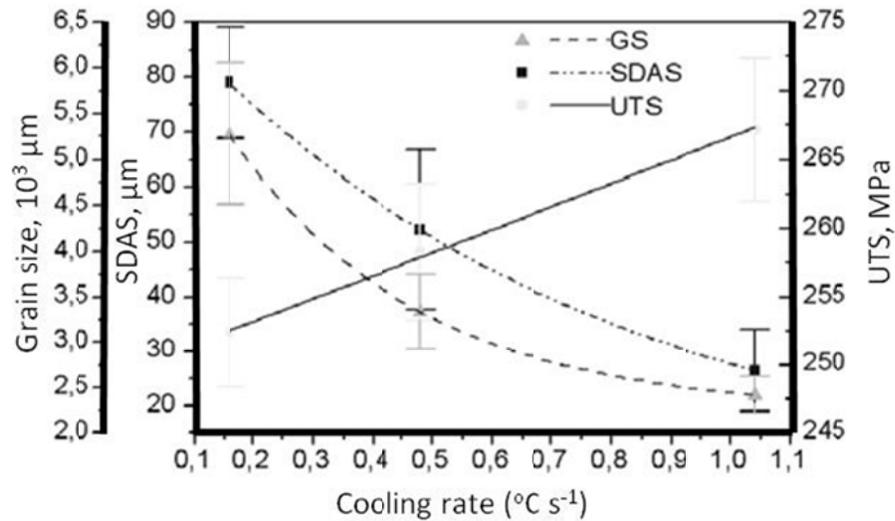
Fig. 3 Variation of grain size, secondary dendrite arm spacing (SDAS) and ultimate tensile strength (UTS) as a function of cooling rate for AlSi9Cu alloy [19].

Fig. 4 shows the relationship between tensile properties and dendrite arm spacing of castings made from A356 alloy [25]. The importance of the cooling rate as a processing parameter in the metal casting process is thus undeniable.

A logical question imposes itself: is there anything that can be done in order to improve the cooling rate during sand casting and thus help refine the microstructure and improve the tensile properties? The answer to this question lies in understanding the structure of a sand mold.
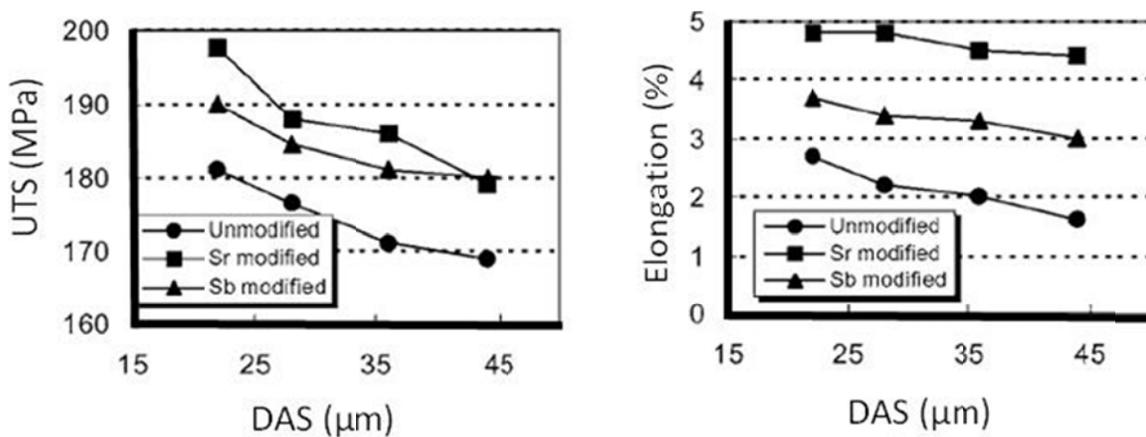
Fig. 4 Tensile properties of as-sand cast A356 specimen as a function of DAS [25]

When sand grains are packed to form the sand mold, voids between the sand grains are inevitable because the grains of sand have different shapes and therefore they don't fill the space in between them completely. Different shapes of sand grains are shown in Fig. 5 [28]. These voids are not necessarily undesirable as sand molds must be permeable so as to allow the gases that form during casting to escape. Important to this investigation is the fact that if air, which is typically present in these voids, is replaced by another gas that has a higher thermal conductivity, there may be an overall enhancement of the rate of heat extraction from the mold and thus an acceleration of the cooling rate of the casting.

Helium and hydrogen are two gases with thermal conductivity that is appreciably higher than that of air [29, 30]. Fig. 6 shows a comparison between the thermal conductivity of various gases at different temperatures [29].
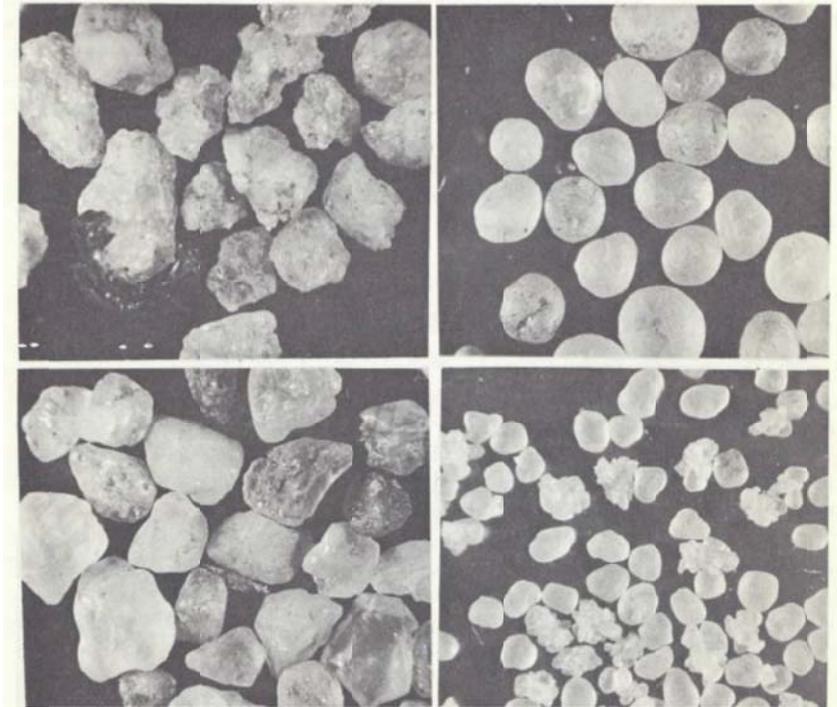
Fig. 5 Angular sand grains (top left); sub-angular sand grains (lower left); rounded sand grains (top right); compounded sand grains (lower right) [28].

The safety concerns associated with hydrogen prevent its use in sand molds [31, 32]. Our choice is thus limited to helium. In the temperature range from 25°C to 500°C, the thermal conductivity of helium is at least 5 times that of air [17]. Helium is a non-toxic, non inflammable and inert gas and is available at relatively low cost [17, 27, 31, 32].
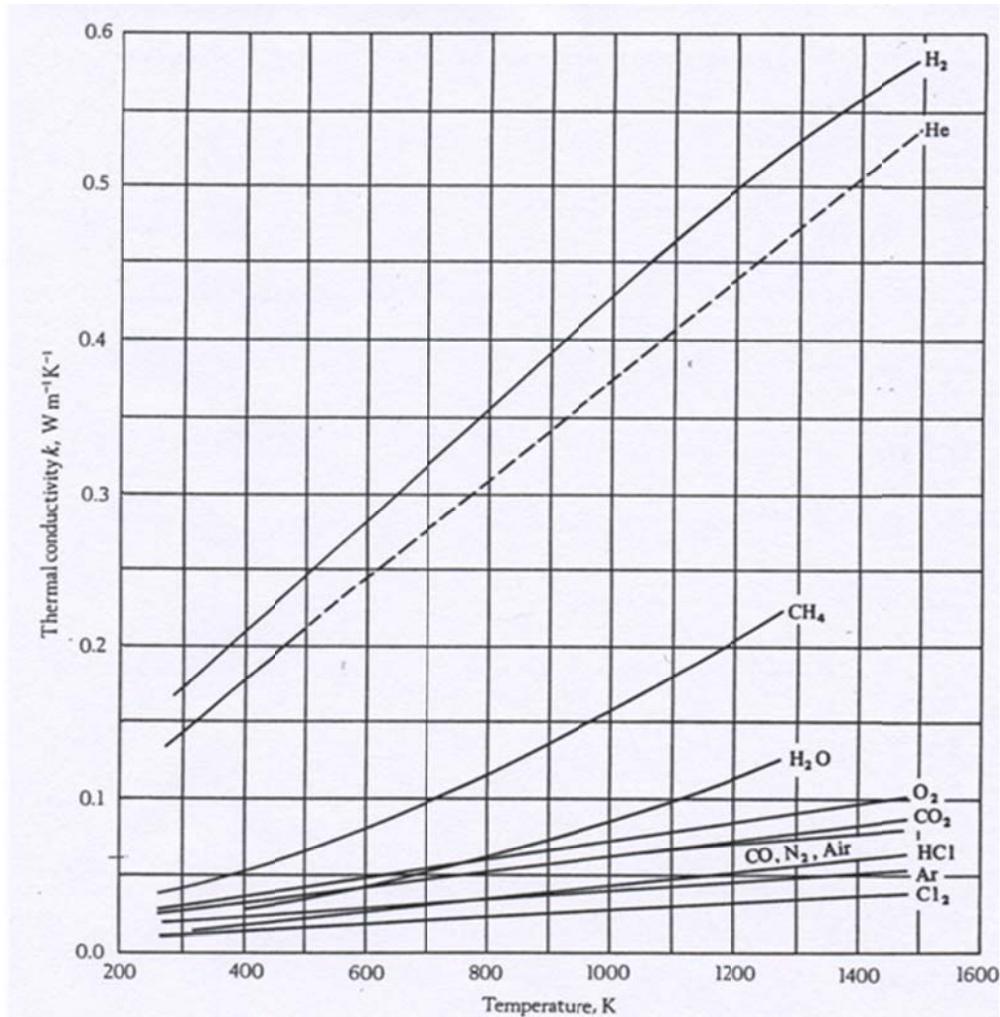
Fig. 6 Comparison of thermal conductivity of various gases at different temperatures. Data valid for upto 10^6 Pa [29].

If helium replaces air inside the voids of the sand mold during sand casting of aluminum alloys, then the rate of heat extraction from the casting would increase resulting in a faster cooling rate with all its associated benefits including microstructure refinement and enhancement of tensile properties.

This window of opportunity: replacing air in mold pores' with helium in order to address the issue of slow cooling rate associated with an otherwise highly versatile casting process is the motivation behind this research.

1.2 Objective

The objective of this research is to investigate the potential benefits of using helium in sand casting. Specifically the objective of this research includes

- Validating the concept of enhancing heat extraction from sand molds by replacing the air in the mold voids by helium

- Identifying a viable approach for application of helium to sand molds

- Designing and constructing an apparatus for using helium in sand molds

- Evaluating the effect of helium on the as-cast microstructure; including

  - Quantitatively characterizing the pores that may form in the cast component

  - Quantitatively characterizing the resulting dendrite arm spacing of the as-cast, un-grain refined cast component

  - Quantitatively characterizing the grain size of the as-cast, un-grain refined cast component

- Evaluating the effect of helium on the room temperature tensile properties of the as-T6 heat treated, un-grain refined cast component

- Analyzing the direct cost impact of using helium and the economical viability of the proposed methodology for employing helium in sand molds

2. Background

Based on their conductive properties; mold materials can be generally classified as insulators or good conductors [15]. Examples of insulating molds include sand molds, ceramic shell molds and plaster molds whereas conducting molds include metallic molds [29]. The difference in the conductive properties of these two mold classifications affects the temperature distribution in the mold as the metal solidifies [29]. The following sections explain the dominant resistances faced by heat flow in both of these mold classifications and present a review of past research related to the use of helium to overcome these resistances [17, 20, 31-34]. The review also helps to identify the research gaps that were targeted by the research work presented herein.

2.1 The Role of Helium in Conducting Molds

Fig. 7 [29] shows the temperature profile in a conducting mold. In this case, most of the resistance to heat transfer occurs at the interface between the solidifying metal and the mold.
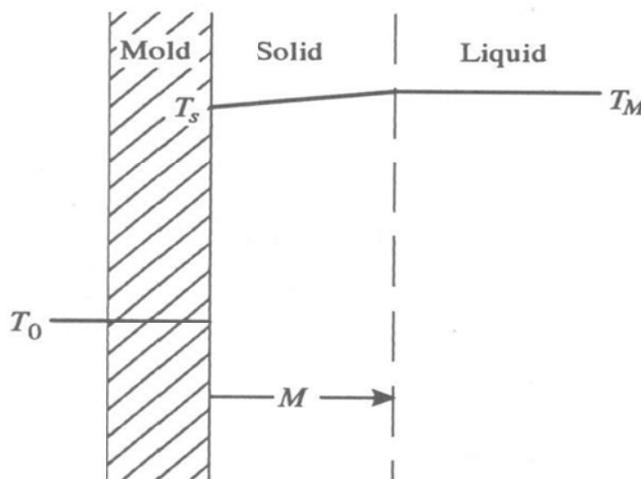
Fig. 7 Temperature profile during solidification of metal in metallic mold [29].

This resistance can be explained in terms of the contact conditions that exist at the interface between the metal and the mold. Two principle resistances to heat transfer across the metal-mold interface have been identified: (1) the resistance presented by the coating that is deposited on the surface of the mold and (2) the resistance presented by a layer of gas that forms between the mold surface and the surface of the solidifying metal (since the gas in this layer is typically air, the layer became known as the "air gap") [35].

Resistance presented by the coating – Metallic molds are coated with a refractory material for a number of reasons: to preferentially control the solidification rate in different areas of the mold, to promote filling of the cavity, to improve die life by reducing thermal shock, to prevent the cast alloy from soldering to the die material, and to lubricate the release of the casting from the mold [35]. Depending on its thickness and type, this coating adds to the insulation at the metal-mold interface [35]. For this reason studies [35, 36] that aimed to determine the interfacial heat transfer coefficient in metallic molds took special measures to carefully control and document the thickness and type of the coating used in their studies.

Resistance presented by the air gap – Although it has been shown that several factors interact to determine the interfacial heat transfer coefficient when a molten alloy solidifies in a conducting mold, among which are the type of the metal, the mold material, its surface condition, the mold and pouring temperature, the casting configuration, and the type of gases at the interfacial air gap [37]; however, it can be readily seen that most if not all of these factors actually influence the thickness of the "air gap" that is formed and thus affect the heat transfer coefficient [37]. The formation of the "air gap" is explained as follows: As the molten metal is poured in the mold and it displaces air from the mold cavity, some air would be entrapped in the roughness troughs of the irregular mold surface [37]. Hallam and Griffiths [35] termed this trapped air the "air layer". The temperature and pressure of this entrapped air increase due to the rise in the temperature at the interface resulting in a gas film whose thickness increases until eventually an "air gap" forms (once a

solid skin forms at the surface of the casting and the casting contracts away from the interface [35, 37]. The mechanism of heat transfer through this gap is conduction with convection and radiation being assumed negligible [37]. Fig. 8 shows a schematic representation of the metal-mold contact region [37].
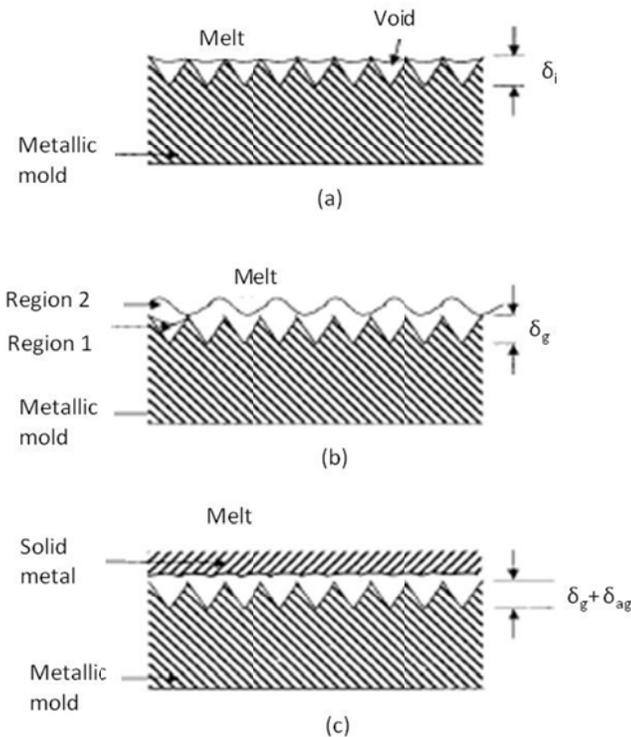
Fig. 8 Schematic of metal/mold contact [37].

It has been reported that the time dependence of the heat transfer coefficient can be roughly divided into three stages [37]: In the first stage, when the metal is still liquid; the magnitude of the heat transfer coefficient is at a maximum and in this stage, the influence of surface roughness, melt superheat and mold preheat temperature are important parameters [37]. In the second stage, the magnitude of the heat transfer coefficient decreases as a thin solid skin starts to form and the contact area between the melt and the mold slightly decreases [37]. The third stage is characterized by the formation of a

continuous air gap between the metal and the mold. In this last stage the alloy composition, the mold type and thickness become important [37].

Hallam and Griffiths [35] calculated the thermal conductivity of insulating coatings by measuring their thermal diffusivity, specific heat capacity, and density. They report that at 500^oC, the thermal conductivity of a typical mold coating (DYCOTE 140ESS from Foseco (FS) Limited, Tamworth, United Kingdom) is approximately 0.8 W/m, which is about 15 times higher than the thermal conductivity of air at 500^oC (0.054 W/m K) [32] This leads to the conclusion that for the same thickness of coating and air gap, the "air gap" dominates heat transfer, particularly during the early stages of solidification.

Several researchers have realized the fact that helium, due to its higher thermal conductivity compared to air, may be used to effectively reduce the resistance to heat flow presented by the "air gap" at the metal-mold interface [17, 20, 31-33]. For example, Doutre [31, 32] injected helium at the interface of metallic molds as the casting solidified and concentrated on the cooling time reductions and productivity aspects. Wan and Pehlke [20] explored the influence of helium injection using basic heat transfer calculations, whereas Argyropoulos and Carletti [17] measured the increased interfacial heat transfer coefficient in metallic molds resulting from the use of helium at the metal-mold interface.

Doutre [31, 32] reported reductions in cooling time ranging between 30% - 50% for a range of aluminum alloys as well as a 29% increase in the production rate when helium was used during production cycle of a complex cored casting. Wan and Pehlke used elementary heat transfer equations to show that the use of helium in metallic molds can result in an increase of 2.3 to 4.3 times in the interfacial heat transfer coefficient across air gaps of varying thickness [20]. Also Argyropoulos and Carletti reported a 48% increase in the average interfacial heat transfer coefficient in the initial phase of solidification (i.e., from

the beginning of the casting operation to the onset of the air gap) when helium was used in a metal mold [17].

Similarly, Griffiths [33] made castings in a purposely-built chamber and reported a 70% increase in the interfacial heat transfer coefficient when helium was used in a permanent mold.

2.2 The Role of Helium in Insulating Molds (Sand Molds)

Fig. 9 [29] shows the temperature profile in an insulating mold. In this case, most of the resistance to heat transfer is presented by the mold material.
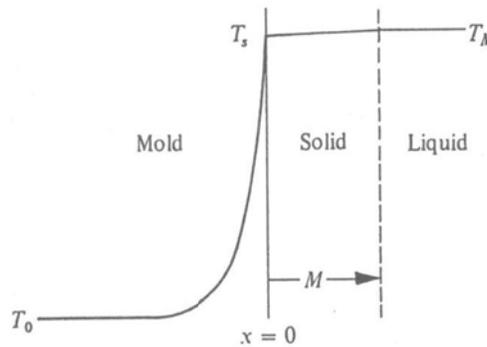
Fig. 9 Temperature profile during solidification of metal in a sand mold [29].

For the temperature distribution shown in Fig. 9, the thickness of solidified metal is given by Eq. (3) [29].

$$M = \frac{2}{\sqrt{\pi}} \frac{(T_M - T_0)}{\rho_s \, \Delta H_s} \sqrt{k_m \, \rho_m \, c_{p_m}} \sqrt{t}$$

(3)

In Eq. (3), T_M is the melt temperature, T_0 is the initial temperature, ρ_s is the density of the metal, and ΔH_s is the latent heat of fusion of the metal. It is clear from Eq. (3) that the thickness of solidified metal (M) at a certain time (t) depends on the properties of the mold material; specifically, its thermal conductivity (k_m), density (ρ_m), and specific heat capacity

(C_{pm}). The product of these three parameters is known as the heat diffusivity of the mold (which is different from the thermal diffusivity of the mold) [15].

The thermal conductivity of the mold is dependent on a number of factors including chemical composition, particle size, type and amount of the binder used to hold the sand particles together, volume fraction of voids, type of gas in the voids, emissivity of the particles, and temperature [15]. The heat transfer within a porous material is a complex phenomenon. On a microscopic level, the heat is transferred by conduction through each particle and by conduction and convection in the gas in the pores [15]. Additionally, there may be radiation from particle to particle across the pore [15].

Keeping all other parameters constant, the heat transfer through the pores can be improved by using a gas with a relatively high thermal conductivity (e.g., helium) in the pores instead of air.

A thorough search of the open literature indicated that there is very limited information on the use of helium in sand molds. In general, there are three possible ways for introducing helium into sand molds.

(1) Helium is directly injected into the mold cavity in a manner similar to what is done with metallic molds. A pending patent application [38] describes this approach where helium is "injected" directly into the cavity of a porous mold to displace air prior to filling the mold cavity with molten metal. In this case, helium is supplied from an opening in the bottom of the mold. The lighter weight of helium compared to air ensures that it displaces air and remains in the mold cavity. The top surface of the mold is encapsulated in order to prevent the escape of helium through the top. It is interesting to note that the main objective of this work is to produce an oxide-free solidification environment and as such, the procedure described in [38] does not call for engulfing the whole mold cavity in helium which would result in a faster cooling rate.

(2) The sand casting process is performed in a controlled helium environment within an enclosed chamber [33]. The results of this study show not only an increase in cooling rate and in IHTC, but also they show significant positive effects on microstructure and mechanical properties. Different sands were used in this study and the study reports a 50% to 90% increase in cooling rate over the entire solidification range together with a 20% increase in IHTC. The study also reports a 20% refinement in the secondary dendrite arm spacing and a 10%-20% improvement in yield strength and ultimate tensile strength of castings in their as cast condition [33]. However, it is also reported that most of the improvements obtained in the as-cast mechanical properties are lost after the castings were subjected to a standard T6 heat treatment [33]. It is also reported that the mold gases diluted the effect of helium at the interface [33].

(3) The sand casting process is performed in a continuous helium flow. In a pending patent application; Hetke [34] describes a "continuous production system" capable of carrying out the whole process (from melting to solidification) in an "oxide" free environment so that light weight metals especially magnesium can be sand cast in a safe manner. Although the main emphasis of this work is performing the whole process in an "oxide" free atmosphere which can be selected from a group consisting of sulfur hexafluoride, nitrogen, argon, helium, or other inert gases and combinations thereof [34]; Hetke claims the potential enhancement in heat transfer rate if prior to pouring the casting, the gas - especially if it is helium - is used to purge the "engineered molds" (these are molds that are at least partially encapsulated) after pulling vacuum through them [34]. Hetke [34] also report that the use of helium in sand molds enhances the cooling rate of the casting and produce castings with tight dendrite arm spacing (of the order of 30 microns or less).

3. *Methodology*

Helium is introduced into the sand mold by the "continued flow" method wherein helium is supplied continually during solidification of the casting. It is important to note the following:

– Helium is introduced into the mold in its as-supplied condition; i.e., without chilling.

– The casting process is conventional "gravity-fed" sand casting.

– The molds are made from recycled silica sand and have properties that are typical of sand molds that are customarily used by the foundry industry.

In order to completely assess the effectiveness of helium in enhancing the casting process, the effects of the following aspects of the process are evaluated:

– The flow rate of helium.

– The mold design; i.e., encapsulating the mold on all its sides – except the bottom where helium is injected and the top where helium is allowed to exit.

– The "helium supply mode"; i.e., the way that helium is made to flow through the mold; i.e., parallel vs. across the surface of the cast part.

In each experiment, the results obtained from the helium-assisted process are compared to the conventional sand casting process.

3.1 Design of Experiments

Table 5 shows the design of experiments.

Table 5 Design of experiments.

Independent variables	Dependent variables	Constants
Gas:	Microstructure characteristics:	Alloy chemical composition:
Helium	Dendrite arm spacing	Aluminum 319
Air	Grain size, porosity	Pouring temperature:
Flow rate[1]:	Tensile properties:	850°C
No flow	Ultimate tensile strength (RT)	Melt conditioning:
1 L/min	Yield strength (RT)	Degassing for 30 minutes
4 L/min	Elongation (RT)	RPT before pouring
8 L/min	Modulus of elasticity (RT)	Part geometry:
Helium supply mode:	Cost	Plate
Cross flow		Mold composition and type:
Parallel flow		Resin bonded silica sand
Mold design:		Mold temperature:
Partially encapsulated mold		Room temperature
Un-encapsulated mold		Helium supply initiation:
		Immediately after mold filling

---

[1] Details of the experiments used to identify the flow rate regime are presented in Appendix A.

3.2 Apparatus

Fig. 10 is a schematic representation of the main apparatus.
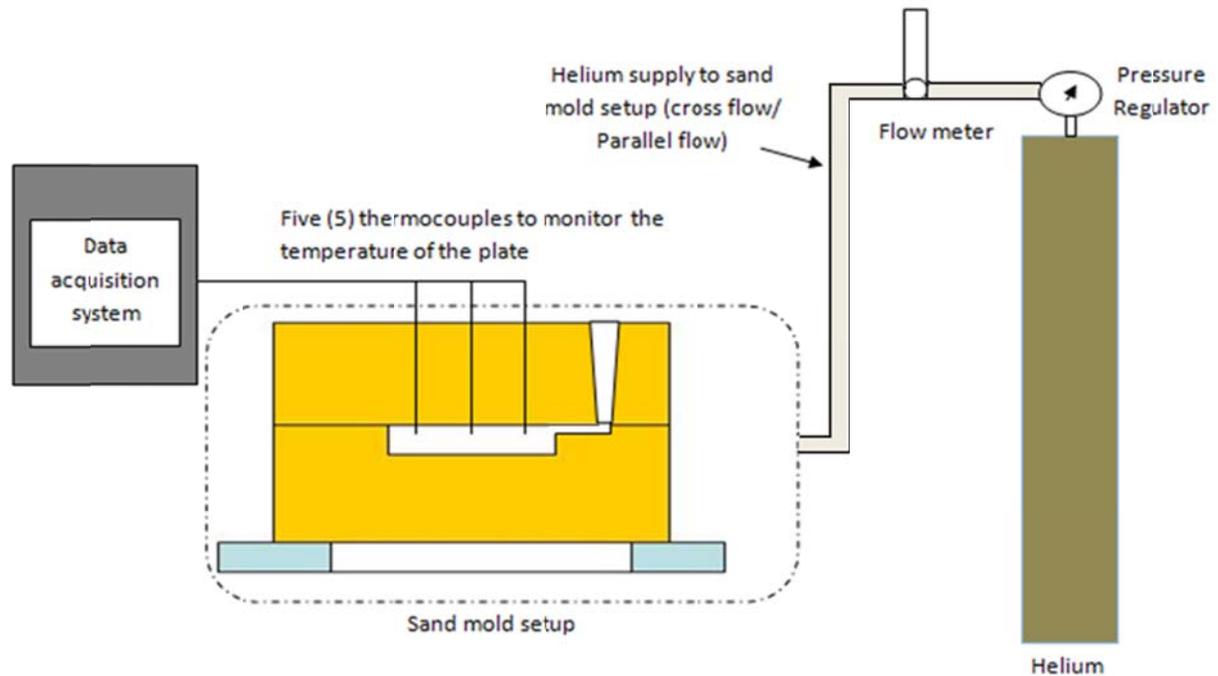
Fig. 10 Schematic representation of the main apparatus.

Five (5) thermocouples are inserted into the mold cavity to monitor the change in temperature during solidification of the casting. As shown in Fig. 11, four (4) of these thermocouples are near the risers and one (1) is at the geometric center of the casting. The placement of the thermocouples was decided with the help of computer simulation of the process with MAGMASOFT® software[2]. Details of the simulation are presented in Appendix B. The thermocouples are inserted and held in place by drilling holes through the cope. A small piece of aluminum tubing (approximately 1.5 inches in length) is placed in each hole with one end of the tubing aligned with the cope's parting surface and fixed in place with a packing of refractory blanket. A thermocouple is pushed through each one of these tubes and into the mold cavity. This arrangement ensures that the thermocouples

---

[2] MAGMA Foundry Technologies Inc., 10 N.Martingale Road, Schaumberg, IL 60173, USA.

remain snug in their place up to the required depth in the casting. The location of the thermocouples in relation to the risers and the casting is shown in the Fig. 11.

(a)   (b)
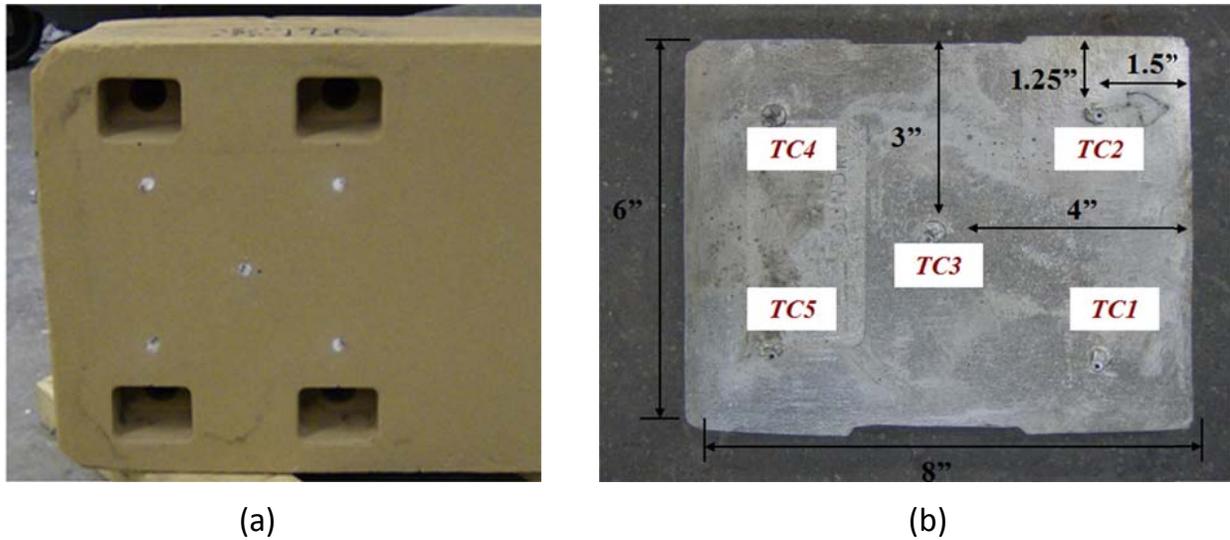
Fig. 11 Location of the thermocouples (a) in relation to the risers, and

(b) in relation to the casting

Note that thermocouples T1 and T2 are nearest to the pouring basin and represent the hot end of the casting. This end is the farthest from the helium supply. Because of symmetry, the average temperature of these two thermocouples is taken to represent the temperature (or cooling rate) at the hot end of the casting. Similarly, thermocouples T4 and T5 are farthest from the pouring basin and represent the cold end of the casting. This end is nearest to the helium supply. Again, because of symmetry, the average temperature of these two thermocouples is taken to represent the temperature (or cooling rate) at the cold end of the casting.

3.3 Alloy Composition

The chemical composition of the alloy was measured using spark emission spectrometry[3] and is shown in Table 6. The alloy is used in the un-grain refined, un-modified state and has a chemical composition that is close to that of 319 alloy.

Table 6 Average composition of the alloy.

	Si	Fe	Cu	Mn	Mg	Ni	Zn	Ti	Others	Al
Measured	6.96	0.62	3.34	0.36	0.42	0.03	0.58	0.03	0.16	rem.
Standard	5.5 - 6.5	1.0	3.0 - 4.0	0.5	0.1	0.35	3.0	0.25	0.5	rem.

3.4 Sand Mold

A two-part (cope and drag) recycled silica sand mold[4] that is specially designed for casting a rectangular plate is used for the experiments. The mold cavity is located completely within the drag. Fig. 12 is a picture of the assembled mold; Table 7 shows its nominal dimensions, and Table 8 shows its relevant technical details. The specific permeability of the sand mold is measured using Darcy's law [29] and details of the measurements are presented in Appendix C.

---

[3] Model Spectro Lab-Max LMXM3, Spectro Analytical Instruments Inc., 91 McKee Drive, Mahwah, NJ 07430, USA.
[4] Courtesy of Palmer Foundry, 22 Mt.Dumplin Road, Palmer, MA 01069, USA.

Fig. 12 The sand mold used in the experiments.

Table 7 Nominal dimensions of the sand mold used for experiments.

Dimensions of mold at the parting surface	16" x 12" (L x W)
Total height of the mold	11"
	Drag height = 5"
	Cope height = 6"

Table 8 Technical details of the sand mold used for experiments.

Sand type	Binder	Filters	AFS grain fineness number	Specific permeability of the sand mold
Recycled silica	Resin (furan based)	Foam 10 ppi	80	$1.51 \times 10^{-11} \text{ m}^2$

3.5 Cast Part

The cast part is a rectangular plate that is 8 inches long and 6 inches wide. The height of the plate measured at its sides is 1 inch. The top surface of the plate has a side web that runs along its periphery. The web is approximately 0.375 inches wide with a height of 0.6 inches so that the effective thickness of the plate is 0.4 inches. Fig. 13 shows a schematic representation of the cast plate, Fig. 14 shows pictures of the plate, and Fig. 15 shows the casting from which the plate is cut together with the risers, runners, and gating system. Fig. 16 is a schematic representation showing the locations on the cast plate where samples for tensile property measurements and microstructure analysis are extracted. Specimens for microstructure analysis are cut from locations adjacent to the 5 thermocouples.
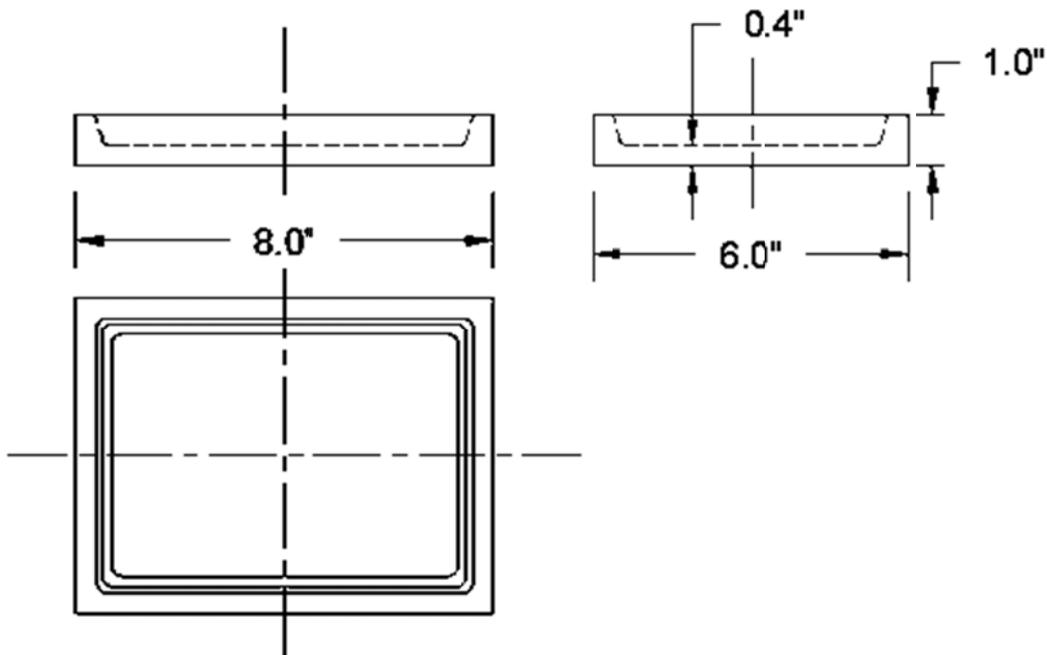
Fig. 13 Schematic representation of the cast plate.

(a)   (b)

Fig. 14 The cast plate: (a) bottom surface and (b) top surface.

Fig. 15 The complete casting.
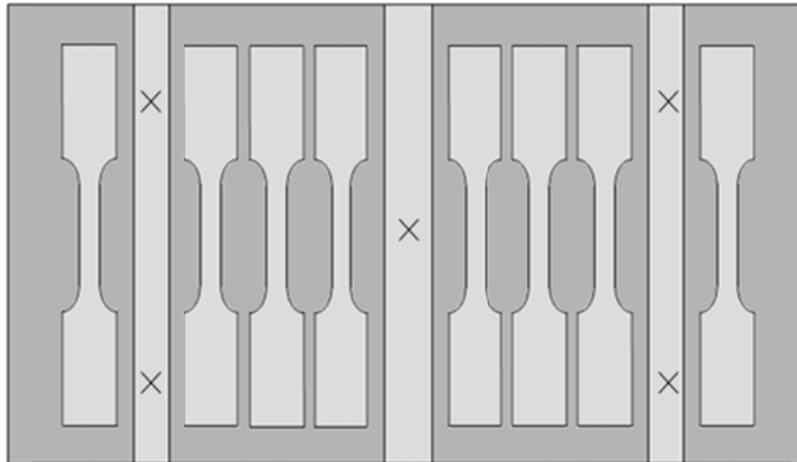
Fig. 16 Schematic representation of the cast plate showing locations where tensile specimens and samples for microstructure analysis are extracted (marked by ×).

3.6 Helium Supply Modes

Three different helium supply modes are investigated. These are:

a) Cross flow in a partially encapsulated mold

b) Cross flow in an un-encapsulated mold

c) Parallel flow in an un-encapsulated mold

Fig. 17 is a schematic representation that illustrates the difference between cross flow and parallel flow.

He

He

(a)   (b)
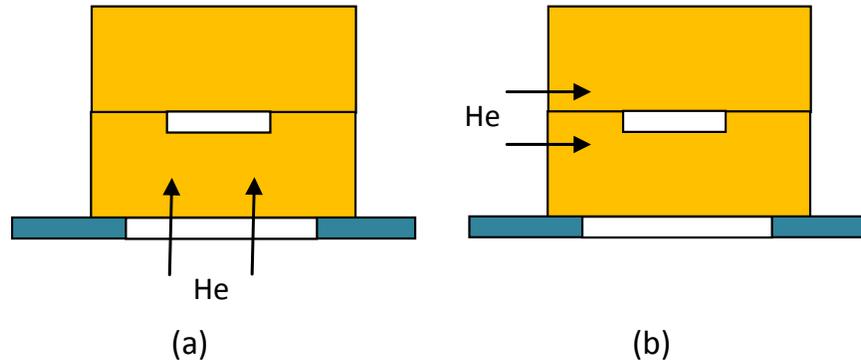
Fig. 17 Schematic representation of (a) cross flow and (b) parallel flow of helium across the casting.

Although the apparatus shown schematically in Fig. 10 is used; some modifications to this apparatus are made in order to accommodate the different helium supply modes. These modifications are described in the following sections.

(a) Cross Flow in a Partially Encapsulated Mold

The partial encapsulation is designed such that it can accommodate sand mold up-to a maximum size of 17.5" x 11.5" (measured at top surface of the mold) with a fixed height of 11 inches. Fig. 18 shows the main components of the device used to partially encapsulate the sand mold and Table 9 lists the purpose that each of these components serves[5]. Fig. 19 together with Table 10 describes the device and its various constituents in more detail. Fig. 20 shows the apparatus when partial encapsulation is employed.

---

[5] Schematic representations of the components are in Appendix D.
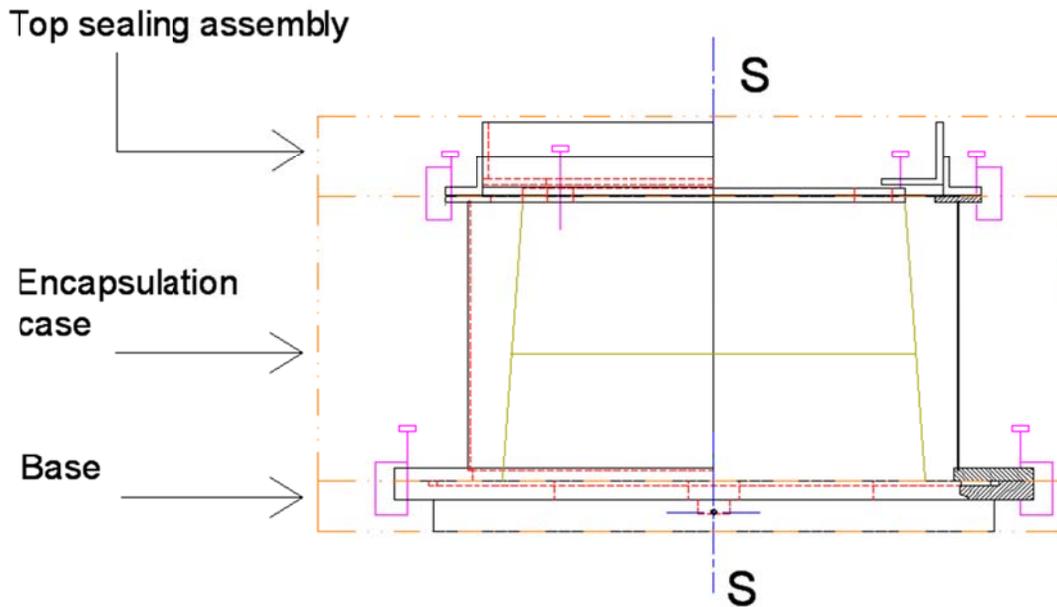
Fig. 18 The main components of the device used to partially encapsulate the sand mold.

Table 9 The main design components of the device used to partially encapsulate the sand mold.

Components	Objectives
Base	Provides a pedestal through which helium is supplied at the bottom of the mold (drag)
Encapsulation case	Provides partial encapsulation of the mold
Top sealing assembly	Seals the peripheral gap (present due to mismatch between mold size and encapsulation case)
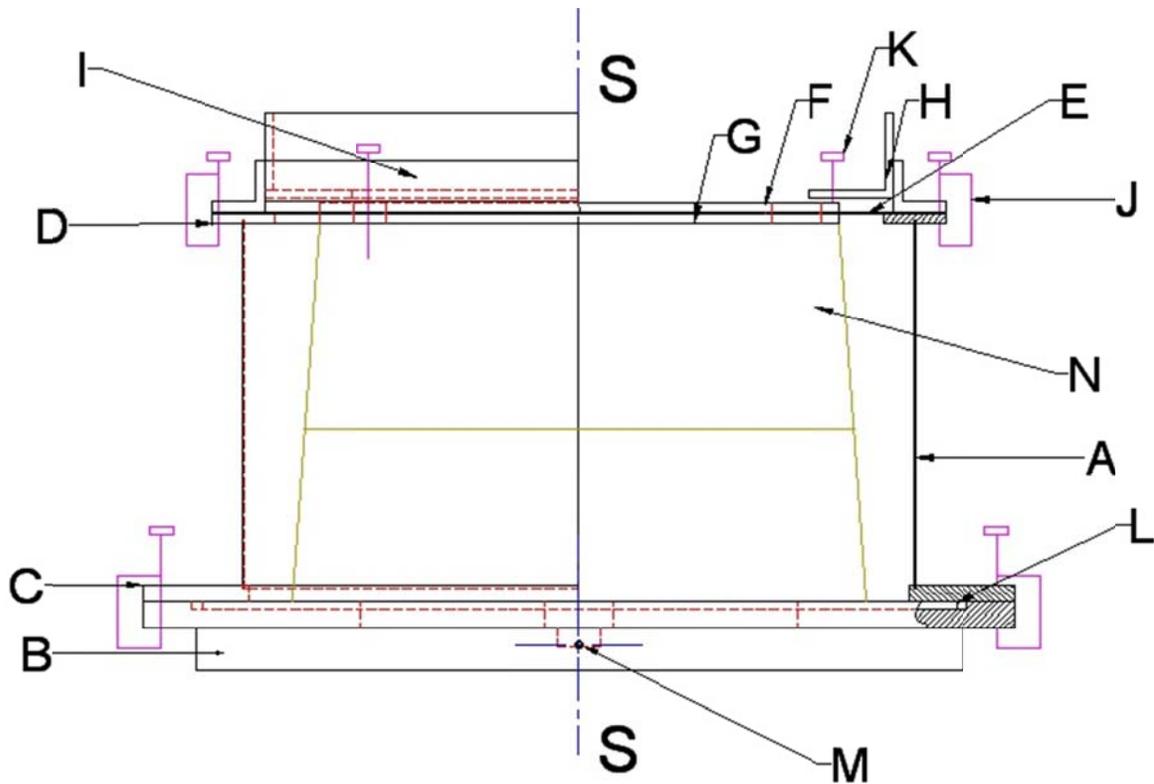
Fig. 19 Detailed schematic of the device used to partially encapsulate sand molds.

Table 10 Description of parts shown in Fig. 19 and details of their fabrication.

Label	Description	Materials	Fabrication details			
			Procedures	Machines	CAD/CAM software assistance	Facility used for fabrication
A	Steel case	16 gauge steel	Sheet metal fabrication (shearing, bending & MIG welding)	(i) Peck, Stow & Wilcox, Co (ii) Tennsmith® (ii) Millermatic® 300 by Miller®	SolidWorks version 2009	Higgins lab & Washburn shops (WPI), Worcester, MA
B	Base plate	C1018	CNC machining	Vertical spindle mold machine VM-3 by Hass Automation, Inc	AutoCAD® 2009 Solidworks version 2009 ESPRIT® version 2009	Washburn shops (WPI), Worcester, MA
C	Bottom flange	C1018	CNC machining	Vertical spindle mold machine VM-3 by Hass Automation, Inc	AutoCAD® 2009 Solidworks version 2009 ESPRIT® version 2009	Washburn shops (WPI), Worcester, MA
D	Top flange	C1018	CNC machining	Vertical spindle mold machine VM-3 by Hass Automation, Inc	AutoCAD® 2009 Solidworks version 2009 ESPRIT® version 2009	Washburn shops (WPI), Worcester, MA

E	Gasket	Graphite fibers with a nitrile binder			AutoCAD® 2009	Purchased from supplier in ready to use form
F	Top plate B	C1018	Water jet cutting		AutoCAD® 2009 SolidWorks version 2009	Outsourced to local fabricator Vangy Tools, Worcester, MA
G	Top plate A	C1018	Water jet cutting		AutoCAD® 2009 Solidworks version 2009	Outsourced to local fabricator: Vangy Tools, Worcester, MA
H	Angle assembly 1	Carbon steel	Abrasive cut off, drilling and Taping	(i) Milwaukee® chop saw (ii) ARBOGA WILTON® A-3008	AutoCAD® 2009	Washburn shops (WPI), Worcester, MA
I	Angle assembly 2	Carbon steel	Abrasive cut off, drilling and Taping	(i) Milwaukee® chop saw (ii) ARBOGA WILTON® A-3008	AutoCAD® 2009	Washburn shops (WPI), Worcester, MA
J	C clamp	Miscellaneous				Purchased from supplier in ready to use form
K	Cap screw	Steel				Purchased from supplier in ready to use form
L	O ring	Viton®				Purchased from supplier in ready to use form
M	Helium supply pin	Brass				Purchased from supplier in ready to use form
N	Sand mold	Silica (sand)				Provided courtesy of Palmer Foundry, MA, USA
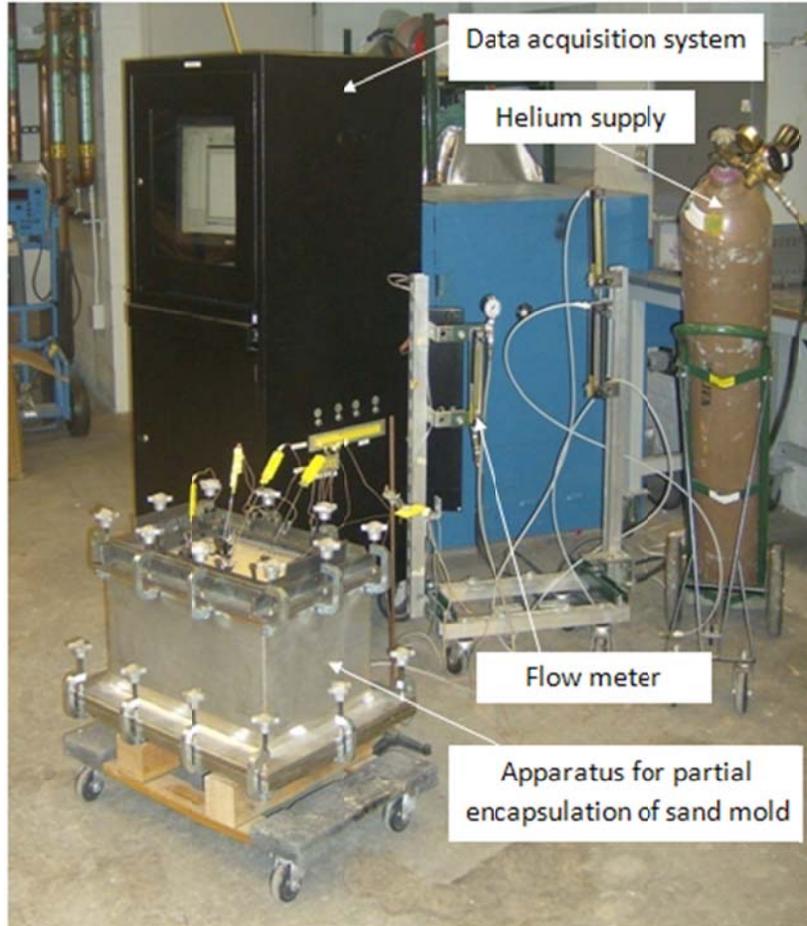
Fig. 20 A photograph of the apparatus when cross flow in partial encapsulation is employed.

(b) Cross Flow in an Un-encapsulated Sand Mold

This mode of helium supply only requires the "base" of the device that is used with the cross flow in partially encapsulated mold. Fig. 21 shows the apparatus when cross flow in an un-encapsulated sand mold is employed. In all cross flow experiments, an epoxy sealant (DURAPOT^{TM} 866)[6] is used to seal the peripheral interface between the mold's base (i.e., the drag) and the base plate (on top of which the mold rests) in order to ensure that helium supplied from the bottom doesn't leak through this interface. However, a good mechanical seal should nullify the need for this chemical sealant.

[6] Cotronics Corporation, 131 47th Street, Brooklyn, NY 11232, USA.
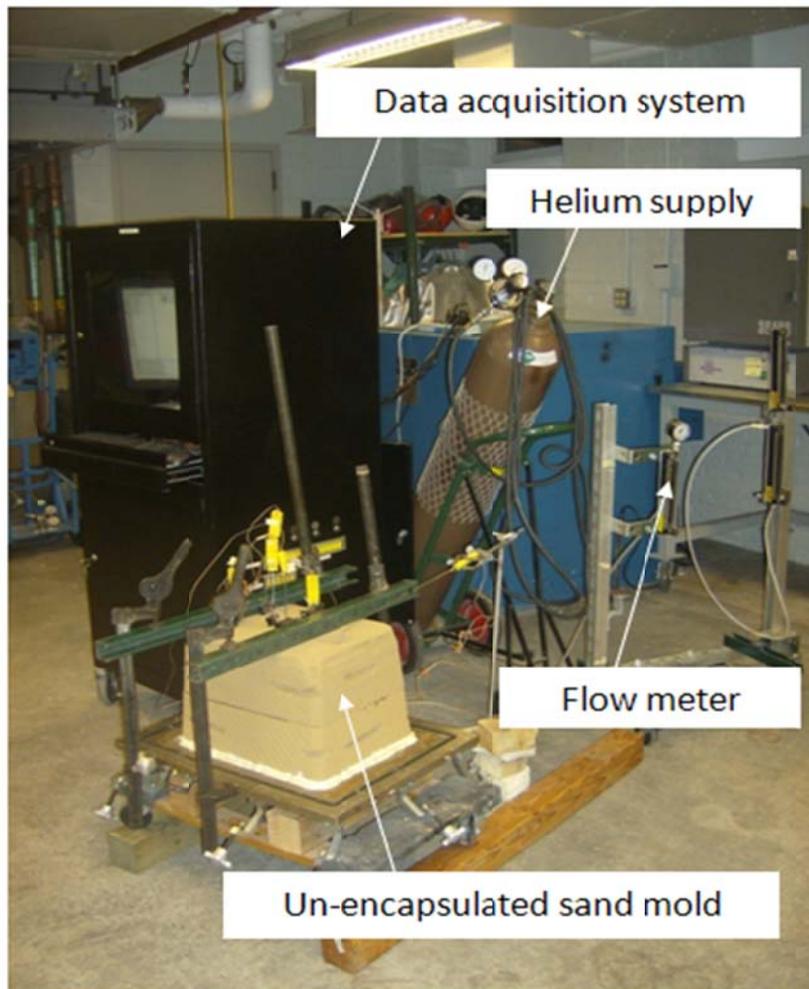
Fig. 21 A photograph of the apparatus when cross flow in an un-encapsulated sand mold is employed.

(c) Parallel Flow in an Un-encapsulated Mold

Two "supply plates" are designed for supplying helium in this mode: one for the "cope" and other for the "drag". These "supply plates" only differ from one another in the location of the point of helium supply. This point is shown as a 1/8"NPT fitting on the schematics in Fig. 22 which shows the two different supply plates. Details for affixing the "supply plates" to the sand mold (including details of the clamping assembly) are

presented in Appendix E. Fig. 23 shows the sand mold with the supply plate attached to the drag and Fig. 24 shows the apparatus when parallel flow in an un-encapsulated mold is employed. Here too, an epoxy sealant (DURAPOT™ 866) is used to seal the peripheral interfaces between the mold and the supply plates in order to ensure that helium doesn't leak through these interfaces. However, a good mechanical seal should nullify the need for this chemical sealant.

Hole for $\frac{1}{8}''$ NPT fitting — 2" — 0.5" — 7" — **(a)**

Hole for $\frac{1}{8}''$ NPT fitting — 2" — 1.0" — 7" — (b)
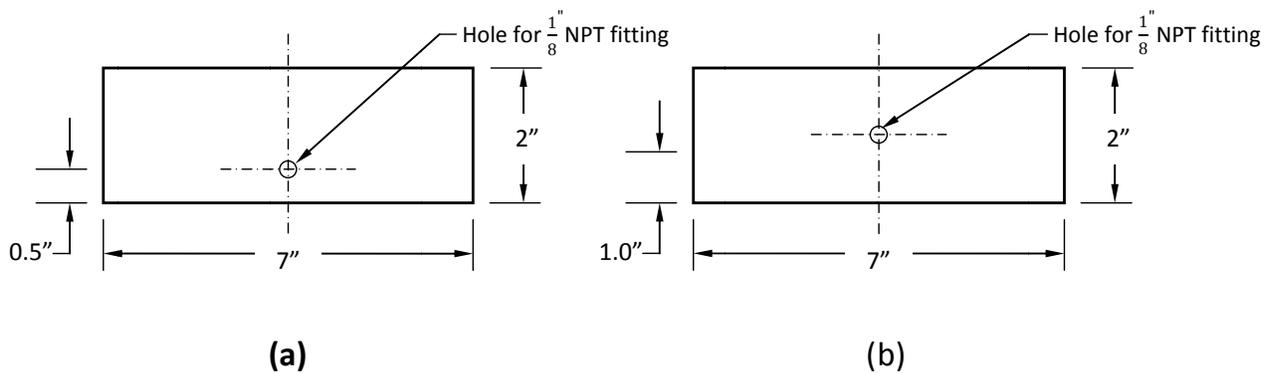
Fig. 22 Supply plates (a) for the cope and (b) for the drag.
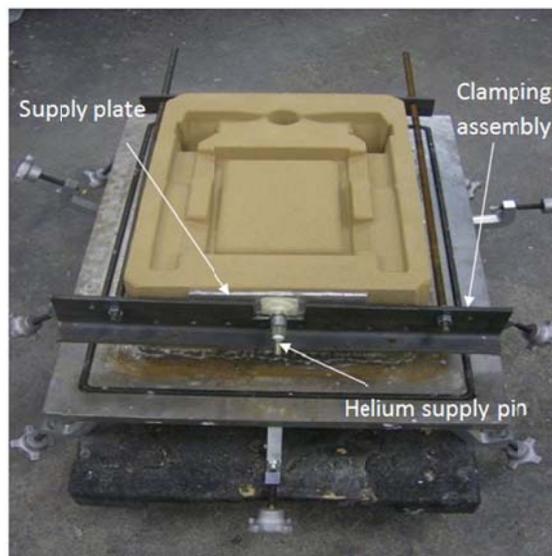
Fig. 23 Apparatus for parallel flow helium supply (drag).
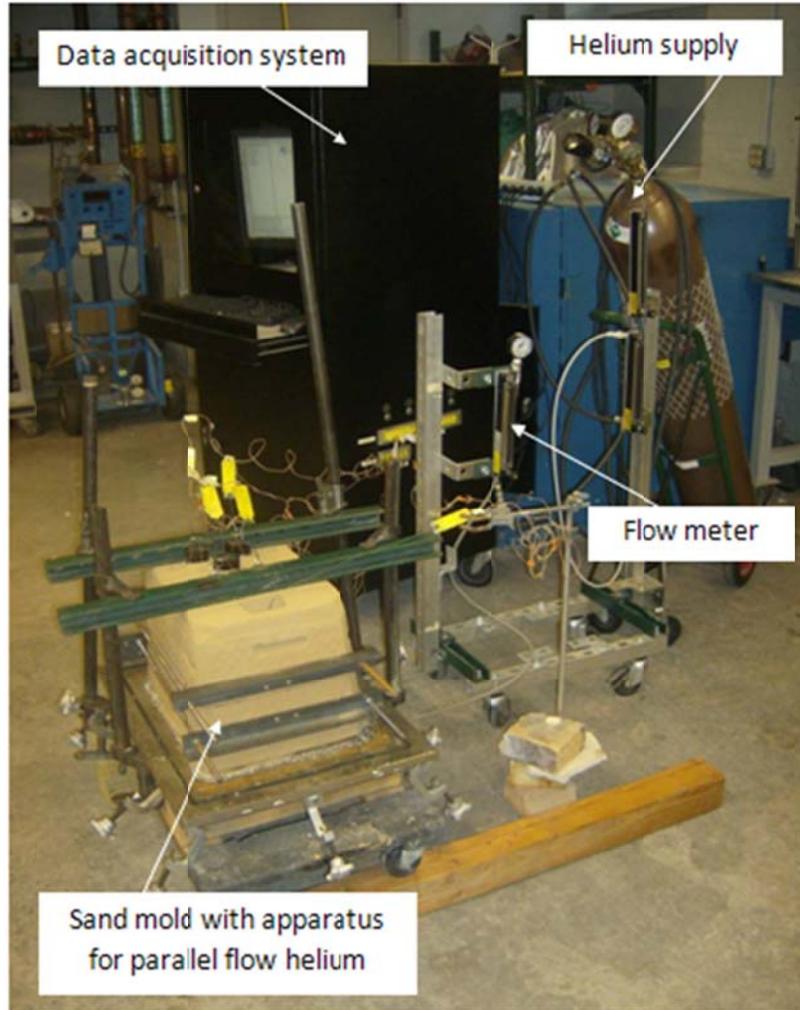
Fig. 24 A photograph of the apparatus when parallel flow in an un-encapsulated mold is employed.

4. Procedures

4.1 Melt Preparation

In each test, 40 pounds of alloy are melted in an induction furnace in a silicon carbide crucible. The melt is heated to 880±5°C and is degassed with argon for half an hour using a rotating impeller degasser. The melt surface is then drossed and an RPT (reduced pressure test) gas sample is taken. If porosity is found inside the solidified RPT sample, or more than three bubbles are detected on the surface of the sample, degassing is continued until a gas-free melt is obtained. At this point a sample is taken for chemical analysis by spark emission spectrometry.

4.2 Measuring the Apparent Thermal Conductivity of the Sand Mold

Apparent thermal conductivity measurements are performed according to the Guarded Comparative Longitudinal Heat Flow method described in ASTM E 1225-4 [39]. Two apparatuses are constructed for the purpose: one to perform measurements on the specimen without introduction of helium, and the other to allow the introduction of helium into the pores between the particles of sand.

Cylindrical specimens that are 45.7 mm (1.8 inches) in diameter and 20 mm (0.79 inches) in height are cut from the sand molds. Two holes that are 11 mm (0.43 inches) apart from each other are made at predefined locations to allow placing thermocouples in the cylinder. Two Macor® machineable ceramic disks[7] are used as reference material. The size and placement of the thermocouple holes in the reference material are the same as those in the sand mold specimen. Fig. 25 is a schematic representation of the specimen and Table 11 gives additional details of the materials used to construct the apparatus.

---

[7] Ceramic Products Inc., 32 MacArthur Ave., Hasbrouck Heights, NJ 07604, USA.

ALL DIMENSIONS ARE IN MM
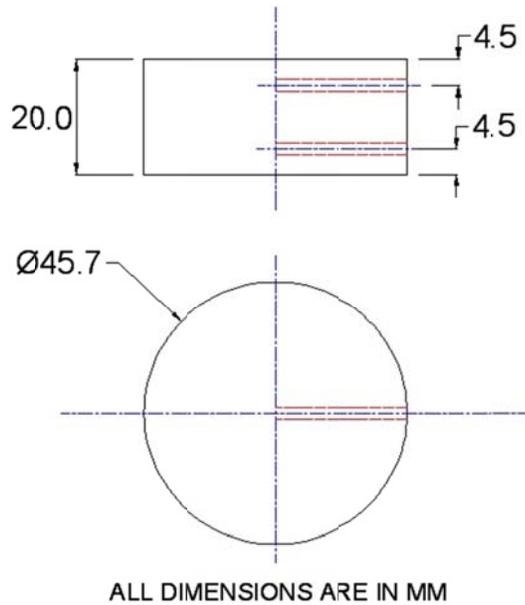
Fig. 25 Specimen used to measure apparent thermal conductivity of sand molds.

Table 11 Details of materials used in the apparatus for measuring apparent thermal conductivity of sand molds.

Length of test stack	60 mm (2.36")
Wall thickness of the metallic guard	0.125"
	(Outer diameter: 4", Inner diameter: 3.75")
Ratio of stack to guard diameter	2.22
Insulation	Commercially available spun ceramic fiber blanket (High Purity Grade: 8 lb)
Heat source	Electric heater
Heat sink	Ice and water mixture
Material used for calibration	Opaque fused quartz[8]

Fig. 26 is a schematic representation of the apparatus used for performing the measurements. Both configurations were calibrated according to the procedures outlined in the Standard's guidelines [39].

---

[8] Technical Glass Products Inc., 881 Callendar Blvd., Painesville Twp, OH 44077, USA.
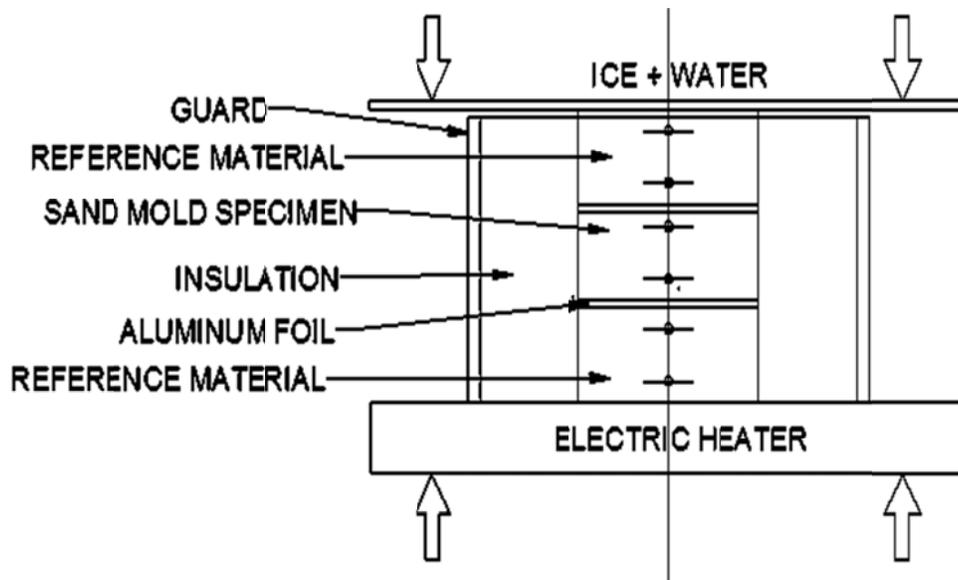
(a)
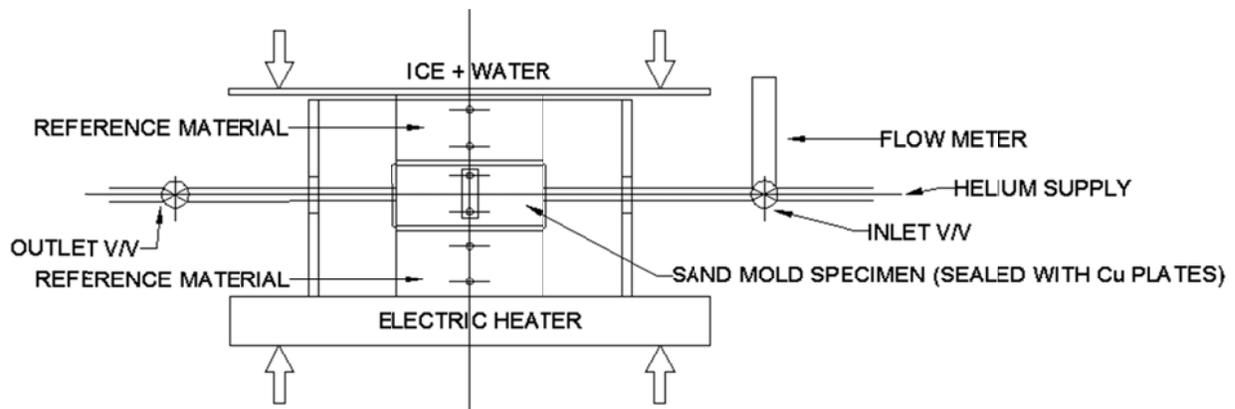
(b)

Fig. 26 Schematic representation of the apparatus used for measuring the apparent thermal conductivity of sand molds. (a) in air, (b) in helium.

Prior to performing the measurements the sand specimens are placed in an oven at about 120°C for about 12 hours in order to drive off moisture that the sand molds may have absorbed during handling and storage.

For measurements in helium, the gas is directly injected into the specimen to displace air from the pores. The side of the specimen are sealed together with two thermocouples and

two tubes (one serves as an entrance and the other as an exit for helium) by a thermally insulating epoxy (DURAPOT[TM] 866, k = 0.216 W/m K). The exposed "ends" of the specimen are covered with 1.5 mm thick copper plates and affixed at both ends. This arrangement ensures that the specimen is completely sealed while maintaining a unidirectional heat flow along the axis of test stack. Helium is introduced into the specimen via the supply tube after passing through a flow meter at a gauge pressure of 12.5 KPa (0.1234 atm. above atmospheric pressure). An On/Off valve is placed downstream of the specimen to control the helium supply as shown in Fig. 26. Prior to performing a measurement, the specimen is purged with helium for a few minutes to push out any air that is present in the pores. The downstream valve is then closed trapping the helium inside the pores while keeping the flow meter v/v open. Therefore, a pressure of 12.5 KPa, which is slightly higher than atmospheric pressure, is maintained in the specimen. Three specimens are used to measure the apparent thermal conductivity of air-filled sand molds and two specimens are used to measure it for helium-filled sand molds. Measurements are performed at 25°C and 125°C for both configurations. The temperature profile developed in the test stack is recorded by six (6) K-type thermocouples that are connected to a data acquisition system[9]. DASYLab® version 5.61.10[10] is used as the data acquisition software. Data is recorded at a sampling rate of 1000 measurements per second and averaged using 100 values to give a time interval of 0.1 second between the recorded data points.

The recorded data is exported to Microsoft® Excel® for analysis and the calculated values are then averaged over the stable range. Eq. (4) [39] is used in the calculation of thermal conductivity. The values reported here are averages of at least six thousand data points.

$$k_S = \left(\frac{\Delta Z_S}{\Delta T_S}\right) \times \left(\frac{k_R}{2}\right) \times \left(\frac{\Delta T_{R1}}{\Delta Z_{R1}} + \frac{\Delta T_{R2}}{\Delta Z_{R2}}\right) \tag{4}$$

---

[9] National Instruments Corporation, 11500 N Mopac Expwy, Austin, TX 78759, USA.
[10] Measurement Computing Corporation, 10 Commerce Way, Norton, MA 02766, USA.

In Eq. (4), k_S is the apparent thermal conductivity of the specimen, ΔZ_S is the distance between the thermocouples in the sample, ΔT_S is the temperature profile developed in the specimen measured as measured by the thermocouples. k_R is the thermal conductivity of the reference material, and ΔZ_{R1} is the distance between the thermocouples in the reference material and ΔT_{R1} is the temperature profile developed in the reference material; both for the reference material disk closest to the heat source. ΔZ_{R2} and ΔT_{R2} are the corresponding values for the reference material closest to the heat sink.

4.3 Measuring the Surface Roughness of the Plate Castings

A contact profilometer[11] is used to characterize the surface roughness of the top surface of the cast plate by measuring R_a and R_z. In each case, twenty (20) measurements are performed and the average is recorded. The conditions used in measuring the surface roughness are presented in Table 12.

Table 12 Measuring conditions used for surface characterization.

Stylus tip	2 μm at 90^0
Measuring speed	0.10 mm per sec
Traveling length	17.50 mm
Point spacing	1.56 μm

R_a (the mean roughness or roughness average) is the arithmetic average of the absolute values of the roughness profile ordinates [40]. It gives a good general description of the height variations in the surface [40]. On the other hand R_z (the mean roughness depth), is

---

[11] Perthometer PRK by Mahr Perthen, 1144 Eddy Street, Providence, RI 02905, USA.

the arithmetic mean value of the single roughness depths of consecutive sampling lengths [40]. Both of these parameters are represented by Fig. 27 [40].
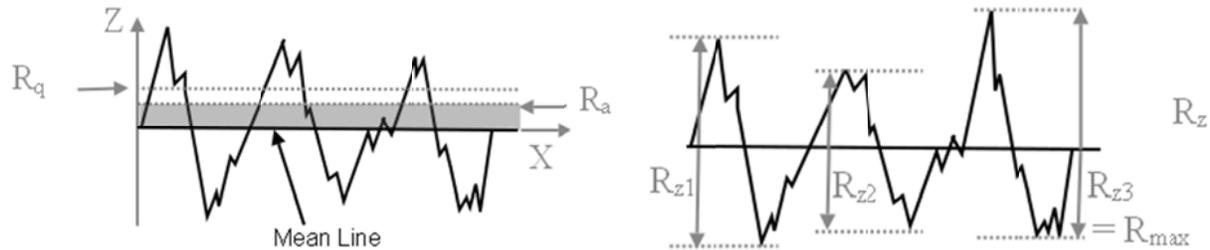
Fig. 27 Explanation of R_a and R_z [40].

The reason for choosing the top surface of the plate for characterization is that it presents the worst case scenario where helium directly impinges on solidifying metal.

4.4 Measuring the Cooling Rate during Solidification of the Plate

In addition to the 5 K-type thermocouples that are placed in the plate casting to record temperature during solidification (see Fig. 11), another K-type thermocouple is placed in the pouring basin to monitor changes in the pouring temperature. These thermocouples are connected to a data acquisition system. DASYLab® version 10.00.01 is used as the data acquisition software. Data is collected at a sampling rate of 20000 measurements per second and averaged using 2000 values to produce a time interval of 0.1 seconds between recorded data points. The recorded data is then exported to Microsoft® Excel® for analysis.

The range selected for thermal analysis is $650^{\circ}C$ to $400^{\circ}C$ with a temperature of $650^{\circ}C$ taken as the starting point for the thermal analysis. There are several reasons for selecting this temperature range for monitoring the temperature, these include:

(i) The melt is poured into the pouring basin when its temperature is $850^{\circ}C$ and starts to cool at a relatively fast rate. Helium is introduced into the system only when the

mold is completely filled. The temperature drop from the pouring temperature (850°C) to 650°C allows sufficient time to manually initiate the introduction of helium so that all measurements are done from the same starting temperature (650°C).

(ii) The temperature range 650°C to 400°C covers all three phases that the alloy under consideration passes through as it solidifies (i.e., the liquidus, the mushy zone - where microstructure forms- and the solidus).

(iii) Unnecessary cluttering of the cooling curve is avoided by presenting the selected range only.

4.5 Measuring the Room Temperature Tensile Properties of the Cast Plate

Eight specimens from each experiment are used to determine the room temperature tensile properties of the cast plate. The specimens are sub-size with a rectangular cross section and are machined from the plate casting from the locations shown in Fig. 16. Tensile property measurements are conducted according to ASTM standard B557-06 [41] with a Universal Testing machine[12]. Strain is measured with an axial extensometer[13] with a gage length of 1 inch. The extensometer is used until the specimen is fractured and the testing machine ramp rate is 0.05 inches/min. The data is digitally captured and analyzed to obtain tensile strength, yield strength, elongation and modulus of elasticity. Prior to measuring the room temperature tensile strength, the specimens are heat treated according to a standard T6 schedule (see Table 13).

---

[12] Series 5500 material testing system, control software Merlin[TM] version 5.11, Instron Worldwide Headquarters, 825 University Ave., Norwood, MA 02062, USA.
[13] Catalogue number: 2630-108, Instron Worldwide Headquarters, 825 University Ave., Norwood, MA 02062, USA.

Table 13 Details of T6 thermal treatment for sand cast aluminum alloy 319 [21].

Soaking	Quenching	Aging
504°C (940°F) for 12 hours	In 75°C water	154°C (310°F) for 3 hours

4.6 Characterizing the Microstructure of the Cast Plate

Microstructure characterizations is done on specimens in the as- cast condition that are cut from locations close to the five thermocouples (see Fig. 16). Each sample is mounted in Bakelite such that metallographic surface is along the thickness of the plate. The samples are then prepared for optical microscopy using typical metallographic preparation procedures. Two optical microscopes[14,15] with ultrahigh definition digital camera[16] are used to examine and capture the microstructure. The captured images are exported to an image processing software[17] to characterize porosity, secondary dendrite arm spacing and grain size. When required, Keller's reagent [42] with the composition shown in Table 14 is used.

Table 14 Composition of Keller's reagent [42].

2 mL HF (48%)
3 mL HCL (concentrated)
5 mL HNO$_3$ (concentrated)
190 mL H$_2$O

---

[14] Model EPIPHOT 200, Nikon Instruments Inc., 1300 Walt Whitman Road, Melville, NY 11747, USA.

[15] Model SMZ1500, Nikon Instruments Inc., 1300 Walt Whitman Road, Melville, NY 11747, USA.

[16] NIKON DXM1200F and NIKON ACT-1 version 2.63 software, Nikon Instruments Inc., 1300 Walt Whitman Road, Melville, NY 11747, USA.

[17] ImageJ 1.42q (http://rsb.info.nih.gov/ij/).

Porosity - Porosity is quantitatively characterized in terms of % area of pores observed at a magnification of 50X in the polished specimen. A total of eighty four (84) micrographs are taken for each experiment the average of the measurements performed on the 84 micrographs, along with the standard deviation is reported.

Grain size - Grain size is measured by Hilliard's circular intercept method [43] on etched specimens observed at a magnification of 10X under polarized light. A total of five (5) micrographs are taken for each measurement and the mean lineal intercept length is reported.

Secondary Dendrite Arm Spacing (SDAS) - SDAS is quantitatively characterized by the linear intercept method from micrographs of etched samples taken at a magnification of 100X. In this procedure, a line is drawn perpendicular to an array of secondary branches of the conveniently oriented primary arm. The length of this line divided by the number of secondary dendrite arms that it intercepts and the magnification gives a measure of the SDAS.

5. Results, Analysis and Discussion

5.1 Apparent Thermal Conductivity of the Sand Mold

Table 15 shows results of measuring the apparent thermal conductivity of the sand mold in air and in helium and Fig. 28 presents the same information in graphical form for better visualization.

Table 15 Apparent thermal conductivity results for all specimens.

Specimen #	Gas	Test pressure	Apparent thermal conductivity measured (W/m K)	
			25°C	125°C
1	Air	Atmospheric	0.529	0.478
2	Air	Atmospheric	0.546	0.495
3	Air	Atmospheric	0.565	0.496
Average	**Air**		**0.547 (0.018)**	**0.49 (0.010)**
4	Helium	12.5 KPa	1.036	1.022
5	Helium	12.5 KPa	1.030	0.929
Average	**Helium**		**1.033 (0.004)**	**0.976 (0.066)**

* Values in parenthesis show the standard deviations.
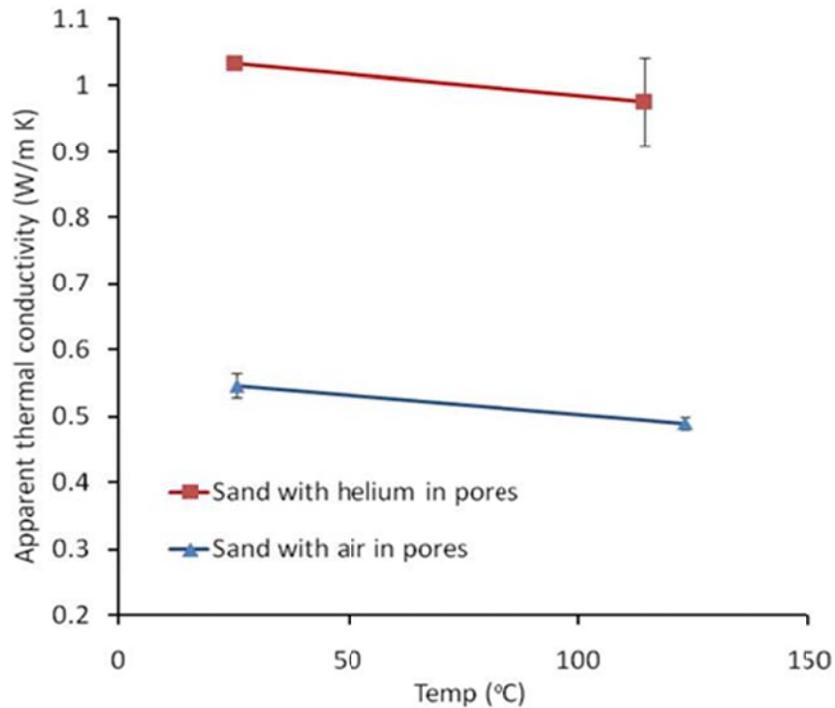
Fig. 28 Results of apparent thermal conductivity experiment.

Table 15 and Fig. 28 clearly show that there is a marked increase in apparent thermal conductivity of sand when helium is present in the pores compared to when air is present in the pores. At 100°C the increase in apparent thermal conductivity due to the presence of helium in the pores is about 94 % increase (apparent thermal conductivity of sand is 0.51 W/m K when air is present the pores compared to 0.99 W/m K when helium is in the pores). Appendix F presents a mathematical analysis that shows the effect of helium on solidification time and heat diffusivity of sand mold.

5.2 Thermal Analysis

(a) Baseline

Cooling curves in the range 650°C to 400°C at different locations on the solidifying plate for the conventional sand casting process are shown in Fig. 29.
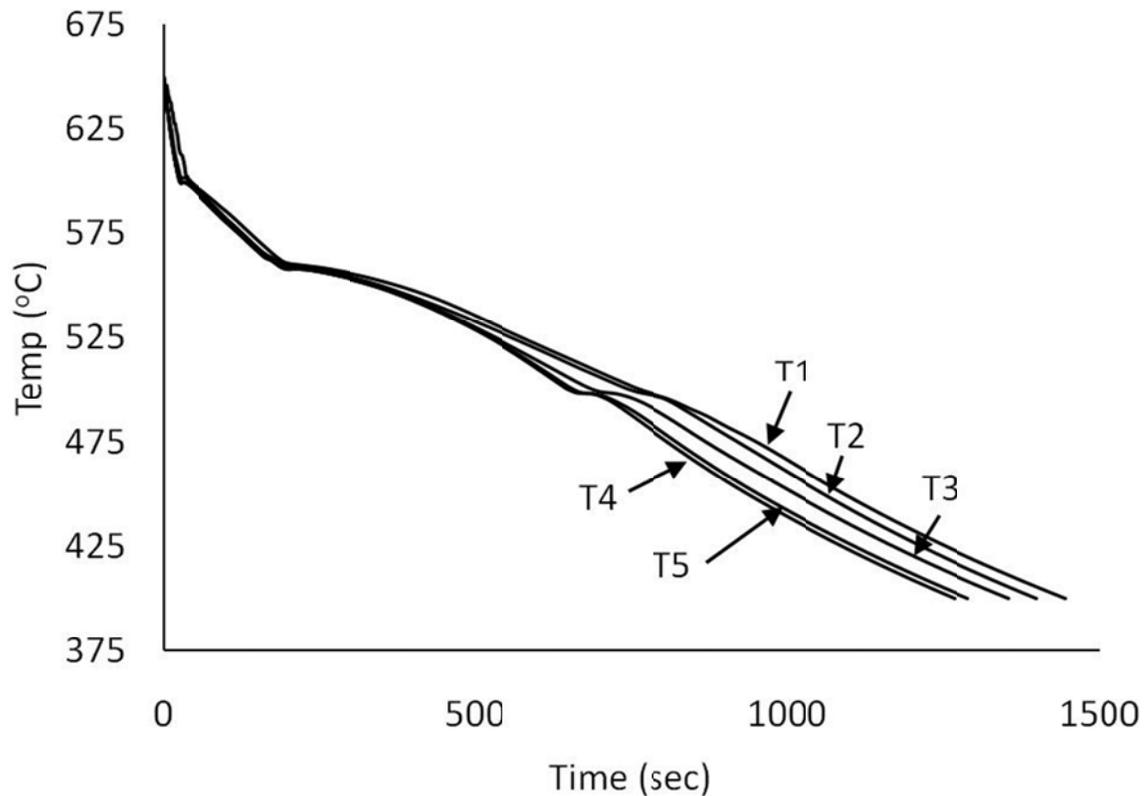
Fig. 29 Cooling curves in the range of 650°C to 400°C for baseline.

Two cooling rates are considered most relevant to this analysis. These are:

1) The cooling rate associated with the region where dendrites grow, since this cooling rate affects the secondary dendrite arm spacing and the overall microstructure of the casting. This cooling rate is calculated in the temperature range 575°C to 560°C.
2) The overall cooling rate of the casting, since it relates to process efficiency. This is calculated over the temperature range 650°C to 400°C.

The average "time to cool" from 650°C to 400°C is shown in the Table 16 and the cooling rates are shown in Table 17.

Table 16 Average "time to cool" from 650°C to 400°C in minutes.

Location on plate		
Nearest to pouring basin "hot end"	Middle	Farthest from pouring basin "cold end"
23.72	22.60	21.15
(0.537)		(0)

* Value in parenthesis shows the standard deviation.

Table 17 Cooling rates for baseline castings.

Cooling rate (^{o}C/s)	Location on plate		
	Nearest to pouring basin, "hot end"	Middle	Farthest from pouring basin, "cold end"
Dendrite growth region	0.22	0.24	0.25
	(0.014)		(0.007)
Overall	0.18	0.19	0.20
	(0.007)		(0.007)

* Value in parenthesis shows the standard deviation.

Table 16 shows that there is only a small variation in the "time to cool" between the "hot end" and the "cold end" of the plate (about 11%). This is due to the directional solidification that occurs towards the source of the feed metal [21]. Similarly, there is only small variation in the cooling rate during the dendrite growth between the "hot end" and the "cold end" of the plate (about 8%). For this reason, microstructure and tensile properties should be constant along the length of the plate.

(b) Helium-Assisted Cross Flow Mode

The cooling curve in the range 650°C to 400°C at the hot end[18] of the solidifying plate for the helium-assisted (cross flow mode) sand casting process are shown in Fig. 30 together with that for the baseline casting.
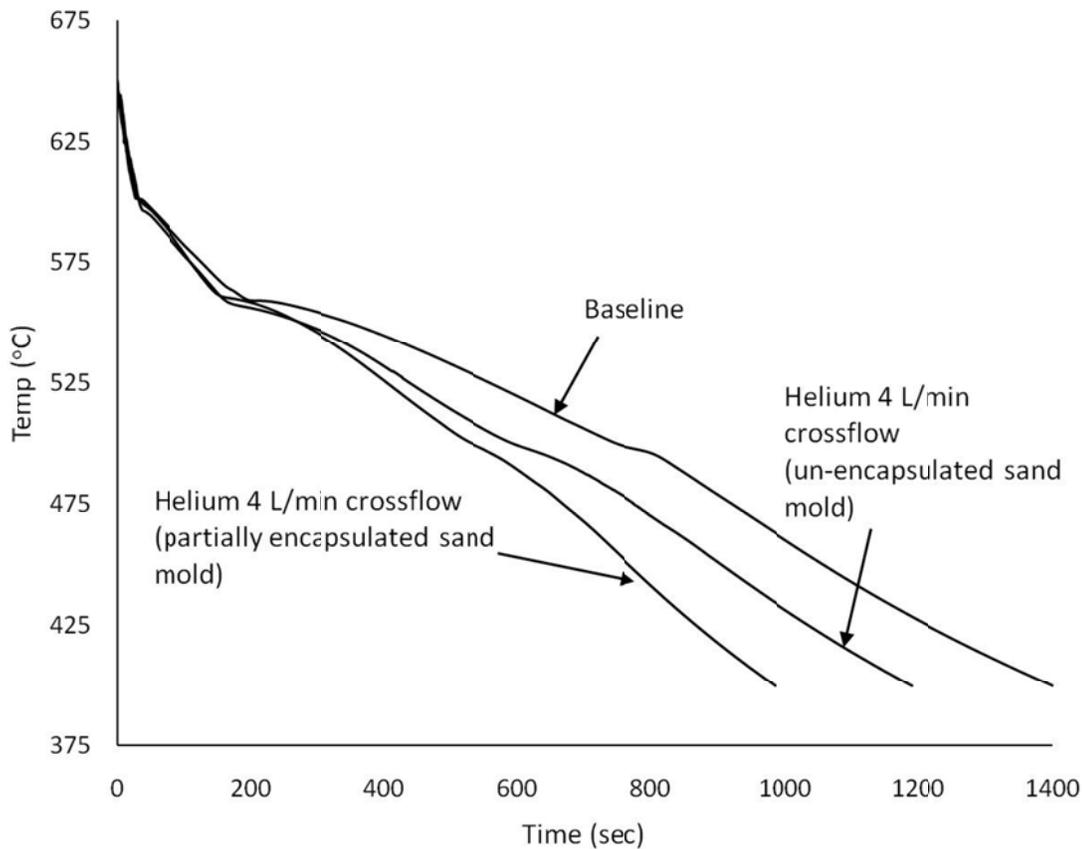
Fig. 30 Cooling curves during helium-assisted (cross flow mode) casting and baseline casting obtained at the "hot end" of the plate.

Table 18 shows the average "time to cool" from 650°C to 400°C for helium-assisted (cross flow mode) casting for a helium flow rate of 4 L/min, and Table 19 shows the reduction in "time to cool" for the helium-assisted (cross flow mode) casting calculated with respect to the baseline.

---

[18] The baseline experiment shows that the "hot end" of the plate takes the longest time to cool.

49

Table 18 Average "time to cool" from 650°C to 400°C in minutes in the helium-assisted (cross flow mode) process - helium flow rate = 4 L/min.

	Nearest to pouring basin "hot end"	Middle	Farthest from pouring basin "cold end"
Un-encapsulated mold	19.84 (0)	19.24	18.22 (0.099)
Partially encapsulated mold	16.33 (0.12)	15.72	15.09 (0.085)

* Value in parenthesis shows the standard deviation.

Table 19 Percent reduction in "time to cool" in the helium-assisted (cross flow mode) process w.r.t. baseline – helium flow rate = 4 L/min.

	Nearest to pouring basin "hot end"	Middle	Farthest from pouring basin "cold end"	Average
Un-encapsulated mold	16.36	14.87	18.58	16.6
Partially encapsulated mold	31.16	30.44	28.65	30.1

Tables 20 and 21 show the cooling rates obtained with the helium-assisted (cross flow mode) process at 4 L/min.

Table 20 Cooling rate in dendrite growth region in ^{o}C/s in the helium-assisted (cross flow mode) casting - helium flow rate = 4 L/min.

	Nearest to pouring basin, "hot end"	Middle	Farthest from pouring basin, "cold end"	Arithmetic average of all values	Increase w.r.t. baseline
Un-encapsulated mold	0.34 (0.042)	0.33	0.33 (0.014)	0.33 (0.023)	43.5 %
Partially encapsulated mold	0.32 (0.085)	0.34	0.33 (0.007)	0.33 (0.043)	43.5 %

* Value in parenthesis shows the standard deviation.

Table 21 Overall cooling rate in ^{o}C/s in the helium-assisted (cross flow mode) castings - helium flow rate = 4 L/min.

	Nearest to pouring basin, "hot end"	Middle	Farthest from pouring basin, "cold end"	Arithmetic average of all values	Increase w.r.t. baseline
Un-encapsulated mold	0.21 (0)	0.22	0.23 (0)	0.22 (0.01)	15.8 %
Partially encapsulated mold	0.26 (0.007)	0.27	0.28 (0)	0.27 (0.013)	42.1%

* Value in parenthesis shows the standard deviation.

The relative advantage of applying helium with respect to the baseline is clear. The results show that the cooling pattern of the plate is not significantly affected by the helium-assisted process in the cross flow mode. Variation in the "time to cool" along the length of the plate is about 8% compared to 11% for the baseline. The same is true for the cooling rates as they are more or less uniform along the length of the plate. The reason for this uniformity in time to cool and cooling rate is that helium, being lighter than air, rises uniformly through the mold from beneath the plate along its entire length.

Effect of encapsulation - Measurements show that the partially encapsulated mold produces better results than the "un-encapsulated mold": The reduction in the average "time to cool" at a flow rate of 4 L/min (compared to the baseline) is about 30% for the partially encapsulated mold compared to only 17% for the un-encapsulated mold. Despite the obvious advantage that mold encapsulation provides in reducing the overall time to cool the casting, in the range of temperature where dendrites grow, mold encapsulation does not give a significant advantage. This may be attributed to the fact that encapsulation hinders the escape of mold gases that evolve during the burn off of the binder. When mixed with helium, these gases seem to adversely affect the efficiency of helium in extracting heat from the solidifying melt. This phenomenon has also been reported by

Griffiths [33] who reported that binder gases dilute the effect of helium when experiments are conducted in a box [33].

(c) Helium-Assisted Parallel Flow Mode

The cooling curve in the range 650°C to 400°C at the hot end[19] and cold end of the solidifying plate for the helium-assisted (parallel flow mode) sand casting process are shown respectively in Figs. 31 and 32 together with cooling curves for the baseline casting; and the "time to cool" from 650°C to 400°C is presented in Table 22.
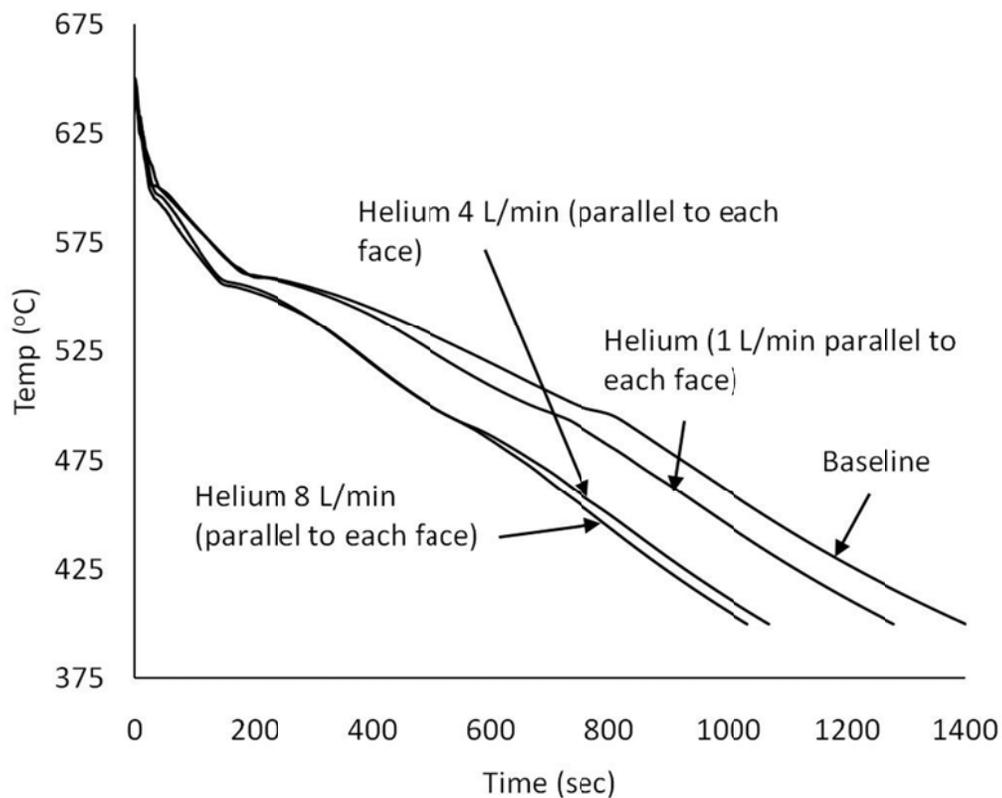
Fig. 31 Cooling curves during helium-assisted (parallel flow mode) casting and baseline casting at the "hot end" of the plate.

---

[19] The baseline experiment shows that the "hot end" of the plate takes the longest time to cool.
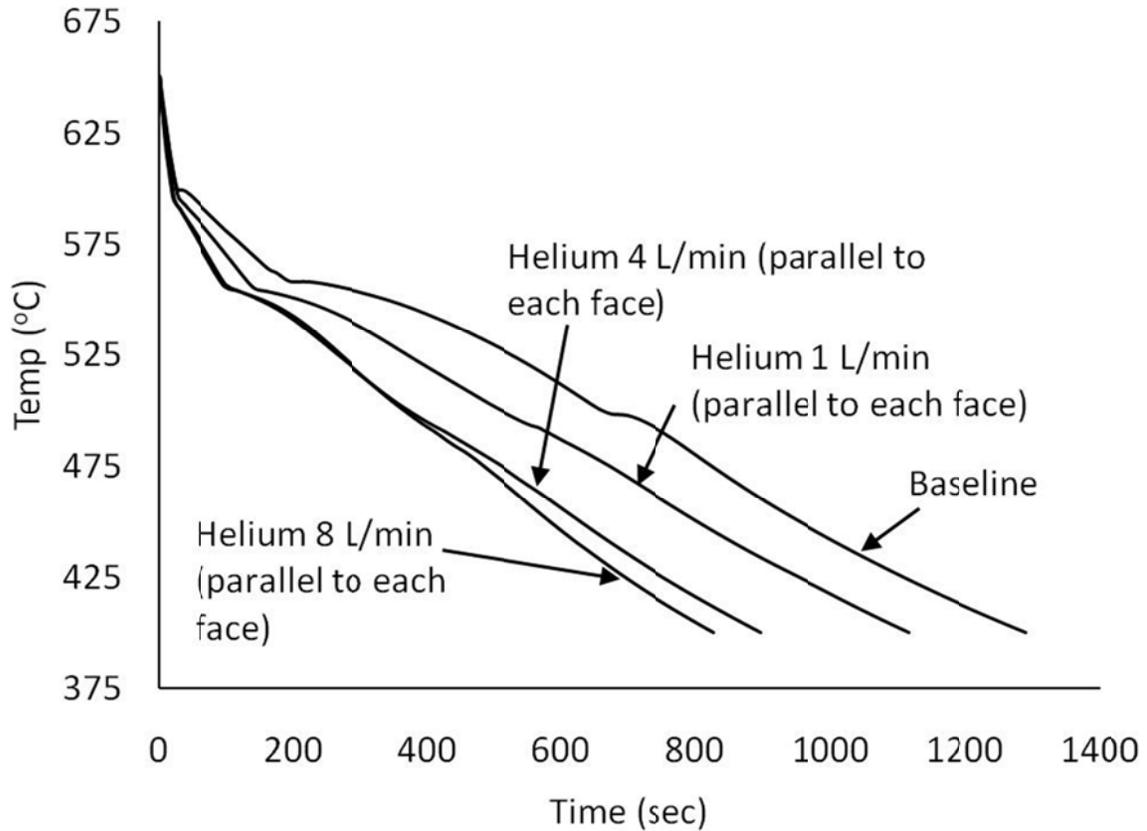
Fig. 32 Cooling curves during helium-assisted (parallel flow mode) casting and baseline casting at the "cold end" of the plate.

Table 22 Average "time to cool" the plate from $650^{o}C$ to $400^{o}C$ in minutes, at various helium flow rates (parallel flow) compared against baseline.

Helium flow rate (parallel to each face)	"Hot end" (farthest from helium supply)	Middle	"Cold end" (nearest to helium supply)
1 L/min	21.32 (0.035)	20.19	18.71 (0.135)
4 L/min	17.97 (0.212)	16.79	15.04 (0.156)
8 L/min	17.24 (0.028)	15.74	13.88 (0.17)

* Value in parenthesis shows the standard deviation.

Fig. 33 shows a comparison between the "time to cool" for helium-assisted sand casting (parallel flow mode) and the baseline; and Table 23 shows calculated percent reduction in "time to cool" compared to the baseline.
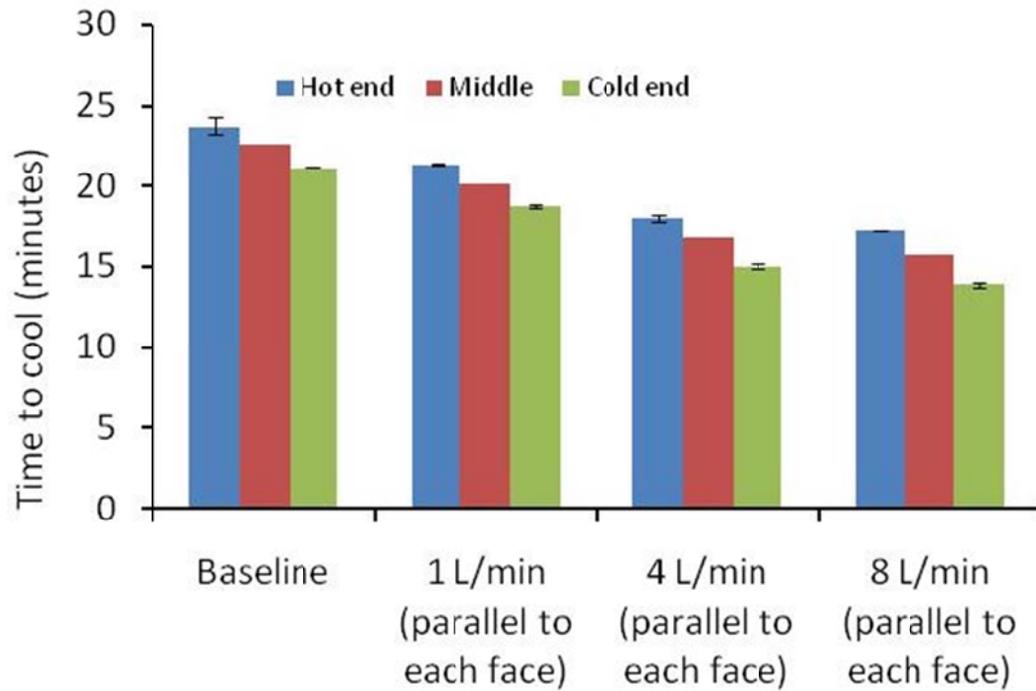
Fig. 33 "Time to cool" from $650^{o}C$ to $400^{o}C$ for helium-assisted (parallel flow mode) sand casting compared with baseline.

Table 23 Percent reduction in "time to cool" from $650^{o}C$ to $400^{o}C$ w.r.t. the baseline.

Helium flow rate (parallel to each face)	"Hot end" (farthest from helium supply)	Middle	"Cold end" (nearest to helium supply)
1 L/min	10.12	10.66	11.54
4 L/min	24.24	25.70	28.89
8 L/min	27.32	30.35	34.37

Table 24 shows the cooling rate in the temperature range where dendrites grow (i.e., 575°C to 560°C) for helium-assisted sand casting (parallel flow mode); Table 25 shows a similar analysis for the overall cooling rate; and Fig. 34 shows the calculated percent increase in cooling rate at the "cold end" for helium-assisted sand casting (parallel flow mode).

Table 24 Cooling rate in ^{o}C/s during dendrite growth.

Helium flow rate (parallel to each face)	"Hot end" (farthest from helium supply)	Middle	"Cold end" (nearest to helium supply)
1 L/min	0.25 (0.041) **[13.63%]**	0.33 **[37.5%]**	0.38 (0.009) **[52%]**
4 L/min	0.35 (0.014) **[59.09%]**	0.40 **[66.67%]**	0.50 (0.028) **[100%]**
8 L/min	0.39 (0.007) **[77.27%]**	0.48 **[100%]**	0.52 (0.001) **[108%]**

* Value in parenthesis shows the standard deviation and the bold number in brackets is the percent increase with respect to the baseline.

Table 25 Overall cooling rate in ^{o}C/sec.

Helium flow rate (parallel to each face)	"Hot end" (farthest from helium supply)	Middle	"Cold end" (nearest to helium supply)
1 L/min	0.20 (0.001) **[11.11%]**	0.21 **[10.53%]**	0.22 (0.001) **[10%]**
4 L/min	0.23 (0) **[27.77%]**	0.25 **[31.58%]**	0.28 (0) **[40%]**
8 L/min	0.24 (0) **[33.33%]**	0.27 **[42.10%]**	0.30 (0.004) **[50%]**

* Value in parenthesis shows the standard deviation and the bold number in brackets is the percent increase with respect to the baseline.
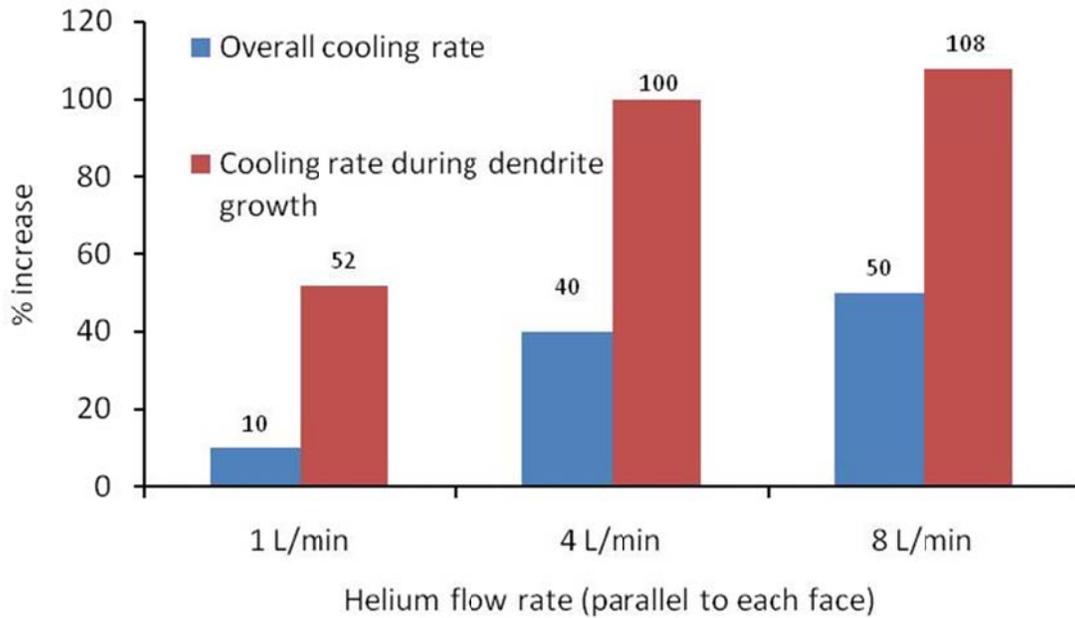
Fig. 34 Percent increase in cooling rate obtained at the cold end the of helium-assisted (parallel flow mode) castings.

Table 26 Percent variation in time to cool along the length of the plate.

1 L/min	12.24 %
4 L/min	16.30 %
8 L/min	19.49 %

It is observed that there is more variation in the magnitude of the "time to cool" along the length of the plate in helium-assisted sand casting with the parallel flow mode as compared to helium-assisted sand casting with the cross flow mode. Table 26 shows the calculated percent variation in "time to cool" along the length of the plate from the "hot end" to "cold end" for helium-assisted sand casting (parallel flow mode); and Fig. 35 shows the percent variation in "time to cool" along the length of the plate compared with the baseline.
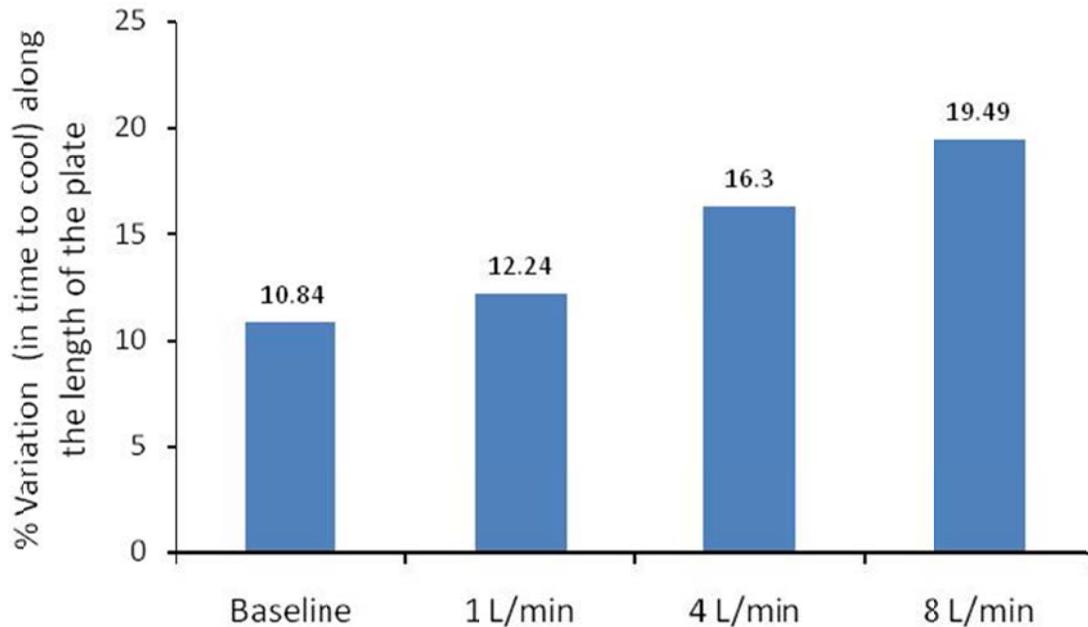
Fig. 35 Percent variation in time to cool along the length of the plate obtained by helium-assisted (parallel flow mode) casting compared with the baseline.

Since the variation in the "time to cool" along the length of the plate for the baseline is 10.84% is most probably caused by directional solidification, then the additional variation observed in the helium-assisted process is most probably caused by the way helium is introduced into the mold. Helium is supplied from only one end of the mold where it has its maximum cooling effect and it loses its effectiveness as it takes heat and moves along the length of the hot plate. A similar trend is observed in the cooling rate (Tables 24 and 25): higher cooling rates at the "cold end" which is nearest to the helium supply point and lower nearest to the "hot end" which is farthest from the helium supply point. This observation is important as it suggests that when helium is to be used in the parallel flow mode, then depending on the size and the design of the part to be cast, more than one input point for helium may be required for correct thermal management. Equally important, helium-assisted sand casting in a parallel supply mode may be used to induce localized cooling of the cast part by carefully designing the locations of the helium input points.

(d) Comparison of Helium-Assisted Sand Casting (Parallel Flow Mode) to Helium-Assisted Sand Casting (Cross Flow Mode in an Un-encapsulated Mold)

Figs. 36 and 37 show respectively the cooling rates during the dendrite growth regime (temperature range 575°C to 560°C), the overall cooling rates (temperature range 650°C to 400°C) for both flow modes together with the corresponding values for the baseline. Fig. 38 shows the percent reduction (with respect to the base line) in the time to cool for all the helium flow rates in all the modes of helium supply investigated in this work. It is evident from Figs. 36 and 37 that introducing helium into the mold by the parallel flow mode is more beneficial than by the cross flow mode. This may be attributed to the following reasons:

– In the parallel flow mode, helium is made to flow in a horizontal direction and so it drives a portion of the heat energy out through the sides of the mold thus leaving only a fraction of the total heat energy to be driven through the larger height of the mold. On the other hand, in the cross flow mode, helium flows normal to the casting and so it has to travel through the entire height of the mold where it picks up thermal energy, heats up, and loses some its effectiveness in cooling the casting.

– In the parallel flow mode helium makes better contact with the surface of the casting than in the cross flow mode.

– In the parallel flow mode there is a stream of helium moving parallel to each one of the two surfaces of the plate thus making the total helium supply double that used in the cross flow mode.
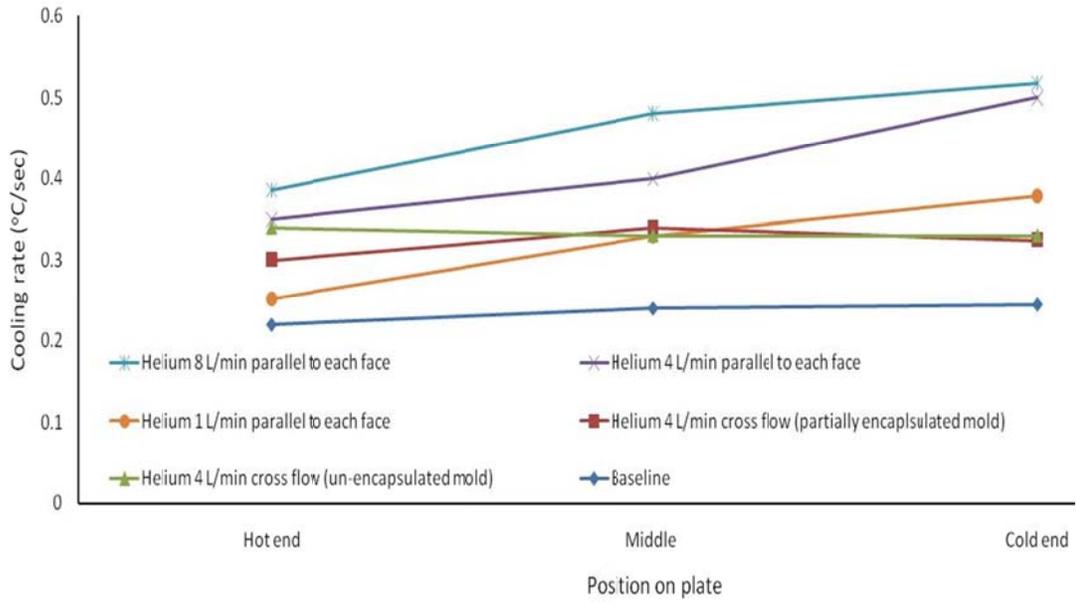
Fig. 36 Cooling rate (during dendrite growth) along the length of the plate.
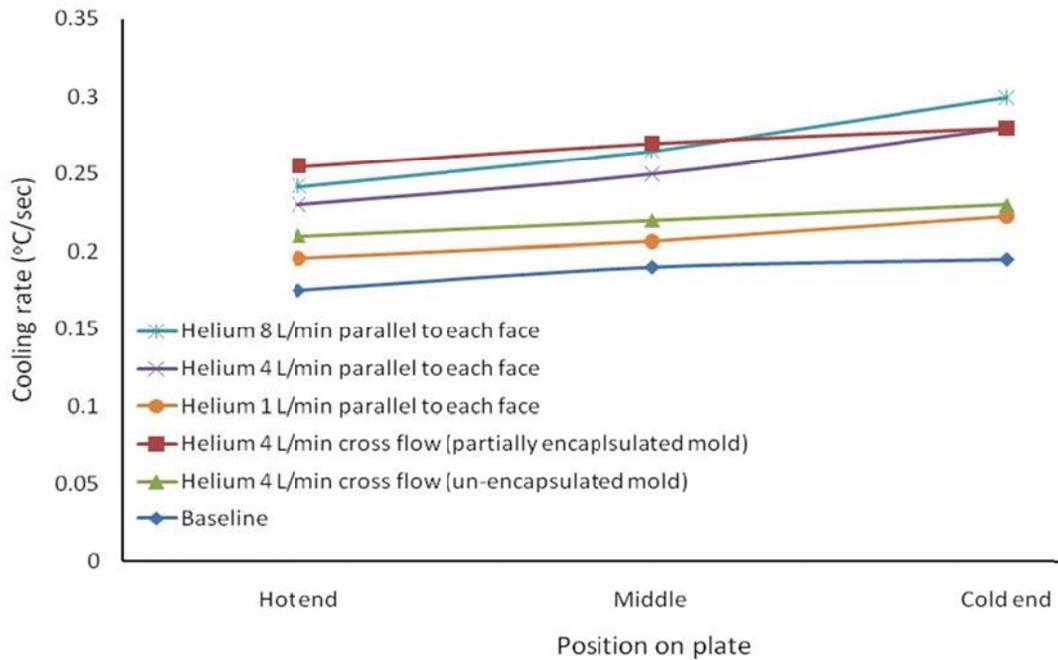
Fig. 37 Overall cooling rate along the length of the plate.
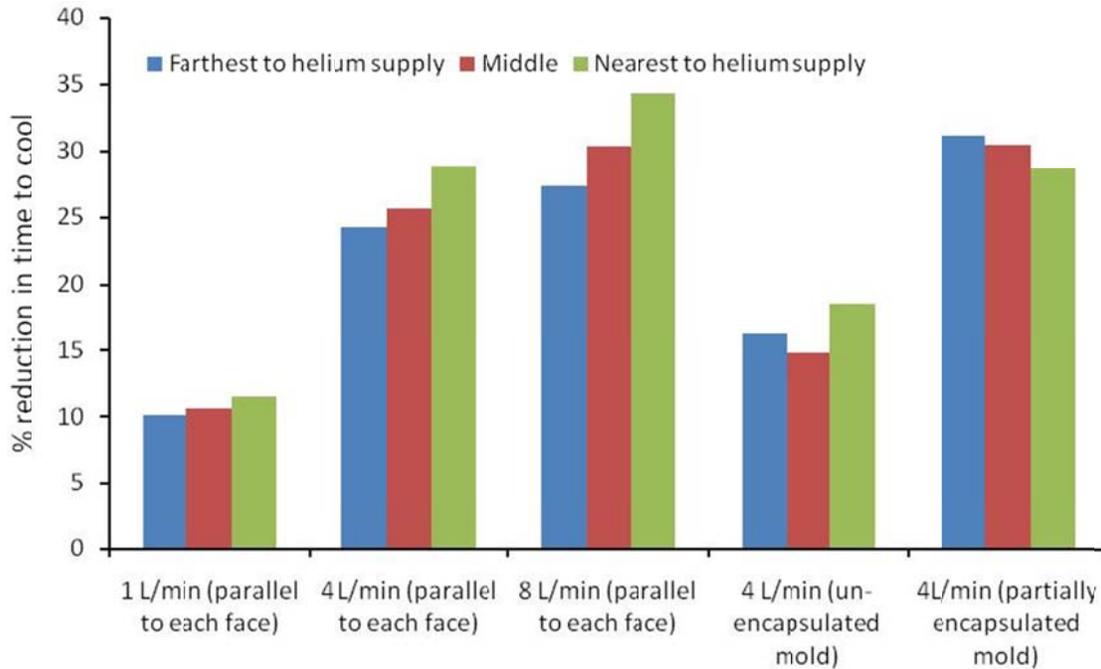
Fig. 38 Percent reduction in the time to cool from 650°C to 400°C (w.r.t.) baseline.

5.3 Surface Roughness Analysis

Table 27 presents R_a and R_z values for helium-assisted sand casting compared with the baseline and Fig. 39 shows a graphical comparison of the measured R_a values for all the castings. Table 27 shows that partial encapsulation of the mold results in the highest surface roughness. This is attributed to the more direct impingement of helium on the solidifying surface. For all the other flow modes the surface condition is not much different from that of the baseline.

Table 27 Surface roughness for helium-assisted sand casting compared with baseline.

Surface roughness (μm)	Baseline	4 L/min partially encapsulated mold	4 L/min un-encapsulated mold	1 L/min parallel to each face	4 L/min parallel to each face	8 L/min parallel to each face
R_a	13.99 (1.6)	16.51 (2.8)	12.35 (0.96)	13.65 (1.35)	13.81 (1.65)	14.24 (1.03)
R_z	79.34 (10.85)	88.72 (12.84)	70.46 (6.48)	77.34 (8.45)	75.85 (8.82)	80.2 (6.99)

*Value in parentheses shows the standard deviation.
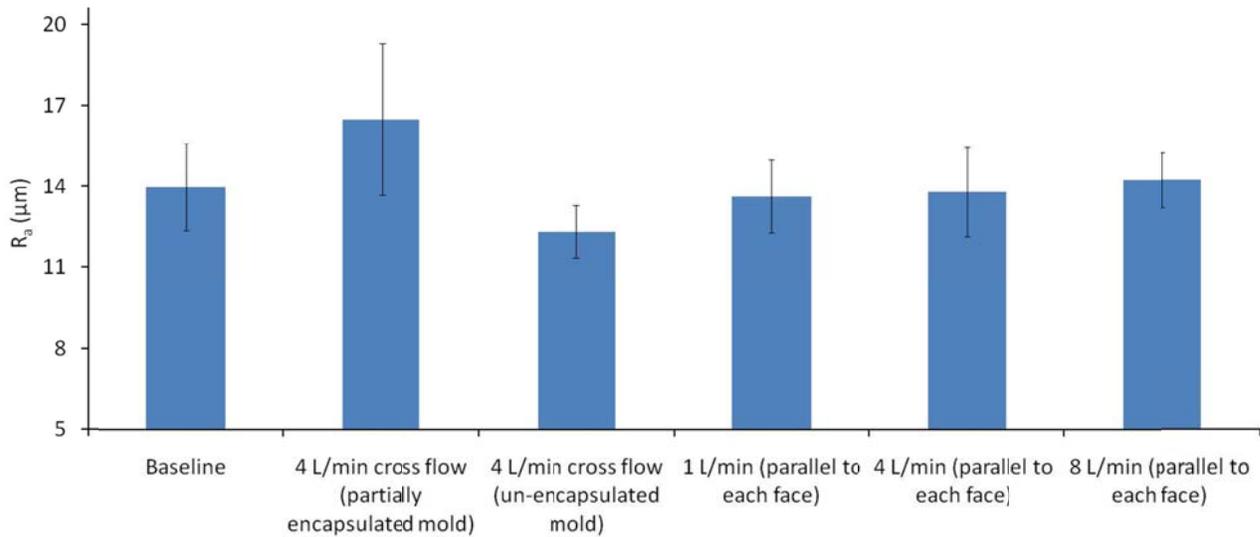
Fig. 39 Comparison of the measured R_a values for all the castings.

5.4 Room Temperature Tensile Properties

(a) Baseline

Table 28 presents the summary of the results for room temperature tensile properties of the plate casting in the T6 heat treated condition for the baseline.

Table 28 Room temperature tensile properties of the plate casting in the T6 heat treated condition for the baseline.

Ultimate tensile strength in ksi	31.65 (1.30)
Yield strength at 0.2 pct. offset in ksi	26.04 (1.77)
Modulus of elasticity x 100 in ksi	101.69 (4.79)
Elongation in pct.	1.11 (0.19)

* Value in parentheses shows the standard deviation.

(b) Helium-Assisted Cross Flow Mode

Table 29 presents the room temperature tensile properties of the plate casting in the T6 heat treated condition for the helium-assisted sand casting (cross flow mode).

Table 29 Room temperature tensile properties (as T6 heat treated) for helium assisted (cross flow) castings at helium flow rate of 4 L/min.

Room temperature tensile properties	Partially encapsulated mold	Un-encapsulated mold
Ultimate tensile strength in ksi	27.07 (2.44)	30 (2.58)
Yield strength at 0.2 pct. offset in ksi	21.29 (3.03)	24.21 (3.19)
Modulus of elasticity × 100 in ksi	95.8 (8.19)	97.25 (6.39)
Elongation in pct.	1.06 (0.14)	1.09 (0.12)

* Value in parentheses shows the standard deviation.

Figs. 40 and 41 show a comparison of the room temperature tensile strength of the helium-assisted sand cast plates with those of the baseline castings. The results show that the room temperature tensile properties have deteriorated with helium-assist. This is due to the increased level of porosity observed in helium-assisted casting with the cross flow mode.
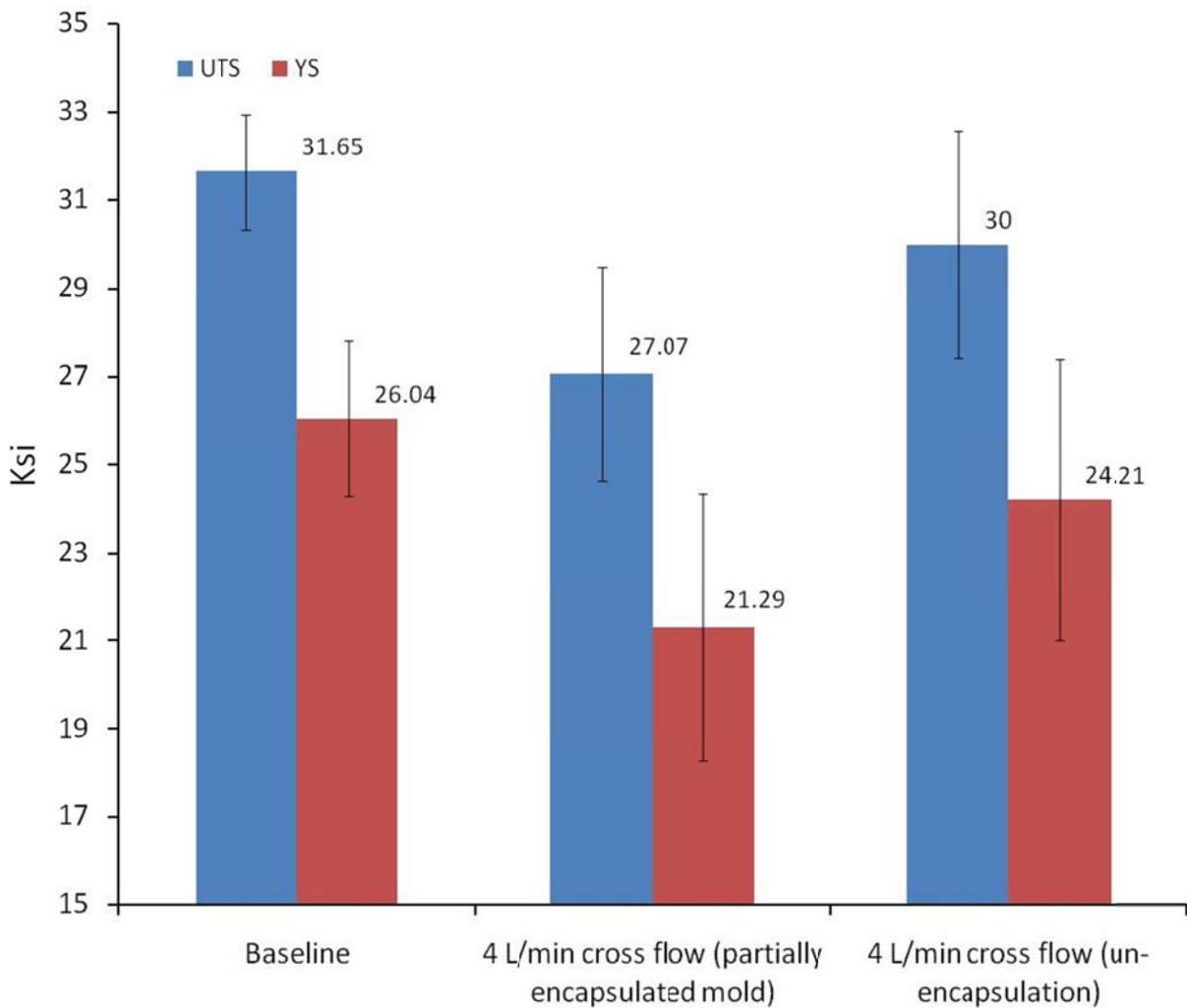
Fig. 40 Ultimate and yield strengths of helium-assisted (cross flow) T6 heat treated castings compared with the baseline.
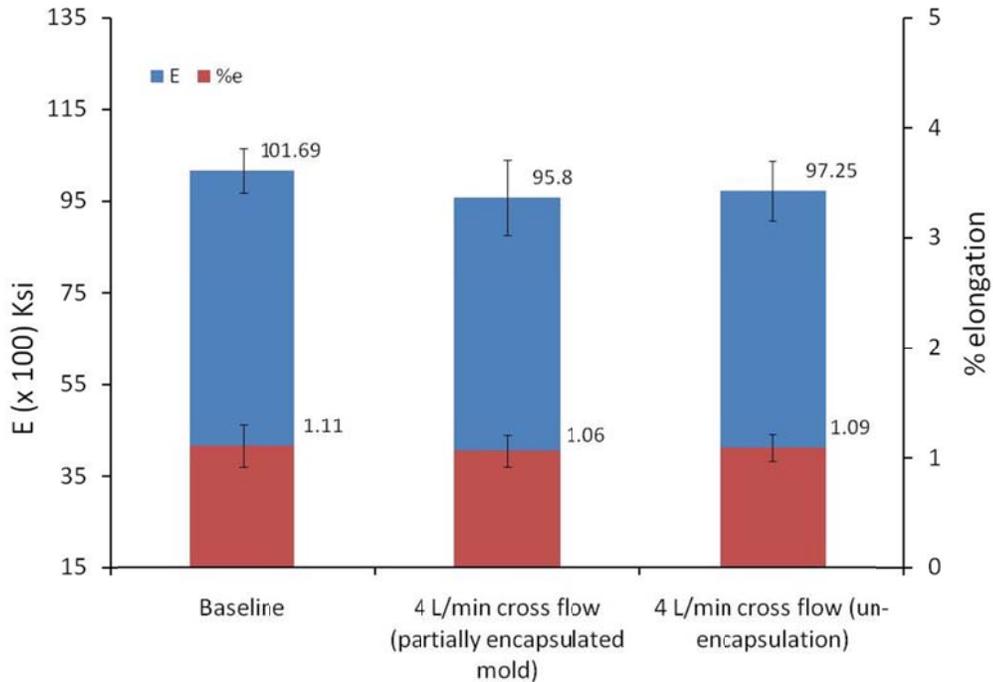
Fig. 41 Modulus of elasticity and elongation of helium-assisted (cross flow) castings compared with the baseline.

(c) Helium-Assisted Parallel Flow Mode

Table 30 presents the average room temperature tensile properties of the plate casting in the T6 heat treated condition for the helium-assisted sand casting (parallel flow mode). Fig. 42 shows the average room temperature ultimate and yield strengths and Fig. 43 shows the average modulus of elasticity and elongation of all the plate castings.

Table 30 Average room temperature tensile properties (as T6 heat treated) for helium assisted (parallel flow) castings compared with baseline.

Property	1 L/min parallel to each face	4 L/min parallel to each face	8 L/min parallel to each face
Ultimate tensile strength in ksi	34.31 (1)	38.75 (1.67)	38.13 (1.83)
Yield strength at 0.2 pct. offset in ksi	28.25 (0.89)	35 (1)	32.92 (1.16)
Modulus of elasticity × 100 in ksi	105.23 (5.38)	106.24 (3.23)	118.07 (8.27)
Elongation in pct.	1.16 (0.17)	0.88 (0.2)	1.05 (0.36)

* Value in parentheses shows the standard deviation.
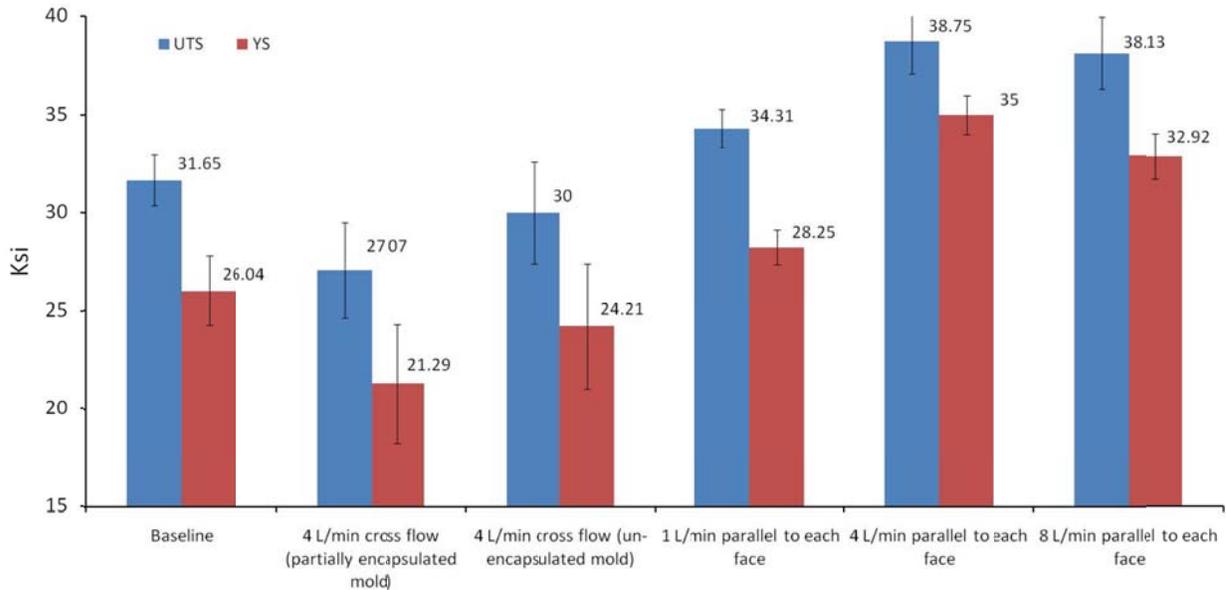
Fig. 42 Average ultimate and yield strengths of all the plate castings.
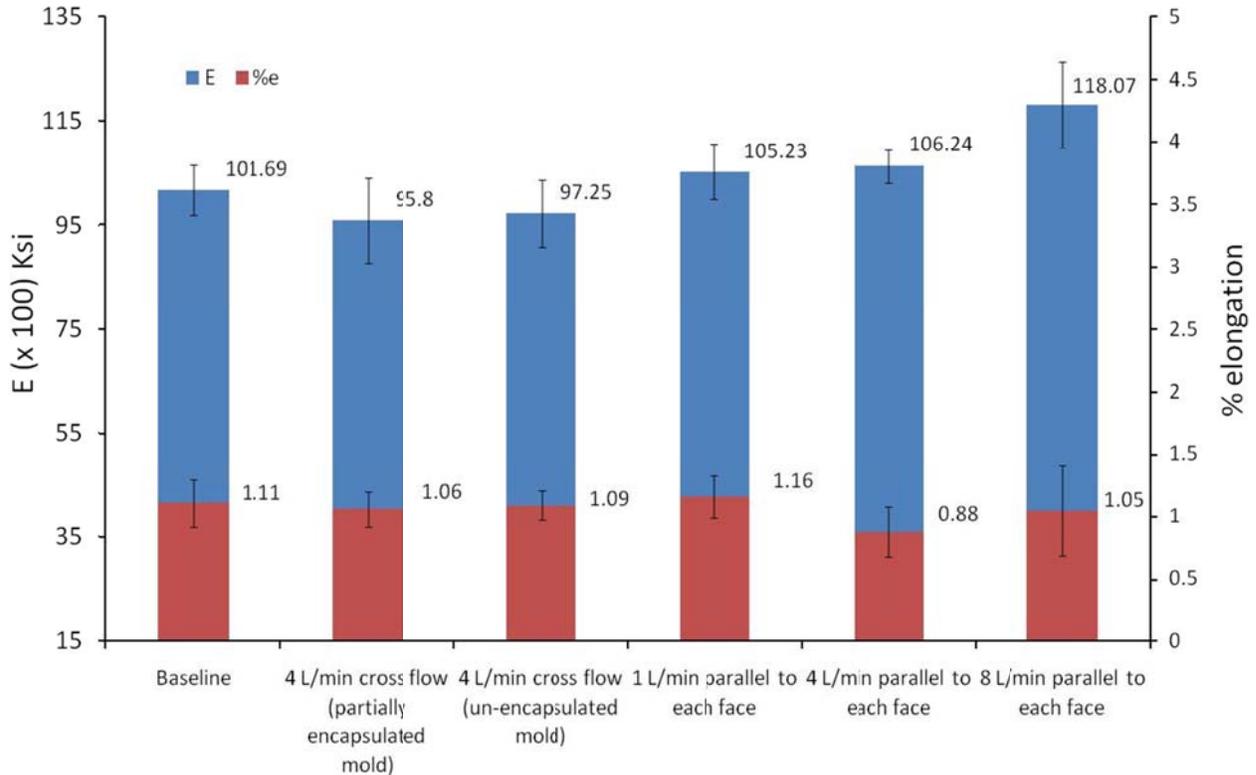
Fig. 43 Average modulus of elasticity and elongation of all the plate castings.

It is clear from Figs. 42 and 43 that the room temperature tensile properties obtained with helium-assisted sand casting in the cross flow mode are inferior to those of the baseline, for this reason the following discussion will be limited to the helium-assisted sand casting with parallel flow. The room temperature tensile properties obtained with helium-assisted sand casting in the parallel flow mode are superior to those of the baseline: At a helium flow rate of 4 L/min parallel to each face of the plate the yield strength increases from 26 ksi to 35 ksi, the ultimate tensile strength increases from 32 ksi to 39 ksi and there is no significant decrease in elongation and modulus of elasticity. It is found that there is no significant enhancement in room temperature tensile properties at helium flow rates higher than 4 L/min parallel to each face of the plate. It is also found that there is a small gradient in the magnitude of ultimate tensile strength and yield strength from a slightly lower value at the hot end of the plate to a slightly higher value at the cold end: the

average ultimate tensile strength is 2 ksi higher at the cold end than at the hot end and the average yield strength is 1 ksi higher at the cold end than at the hot end.

5.5 Microstructure Analysis

The aspects of microstructure of interest in this work are (a) the porosity, (b) the grain size, and (c) the dendrite arm spacing.

(a) Porosity

Baseline - Fig. 44 shows micrographs representative of the microstructure and distribution of pores in the baseline castings. The average volume percent of pores is 0.52%.
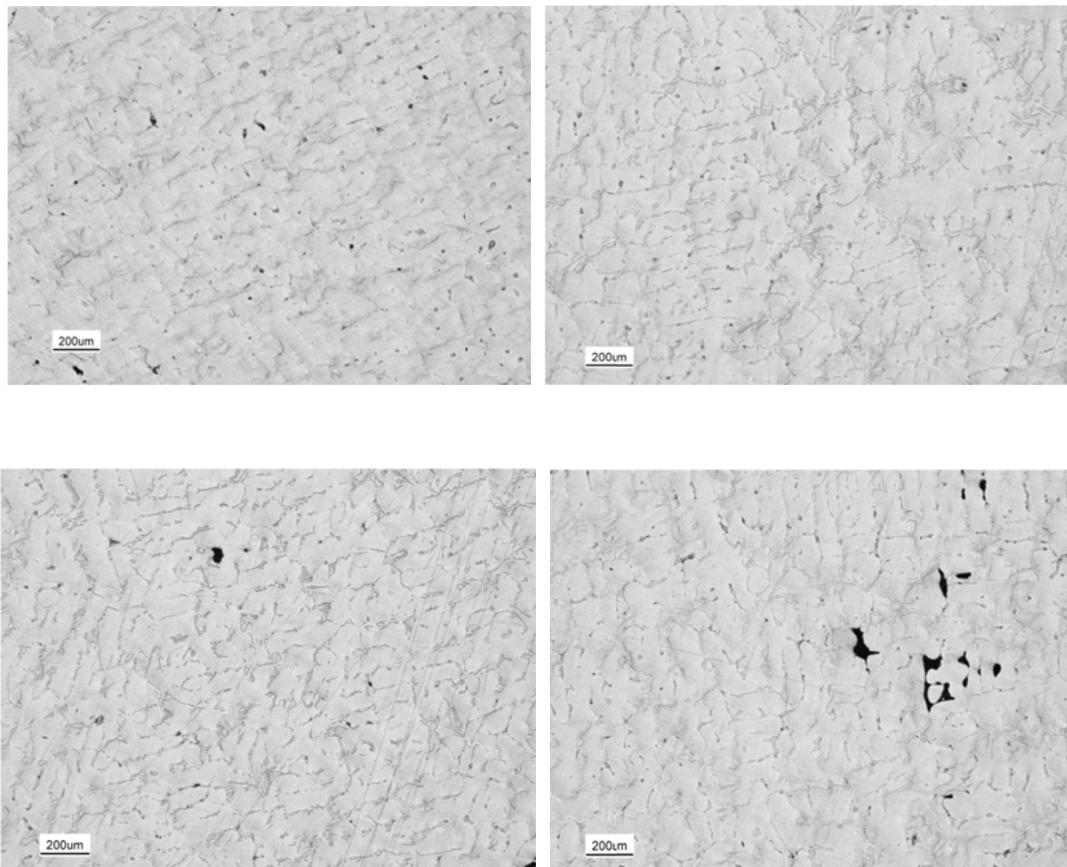
Fig. 44 Microstructure of baseline casting.

Helium-assisted cross flow mode - As observed in Table 31, more pores are present in the helium-assisted (cross flow mode) castings than in the baseline castings. Fig. 45 shows micrographs representative of the microstructure and distribution of pores in the helium-assisted (cross flow) sand castings. It is clear that not only the average area of porosity is increased in the helium-assisted (cross flow) sand casting compared to the baseline, but also the size of the average pore is increased – more so in the partially encapsulated mold than in the un-encapsulated mold.

Table 31 Porosity (%) in helium-assisted (cross flow) castings compared with baseline.

Baseline	4 L/min Partially encapsulated mold	4L/min un-encapsulated mold
0.52	1.86	0.72
(0.52)	(1.42)	(0.59)

* Value in parenthesis shows the standard deviation.
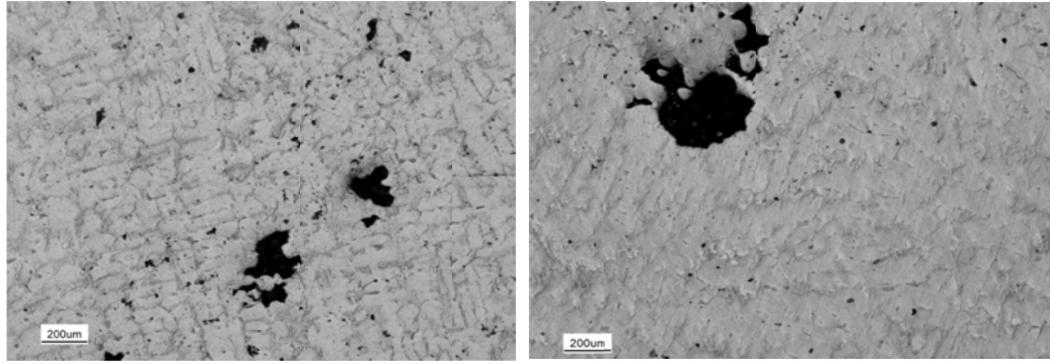
(a)
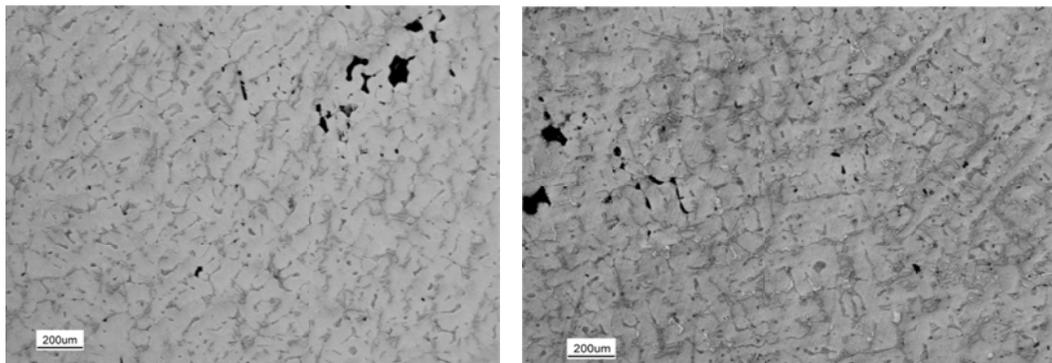
(b)

Fig. 45 Microstructure of helium-assisted (cross flow) castings at 4 L/min helium flow rate (a) in partially encapsulated mold (b) in an un-encapsulated mold.

Helium-assisted parallel flow mode - As observed in Table 32, less pores are present in the helium-assisted (parallel flow mode) castings than in the helium-assisted (cross flow mode) castings and also less than in the baseline. Fig. 46 shows micrographs representative of the microstructure and distribution of pores in the helium-assisted (parallel flow) sand castings.

Table 32 Porosity (%) in helium-assisted (parallel flow) castings compared with baseline.

Baseline	1 L/min parallel to each face	4 L/min parallel to each face	8 L/min parallel to each face
0.52 (0.52)	0.39 (0.35)	0.33 (0.25)	0.41 (0.41)

*Value in parentheses shows the standard deviation.
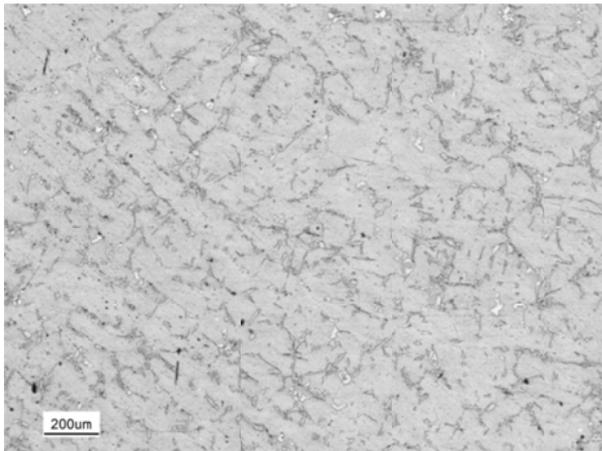
(a) Helium supply: 1 L/min parallel to each face.
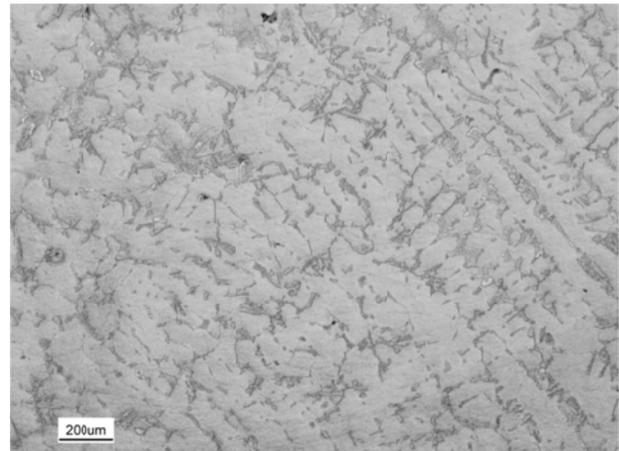
(b) Helium supply: 4 L/min parallel to each face.
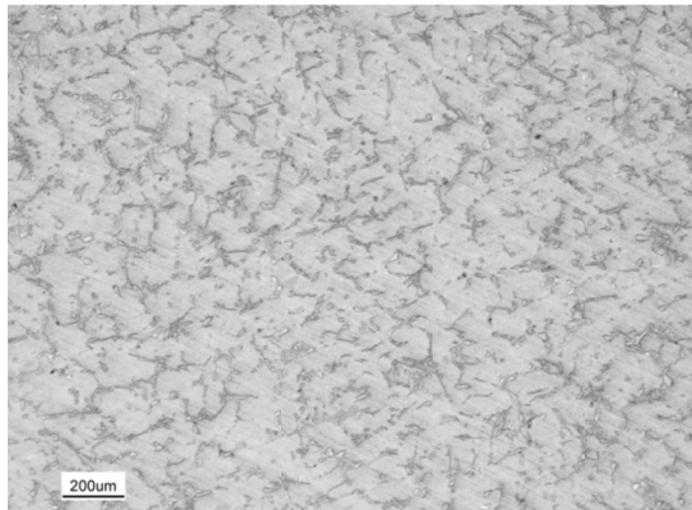
(c) Helium supply: 8 L/min parallel to each face.

Fig. 46 Microstructure of helium-assisted sand castings (parallel flow mode).

(b) Grain Size

Baseline - Fig. 47 shows representative micrographs of the grain structure of the baseline castings. The mean lineal intercept length method gives a grain size = 2.15 mm.
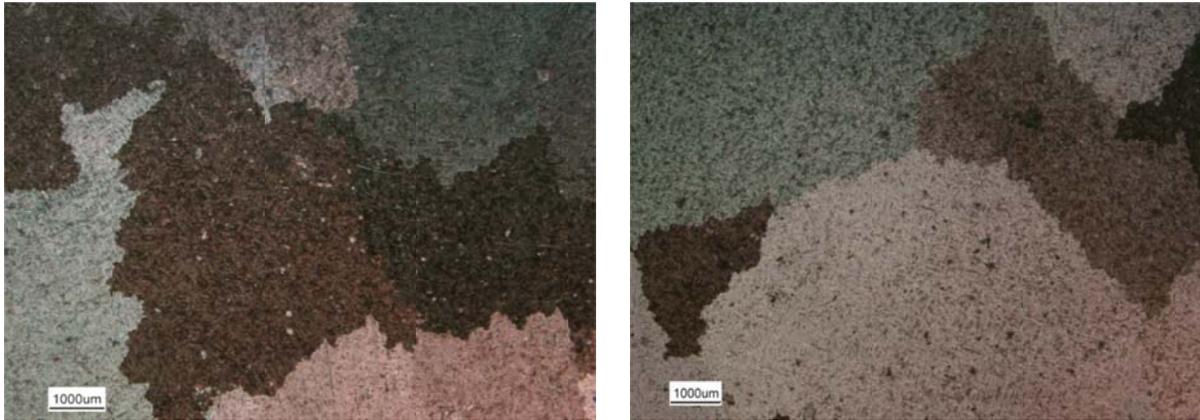
Fig. 47 Grain structure of the baseline casting (viewed with polarized light).

Helium-assisted cross flow mode - Table 33 presents the grain size for helium-assisted sand castings (cross flow mode) compared with the baseline, and Fig. 48 shows representative micrographs of the grain structure.

Table 33 Grain size (mean lineal intercept length, mm) of helium assisted (cross flow mode) castings compared with the baseline.

Baseline	4 L/min partially encapsulated mold	4 L/min un-encapsulated mold
2.15	1.91	1.81
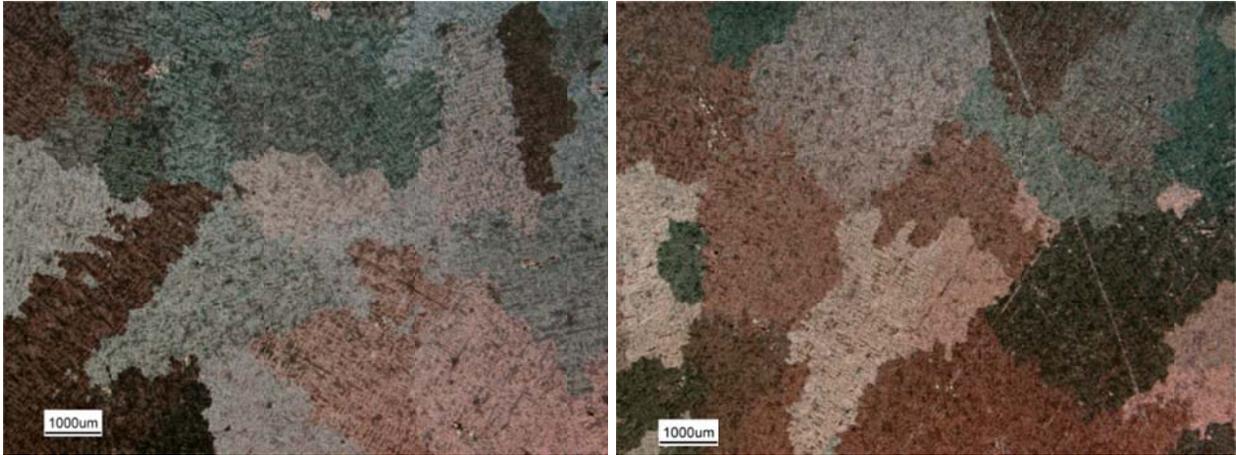
<div align="center">(a) Partially encapsulated sand mold.   (b) Un-encapsulated sand mold.</div>

Fig. 48 Micrographs of helium-assisted castings (cross flow mode, helium flow rate 4 L/min, viewed with polarized light).

Helium-assisted parallel flow mode - Table 34 presents the grain size for helium-assisted sand castings (parallel flow mode) compared with the baseline, and Fig. 49 shows representative micrographs of the grain structure.

Table 34 Grain size (mean lineal intercept length, mm) of helium-assisted (parallel flow mode) castings compared with the baseline.

Baseline	1 L/min parallel to each face	4 L/min parallel to each face	8 L/min parallel to each face
2.15	1.90	1.54	1.64

(a) Helium supply: 1 L/min
parallel to each face.

(b) Helium supply: 4 L/min
parallel to each face.
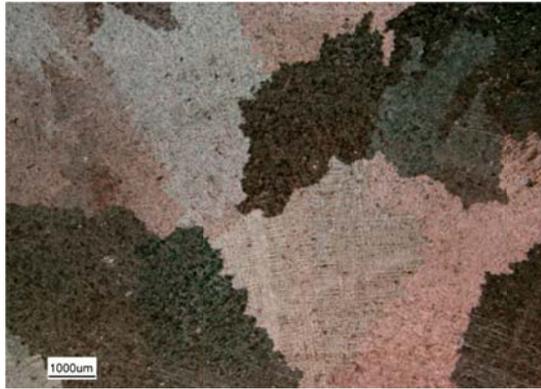
(a) Helium supply: 8 L/min
parallel to each face.

Fig. 49 Micrographs of helium-assisted castings (parallel flow mode viewed with polarized light).

(c) Secondary Dendrite Arm Spacing (SDAS)

Table 35 presents the average SDAS values for all the plate castings.

Table 35 Average SDAS in µm of helium-assisted castings compared with the baseline.

Baseline	4 L/min cross flow mode (partially encapsulated mold)	4 L/min cross flow mode (un-encapsulated mold)	1 L/min parallel to each face	4 L/min parallel to each face	8 L/min parallel to each face
60.06 (5.5)	50.7 (5.47)	51.07 (5.29)	52.33 (5.68)	46.04 (4.05)	47.99 (4.61)

    * Value in parenthesis shows the standard deviation.

Figs. 50-53 present a summary of the microstructure analysis. It is clear from these Figs. that the grain size and the SDAS are refined in the helium-assisted castings. However more porosity is obtained with the cross flow mode compared to the parallel flow mode. It is also clear from Fig. 50 that encapsulation results in more porosity.
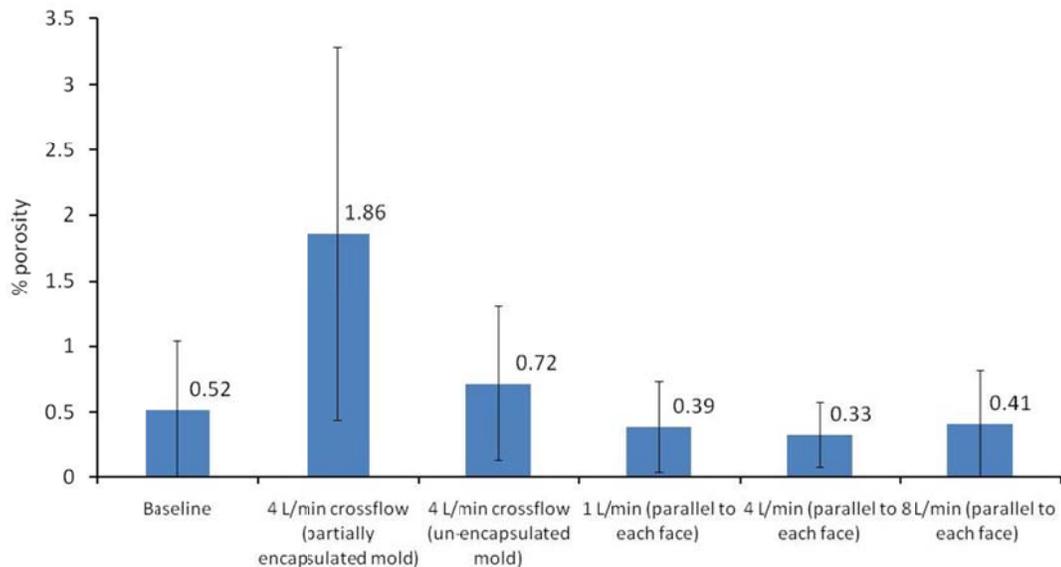
Fig. 50 Comparison of percent porosity for all the castings.
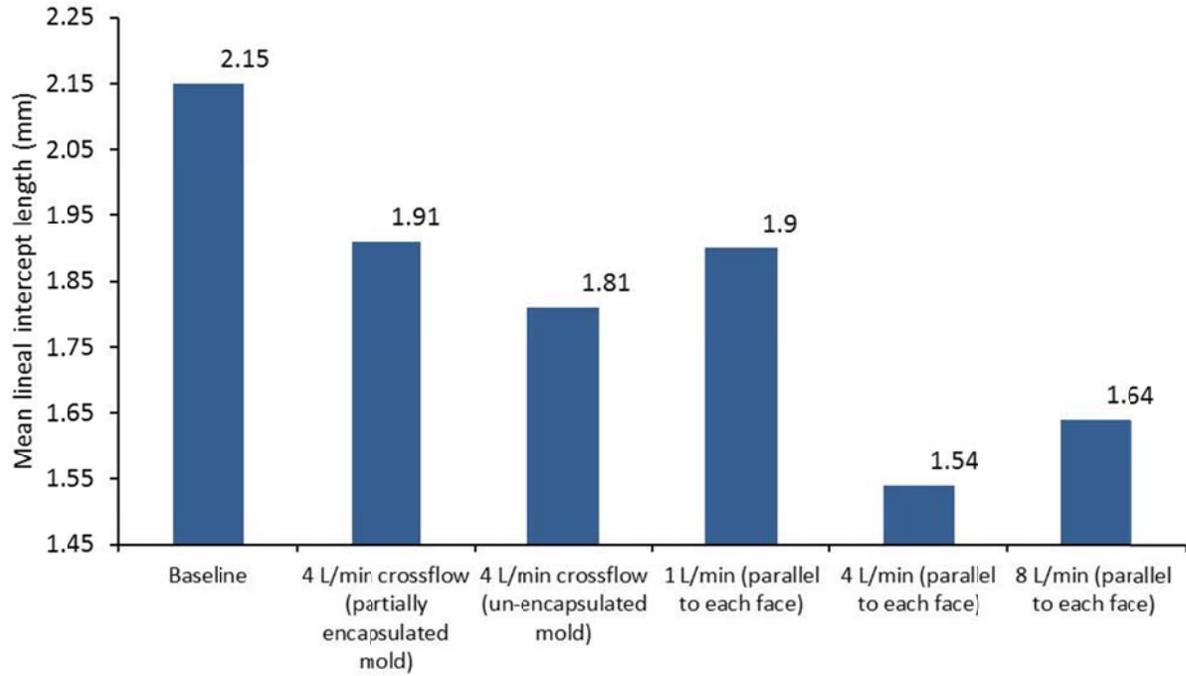
Fig. 51 Comparison of grain size for all the castings.
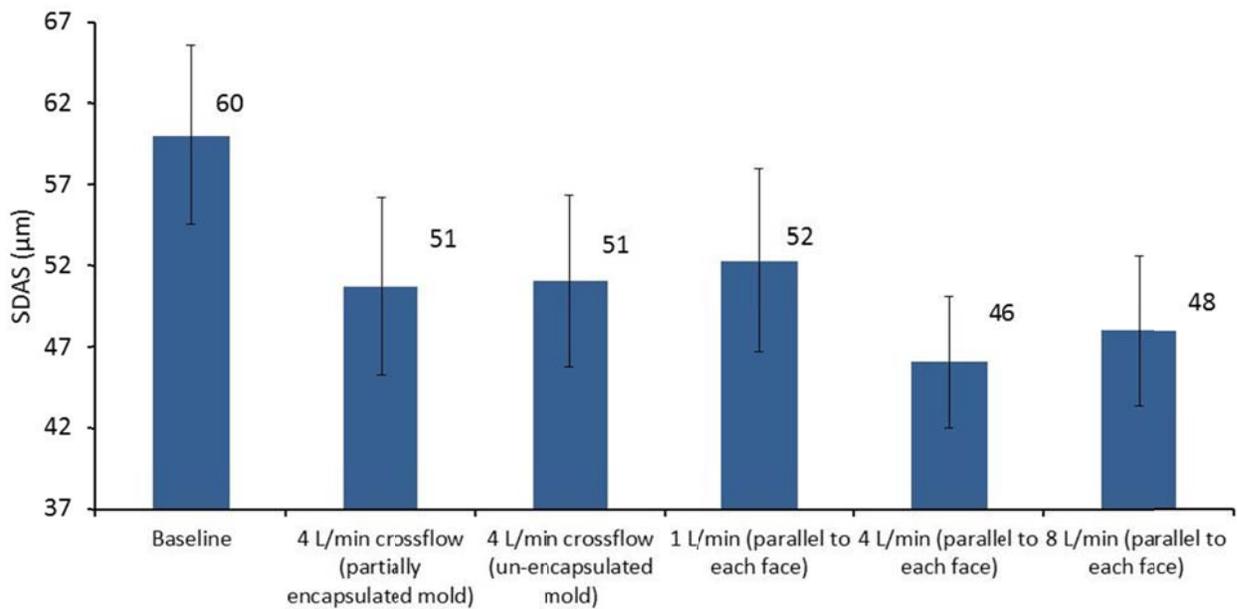
Fig. 52 Comparison of SDAS for all the castings.
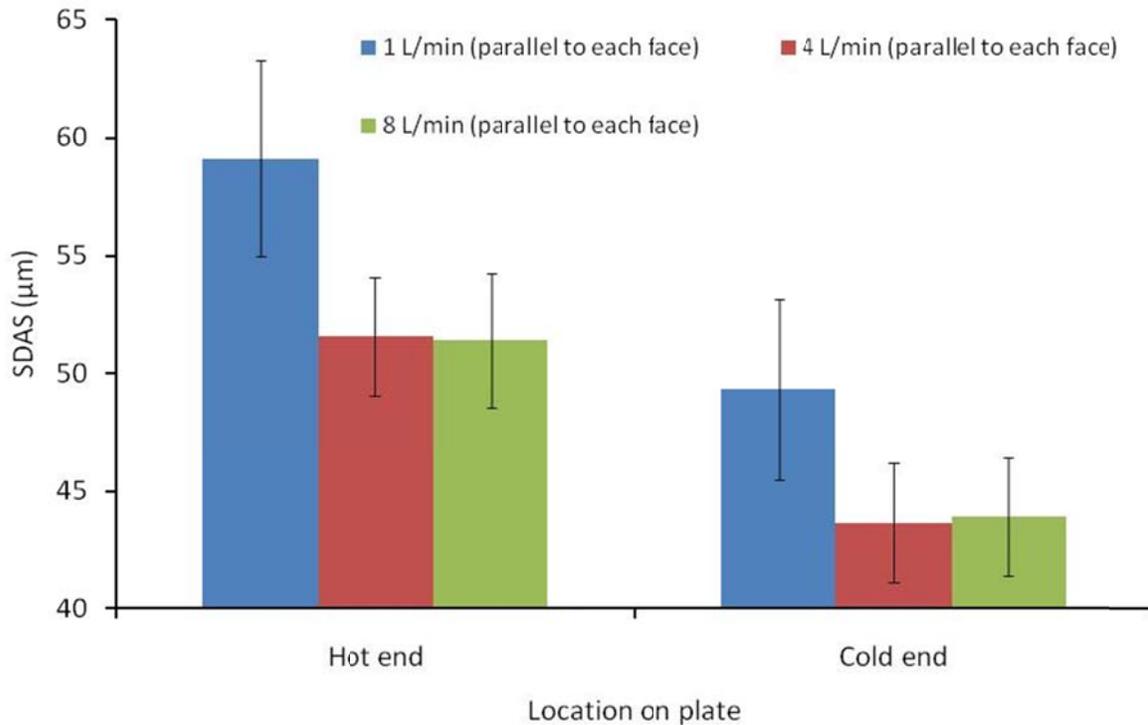
Fig. 53 Variation in SDAS along the length of the plate as observed in helium assisted (parallel flow) castings.

5.6 Cost Analysis

Apparently it may seem that employing helium would add cost to the "conventional" sand casting process; however it must be realized that castings made with the helium-assisted (parallel flow mode) process have better yield strength, and this increased yield strength translates into a reduction in section size, which in turn translates into a smaller casting weight and material savings. The casting weight is related to labor cost and total weight poured [44], therefore any reduction in casting weight translates into a reduction in alloy cost, labor cost and melting cost. The following analysis weighs the cost of applying helium against the reduction in direct cost, specifically alloy cost and labor cost.

$$Alloy\ cost = casting\ weight\ \times unit\ price\ of\ alloy \qquad (5)$$

$$Labor\ cost = labor\ time\ \times wage\ rate \qquad (6)$$

In order to estimate the labor time, we use Eqs. (7) and (8) [44].

$$Mold\ time\ (\text{min}) = 6.8 \times CW + 14 \tag{7}$$

$$Finishing\ time\ (\text{min}) = 5.2 \times CW \tag{8}$$

Where CW (casting weight) is in kg.

First, it is important to consider the following:

- The unit cost of the alloy may not be constant and quantity discounts result in variation in unit price for the same market conditions. This would be dictated by inventory levels maintained by individual companies.

- Alloy cost forms only one aspect of material cost.

- Labor costs are difficult to estimate and very little data is available [44].

- Labor wage rates may be different for different functions and will vary from company to company.

- Different companies may use different costing methods.

For these reasons, the analysis presented in this work is not absolute but rather it is relative and compares the helium-assisted (parallel flow mode) sand casting process to a relevant baseline. The parallel flow mode is chosen for the cost analysis because it shows the largest improvement in yield strength compared to the base line.

Tables 36 and 37 present information that is used in the cost analysis and Table 38 shows the results.

Table 36 Dataset used for cost analysis.

Density of aluminum 319 (g/cc)	2.79 [45]
Unit price of alloy ($/lb)	1.85 [46]
Wage rate ($/hr)	25 [47]
Helium price ($ per 300 cu ft cylinder)	89.05 [48]

Table 37 Results obtained in this project that are used for cost analysis.

	Baseline	Helium 1 L/min parallel to each face (Total: 2 L/min)	Helium 4 L/min parallel to each face (Total: 8 L/min)	Helium 8 L/min parallel to each face (Total: 16 L/min)
Yield strength (ksi)	26.04	28.25	35	32.92
Casting volume (cc)	446.70	411.71	332.37	353.40
Weight of casting (kg)	1.25	1.15	0.93	0.99
Time of helium application (min)	0	21.32	17.97	17.24

Table 38 Results of the cost analysis.

	Baseline	Helium 1 L/min parallel to each face (Total: 2 L/min)	Helium 4 L/min parallel to each face (Total: 8 L/min)	Helium 8 L/min parallel to each face (Total: 16 L/min)
Alloy cost factor ($)	5.10	4.69	3.79	4.04
Labor cost factor ($)	12.08	11.58	10.48	10.78
Helium cost factor ($)	0	0.45	1.51	2.89
Total cost factor ($)	17.18	16.72	15.78	17.71

The cost analysis shows that the enhanced properties obtained by the use of helium can result in net cost reductions making the technique economically feasible up-to at least 4 L/min (parallel on each face of the plate). It is worth mentioning that the analysis performed here is based on experiments in which helium is supplied over the temperature range between 650°C to 400°C. More control over the process may allow shortening the time of helium use and thus reducing the cost even further.

Because of its complexity, the cost of melting warrants further analysis. Melting is the most energy intensive step of the metal casting process and accounts for 55% of the total casting cost [49]. Although the actual cost of melting depends on the particular melting practice and the production activity, nevertheless, a comparison between melting costs for the helium-assisted sand casting process and the baseline is useful. The following equations can be used to estimate the cost of melting:

$Energy\ (heat)\ cost\ factor =$
$Total\ heat\ energy\ taken\ by\ alloy\ \times unit\ price\ of\ heat\ energy$ $\qquad\qquad$ (9)

$Total\ heat\ energy\ taken\ by\ alloy =$
$total\ weight\ poured$[20] $\times$
$total\ heat\ content\ of\ the\ alloy\ per\ unit\ weight\ (thermal\ capacity\ of\ alloy)$ $\qquad$ (10)

$unit\ price\ of\ heat\ energy = \frac{unit\ price\ of\ electricity}{furnace\ efficiency}$ $\qquad\qquad$ (11)

Total weight poured is [44].

$Total\ weight\ poured = casting\ weight\ \times \frac{1}{(1-casting\ scrap\ rate)} \times \frac{1}{(yield)} \times \frac{1}{(1-melt\ loss)} \times$
$\frac{1}{(1-finishing\ scrap\ rate)}$ $\qquad\qquad$ (12)

Since casting scrap rate and finishing scrap rate are not likely to be affected by the use of helium since no adverse effects are seen in the castings made with helium assistance in the

---

[20] Total weight poured and total weight melted, are considered approximately equal.

parallel flow mode and also the use of helium does not affect melt losses; therefore these terms can be considered constant for both the baseline and the helium- assisted processes. Thus Eq. (12) is reduced to

$$Total\ weight\ poured = casting\ weight\ \times \frac{1}{yield} \times constant \qquad (13)$$

For simplicity, we take the constant to be 1 in our calculations as specific values are very much dependent on the specific shop practices. Additionally, taking the efficiency term in Eq. (11) to be 1 and using the data in Table 39, Table 40 is produced to show the energy cost factor.

Table 39 Dataset used for calculating energy cost factor.

Yield (%) [21]	24
Thermal capacity of aluminum at ~850°C, BTU/lb (KJ/Kg)	550 [21] (1278.42)
Unit price of energy[22] (cents/KWhr)	13.29 [50]

Table 40 Energy cost factor for helium-assisted (parallel flow) sand casting compared with the baseline.

	Baseline	Helium 1 L/min parallel to each face (Total: 2 L/min)	Helium 4 L/min parallel to each face (Total: 8 L/min)	Helium 8 L/min parallel to each face (Total: 16 L/min)
Energy cost factor ($)	0.25	0.23	0.18	0.21

---

[21] Measured by considering the volume of the plate and the volume of the total casting (without filters). Assumed constant for all the analyses presented here.
[22] Average retail price of electricity to industrial customer in Massachusetts, USA during Nov. 2010.

There is one more important benefit gained by using helium in the sand casting process which can result in further cost saving: A reduction in homogenization time (during heat treatment) brought about by the refined SDAS.

The segregation index (δ) is given by [29]

$$\delta = exp\left[-\frac{\pi^2 D t}{L^2}\right]$$ (14)

Where D is the diffusion coefficient in m^2/s, t is the homogenization time in seconds and L is the secondary dendrite arm spacing in meters. Using a diffusion coefficient of 4.74 × 10^{-14} m^2/s for copper in aluminum at 504°C [51]) and the average SDAS values shown in Table 35, we calculate the homogenization times required to achieve the various segregation indices as shown in Fig 54. Concomitant cost savings can be calculated based on these shorter homogenization times.
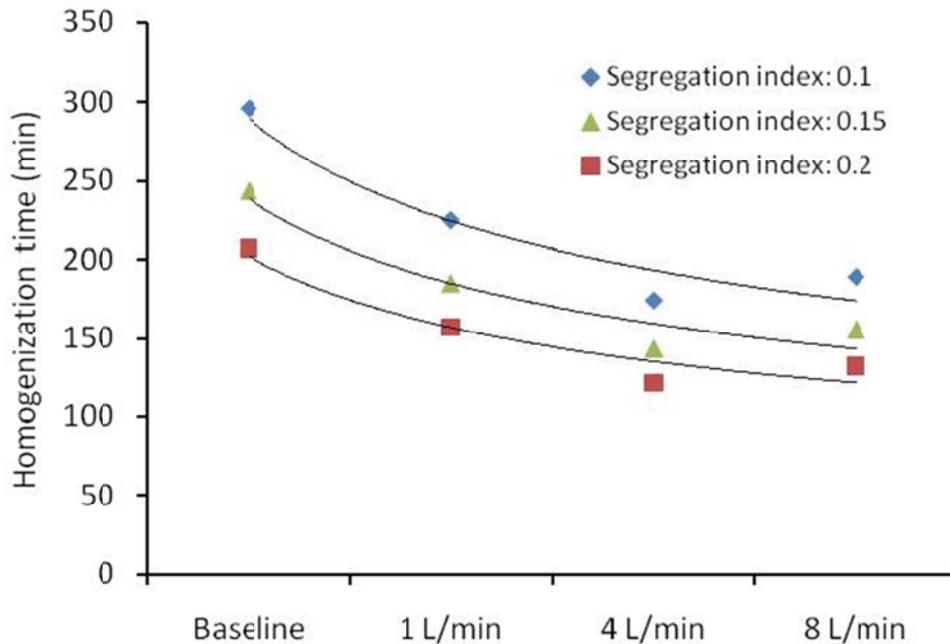
Fig. 54 Homogenization times required to achieve various segregation indices.

5.7 Performance Index and Determination of the Optimum Flow Rate

It is clear from the results that beyond a certain flow rate, the benefits (i.e., the increase in cooling rate, refinement of the microstructure, improvement of the tensile properties, etc.) begin to show diminishing returns with increasing helium flow rate. Therefore, it is important to determine the optimum helium flow rate. Since it is an improved yield strength of the casting that is the targeted outcome of the helium-assisted process (and since this will occur at a cost penalty), then the optimum flow rate would be the one that would give maximum increase in yield strength with respect to the baseline at the minimum flow rate of helium. Based on this logic, a performance index for the process is defined as given in Eq. (15)

$$Performance\ index = \frac{\%\ increase\ in\ yield\ strength\ w.r.t\ the\ baseline}{Helium\ flow\ rate}$$

(15)

Table 41 shows the % increase in yield strength with respect to the baseline and the corresponding performance index for the flow rates employed in this work and Fig. 55 shows a plot of the performance index vs. helium flow rate.

Table 41 Performance indices.

Helium flow rate (parallel to each face)	% increase in yield strength w.r.t the baseline	Performance index
1	0.085	0.085
4	0.344	0.086
8	0.264	0.033
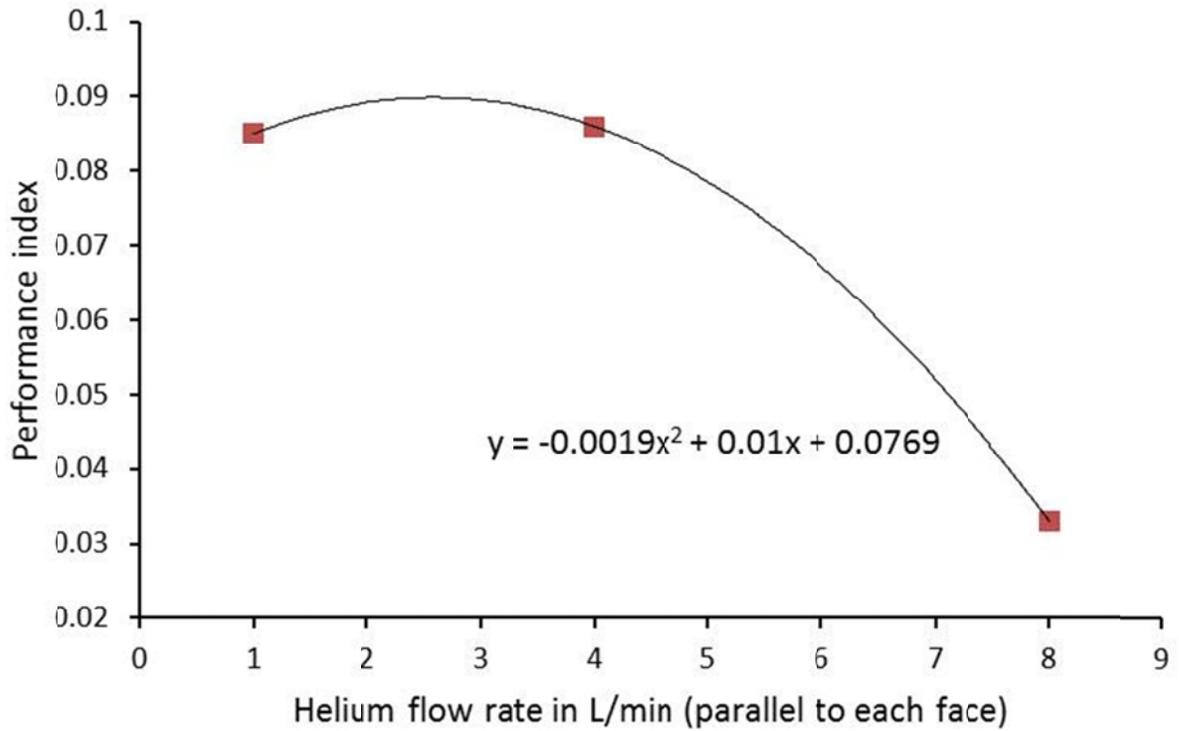
Fig. 55 Performance index vs. helium flow rate.

The maxima of the curve shown in Fig. 55 occurs at a flow rate of 2.63 L/min parallel to each face and is thus the optimum flow rate beyond which the relative advantage of improved yield strength compared to the baseline casting would begin to diminish.

6. Conclusions and Recommendations for Future Work

6.1 Conclusions

1. Helium-assisted sand casting with a cross flow of helium in either an un-encapsulated mold or a partially encapsulated mold is not viable for making castings with thin sections as it increases porosity in the cast component. Partial encapsulation also seems to cause entrapment of the process gases in the cast component.

2. Helium-assisted sand casting with a parallel flow of helium is viable for making castings irrespective of part thickness. The only additional required equipment for the process is a "supply plate". If this plate is made to be part of the mold during the molding process, then clamping and sealing the plate to the sand mold can be eliminated.

3. At a helium flow rate of 4 L/min in parallel flow mode, the cooling rate during dendrite formation increases by about 100% at locations near the point of supply of helium (compared to regular sand casting). Under similar conditions, in the cross flow mode, the increase is only 43%.

4. In the parallel flow mode, the role of heat convection is limiting and a point of diminishing return is reached. Accordingly, a "Performance Index" is defined as a ratio of one of the main benefits of the helium-assisted sand casting process (i.e., the increase in yield strength compared to traditional sand casting) to the cost penalty of using helium (as represented by the helium flow rate). It is found that 2.63 L/min (parallel to each face) is the optimum flow rate that maximizes this performance index.

5. Helium-assisted sand casting with parallel flow or cross flow mode result in refinement of the secondary dendrite arm spacing and the grain size; however the room temperature tensile properties for T6 heat treated specimens are improved

only in castings that are made with the parallel flow mode. This is attributed to the higher porosity obtained when the cross flow mode is used.

6. The average SDAS in plates that are sand cast with the helium-assisted process at a helium flow rate of 4 L/min parallel to each face is 46 µm. The average SDAS in the baseline castings is 60 µm. This corresponds to a 23% reduction in SDAS due to the use of helium.

7. The average yield strength of specimens machined from plates that are sand cast with the helium-assisted process at a helium flow rate of 4 L/min parallel to each face is 35 ksi. The average yield strength of specimens machined from the baseline castings is 26 ksi. This corresponds to a 34% increase in yield strength due to the use of helium.

8. The average ultimate tensile strength of specimens machined from plates that are sand cast with the helium-assisted process at a helium flow rate of 4 L/min parallel to each face is 38 ksi. The average ultimate tensile strength of specimens machined from the baseline castings is 31 ksi. This corresponds to a 22% increase in ultimate tensile strength due to the use of helium.

9. Helium-assisted sand casting with parallel flow mode produces a thermal gradient in the cast part. For this reason, there is a small gradient in SDAS and also in properties. Although the gradient observed in the plates is insignificant (due to their small length), it can be significant in larger parts. In order to mitigate this gradient, helium should be introduced into the mold at more than one location. The location of the helium input points may be determined be computer simulation of the casting process. On the other hand, when needed, the flow of helium may be used to cause localized cooling or to induce directional solidification. In essence, helium would replace chills which may simplify the design of the mold.

10. The surface of the cast plate is not affected by helium when it is supplied in the parallel flow mode.

11. Cost analysis shows that helium-assisted sand casting in the parallel flow mode compares favorably to traditional sand casting up to a flow rate of 4 L/min (parallel to each face). Although the analysis performed as part of this work is relative and based on assumptions and relations obtained from the open literature, it can serve as basis for company-specific analyses.

6.2 Recommendations for Future Work

1. Although it was found that the helium cross flow mode is not viable for casting thin sections, the approach may be viable for casting thick sections. In this case, helium would be supplied after a certain time delay that allows a solid "skin" to form and mitigate the incursion of gas into the molten metal. It is suggested that the helium cross flow mode in both encapsulated and partially-encapsulated molds be investigated for making thick section parts.

2. Since in the current design, helium is supplied in an "open loop" where it flows into the work environment, its effect on safety in the work environment should be investigated. In any case, design and implementation of a "closed helium loop" is recommended.

References

[1] Totten, G.E. and MacKenzie, D.S., Eds., "Handbook of Aluminum: Volume 1; Physical Metallurgy and Processes", Marcel Dekker, Inc. (2003).

[2] Totten, G.E. and MacKenzie, D.S., Eds., "Handbook of Aluminum: Volume 2; Alloy Production and Materials Manufacturing", Marcel Dekker, Inc. (2003).

[3] Shackelford, J.F., "Introduction to Materials Science for Engineers", Pearson Prentice Hall (2005).

[4] Askeland, D.R. and Phule`, P.P., "Essentials of Materials Science and Engineering", Thomson (2004).

[5] Davis, J.R., Ed.,"ASM Specialty Handbook for Aluminum and Aluminum Alloys", ASM International (1993).

[6] Kaufman, J.G. and Rooy, E.L., "Aluminum Alloy Castings: Properties Processes and Applications", ASM International (2004).

[7] "Industry Statistics", The Aluminum Association Inc., http://www.aluminum.org/Content/NavigationMenu/NewsStatistics/StatisticsReports/FactsAtAGlance/factsataglance.pdf, Access Date: 12/29/2010.

[8] "Aluminum in Transportation", The Aluminum Association Inc., http://aluminumintransportation.org/main/growth/auto-aluminum-growth, Access Date: 12/29/2010.

[9] Krupinski, M., Dobrzanski, L.A. and Sokolowski, J.H., "Microstructure Analysis of the Automotive Al-Si-Cu Castings", Archives of Foundry Engineering, vol. 8(1/2008), pp. 71-74 (2008).

[10] Saha, D., "Novel Processing Methods and Mechanisms to Control the Cast Microstructure in Al Based Alloys-390 and Wrought Alloys", PhD Thesis, Worcester Polytechnic Institute (2005).

[11] Heine, R.W., Loper Jr., C.R. and Rosenthal, P.C., "Principles of Metal Casting", Tata McGraw-Hill (2003).

[12] Ravi, B., "Metal Casting: Computer-Aided Design and Analysis", Prentice Hall of India (Pvt.) Ltd. (2005).

[13] Kelpakjian, S., "Manufacturing Engineering Technology", Addison Wesley (1995).

[14] Website of "Custompartnet", http://www.custompartnet.com/wu/SandCasting, Access Date: 12/30/2010.

[15] Poirier, D.R. and Poirier, E.J., "Heat Transfer Fundamentals for Metal Castings, Second Edition with SI Units", The Minerals, Metals and Materials Society (TMS) (1994).

[16] "Recommended Practices for Aluminum and Magnesium Alloys", American Foundrymen's Society, Inc. (1965).

[17] Argyropoulos, S.A. and Carletti, H., "Comparisons of the Effects of Air and Helium on Heat transfer at the Metal-Mold Interface", Metallurgical and Materials Transactions B, vol. 39(3), pp. 457-468 (2008).

[18] Zhang, L.Y., Jiang, Y.H., Ma, Z., Shan, S.F., Jia, Y.Z., Fan, C.Z. and Wang, W.K., "Effect of Cooling Rate on Solidified Microstructure and Mechanical Properties of Aluminium-A356 Alloy", Journal of Materials Processing Technology, vol. 207(1-3), pp. 107-111 (2008).

[19] Dobrzanski, L.A., Maniara, R. and Sokolowski, J.H., "The Effect of Cast Al-Si-Cu Alloy Solidification Rate on Alloy Thermal Characteristics", Journal of Achievements in Materials and Manufacturing Engineering, vol. 17(1-2), pp. 217-220 (2006).

[20] Wan, X. and Pehlke, R.D., "Using Helium to Increase Heat Transfer at the Metal/Mold Interface in Permanent Mold Casting", Transactions of the American Foundry Society, vol. 112, pp. 193-207 (2004).

[21] Zalensas, D.L., Ed., "Aluminum Casting Technology", The American Foundrymen's Society (2001).

[22] Caceres, C.H., Davidson, C.J., Griffiths, J.R. and Wang, Q.G., "The Effect of Mg on the Microstructure and Mechanical Behavior of Al-Si-Mg Casting Alloys", Metallurgical and Materials Transactions A, vol. 30A, pp. 2611-2618 (1999).

[23] Ceschini, L., Morri, A., Morri, A., Gamberini, A. and Messieri, S., "Correlation Between Ultimate Tensile Strength and Solidification Microstructre for the Sand Cast A357 Aluminum Alloy", Materials and Design, vol. 30(10), pp. 4525-4531 (2009).

[24] Wang, Q.G., Apelian, D. and Lados, D.A., "Fatigue Behavior of A356/357 Aluminum Cast Alloys. Part II – Effect of Microstructural Constituents", Journal of Light Metals, vol. 1(1), pp. 85-97 (2001).

[25] Shabestari, S.G. and Shahri, F., "Influence of Modification, Solidification Conditions and Heat Treatment on the Microstructure and Mechanical Properties of A356 Aluminum Alloy", Journal of Material Science, vol. 39(6), pp. 2023-2032 (2004).

[26] Jeong, C.Y., Kang, C.-S., Cho, J.-I., Oh, I.H. and Kim, Y.-C., "Effect of Microstructure on Mechanical Properties of A356 Casting Alloy", International Journal of Cast Metals Research, vol. 21(1-4), pp. 193-197 (2008).

[27] "Wikipedia Encyclopedia", http://www.wikipedia.org.

[28] "Foundry Sand Handbook", American Foundrymen's Society, Inc. (1963).

[29] Poirier, D.R. and Geiger, G.H., "Transport Phenomena in Materials Processing", The Minerals, Metals & Materials Society (TMS) (1994).

[30] Kreith, F. and Bohn, M.S., "Principles of Heat Transfer", Brooks/Cole, 2001.

[31] Doutre, D., "Increasing the Production Rate of Permanent Mold Casting Through the Use of Helium Injection", Advances in Industrial Materials, Proceedings of the International Symposium on Advances in Industrial Materials, Calgary, Alberta, pp. 289-301 (1998).

[32] Doutre, D., "The Influence of Helium Injection on the Cooling Rate and Productivity of Permanent Mold Casting Process", AFS International Conference on Permanent Mold Casting of Aluminum, 5th, Milwaukee, WI, pp. 86-96 (2000).

[33] Griffiths, W.D., "Enhanced Mechanical Properties in Al Castings by the Application of Helium", Engineering and Physical Sciences Research Council, (Grant reference: EP/C514718/1), http://gow.epsrc.ac.uk/ViewGrant.aspx?GrantRef=EP/C514718/1, Access Date: 12/6/2009.

[34] Hetke, A., U.S. Patent Application No. 12/159924, "Metal Casting System, Engineered Mold, Process and Articles Made Thereby", (2008), http://www.freepatentsonline.com/20080308249.pdf.

[35] Hallam, C.P. and Griffiths, W.D., "A Model of the Interfacial Heat Transfer Coefficient for the Aluminum Gravity Die Casting Process", Metallurgical and Materials Transactions B, vol. 35B (2004).

[36] Carroll, M., Walsh, C. and Makhlouf, M.M., "Determination of Effective Interfacial Heat Transfer Coefficient Between Metal Molds and Al Alloy Castings," Transactions of the American Foundrymen's Society, pp. 307-314 (1999).

[37] Taha, M.A., El-Mahallawy, N.A., El-Mestekawi, M.T. and Hassan, A.A., "Estimation of Air gap and Heat Transfer Coefficient at Different Faces of Al and Al-Si Castings Solidifying in Permanent Mould", Materials Science and Technology, vol. 17 (2001).

[38] B. L. Hohenstein and J. R. Bennett, U.S. Patent Application No. 11/293382, "Aluminum Casting Method With Helium Insertion", (2007) http://www.freepatentsonline.com/20070125509.pdf.

[39] ASTM Standard E1225-04, "Standard Test Method for Thermal Conductivity of Solids by Means of the Guarded-Comparative-Longitudinal Heat Flow Technique", Annual Book of ASTM Standards, vol. 14.02 (2008).

[40] Website of "Rubert & Co.", http://www.rubert.co.uk/, Access Date: 5/31/2010.

[41] ASTM Standard B557-06, "Standard Test Methods for Tension Testing Wrought & Cast Aluminum- and Magnesium-Alloy Products", Annual Book of ASTM Standards, vol. 02.02 (2010).

[42] "ASM Handbook: Metallography and Microstructure, Volume 9", ASM International (1992).

[43] ASTM Standard E112-96 (Re-approved), "Standard Test Methods for Determining Average Grain Size", Annual Book of ASTM Standards, vol. 03.01 (2010).

[44] Srinivasan, N.K., "Foundry Engineering", Khanna Publishers (2000).

[45] Website of "Material Property Data", http://www.matweb.com, Access Date: 9/2/2010.

[46] Price Quote of aluminum alloy 319 (Mr. Brian Livingstone, Aluminum Resources, Inc., Smyrna, TN, USA), 2/10/2011.

[47] Personal Communication (Mr. Bob Logan, Palmer Foundry, Palmer, MA, USA), 12/15/2010.

[48] Price Quote of Industrial Grade Helium Gas (Kristina L. Daubney, AIMTEK, INC., Auburn, MA, USA), 1/20/2011.

[49] "Energy and Environmental Profile of the US Metal Casting Industry", Office of Industrial Technologies, Energy Efficiency and Renewable Energy, US Department of Energy (2000).

[50] Website of "U.S. Energy Information Administration", http://www.eia.doe.gov, Access Date: 2/17/2011.

[51] Anand, M.S., Murarka, S.P. and Agarwala, R.P., "Diffusion of Copper in Nickel and Aluminum", Journal of Applied Physics, vol. 36(12), pp. 3860-3862 (1965).

[52] "Air property calculator", http://www.frigprim.com/online/air_properties.html , Access Date: 10/2/2010.

[53] Website of "National institute of standards & technology (NIST)", http://webbook.nist.gov/chemistry/fluid/, Access Date: 5/26/2010.

[54] "Engineering toolbox", http://www.engineeringtoolbox.com/specific-heat-capacity-d_391.html, Access Date: 4/13/2009.

[55] Mills, A.F., "Heat and Mass Transfer", Richard D. Irwin. Inc. (1995).

APPENDIX A

Physical Simulation

Physical simulation was performed during the early stages of the work in order to determine the range of helium flow rate that is capable of producing significant reduction in the casting's time to cool. Fig. A-1 shows a schematic representation of the apparatus used. A 6" x 6" aluminum plate is placed in the mold cavity and a 500 watts strip heater is secured to it as shown in Fig. A-2. The cope and the drag are then clamped together and the assembly is placed in the apparatus designed for investigating helium-assisted sand casting (cross flow mode) with partial encapsulation. The complete setup is shown in Fig. A-3.
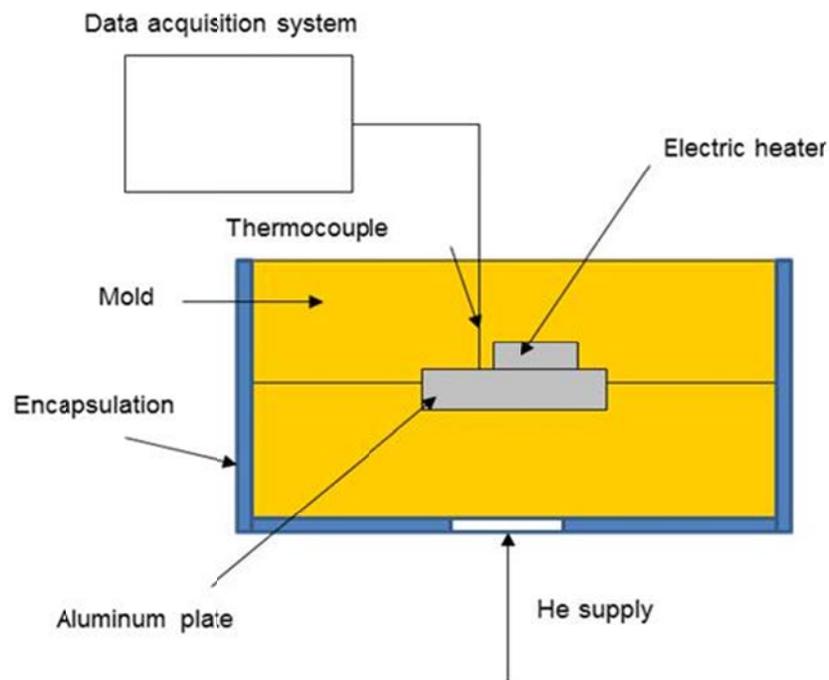

Fig. A-1 Schematic representation of the apparatus used to simulate the helium-assisted sand casting process during the early stages of the work.

Fig. A-2 Aluminum plate and strip heater assembly placed in mold cavity.
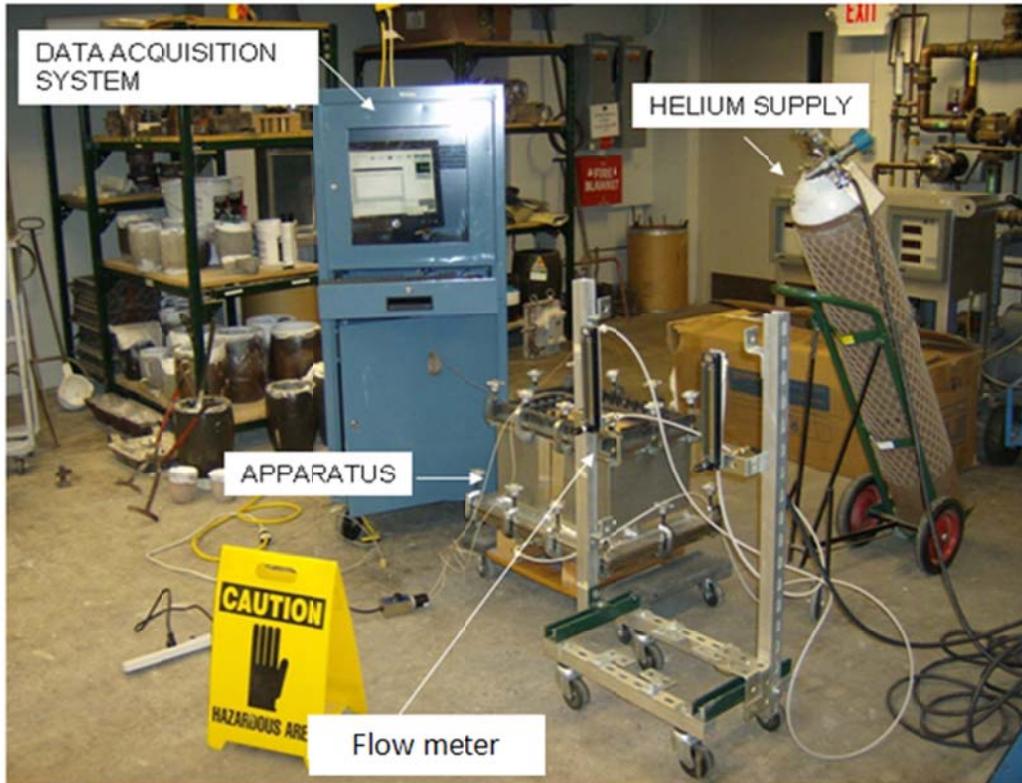

Fig. A-3 Setup used for physical simulation.

One K type thermocouple is attached to the data acquisition system and data is recorded at a sampling rate of 20000 measurements per second and averaged using 10,000 values to get a time interval of 0.5 seconds between recorded data. The recorded data is exported to Microsoft® Excel® for further analysis. The heater is activated and the plate temperature is brought up to 250°C and then the heater is shut off and the cooling curve is recorded as the plate cools down to 100°C without helium. This establishes the baseline for the simulation. The procedure is then repeated with helium flowing through the mold at various flow rates and, for each flow rate, the cooling curve is recorded. Fig. A-4 and Table A-1 show the results.
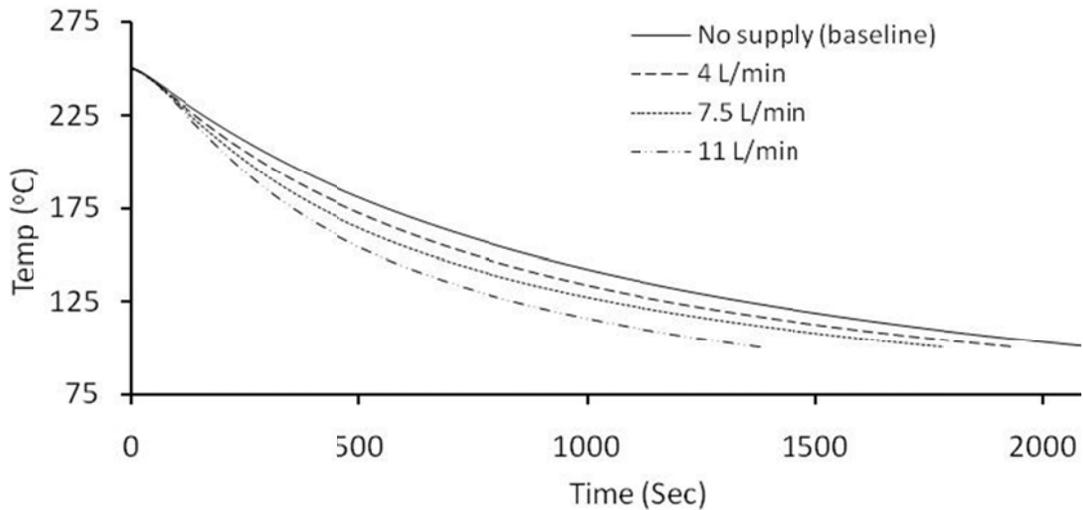

Fig. A-4 Time to cool an aluminum plate from 250°C to 100°C.

Table A-1 Results of the physical simulation experiments.

Flow rate (L/min)	Time to cool from 250°C to 100°C (minutes)	% change
Baseline	35.16	
4	32.35	7.99
7.5	29.7	15.53
11	22.98	34.64

Computer Simulation of the Solidification Process

The solidification simulation software MAGMASOFT® version 5.0.0 is used to simulate
the conventional sand casting process for three reasons: (1) in order to determine the
general cooling pattern of the plate casting, (2) in order to characterize the overall
quality of the casting (presence of hot tears, excessive porosity, etc.), and (3) in order to
locate the placement of thermocouples for monitoring the process. The simulation is
performed with the following parameters: Alloy = A319, mold = cold box silica, melt
temperature = 850°C, mold temperature = 20°C. Fig B-1 shows the CAD model of the
plate casting which is imported into the simulation software.
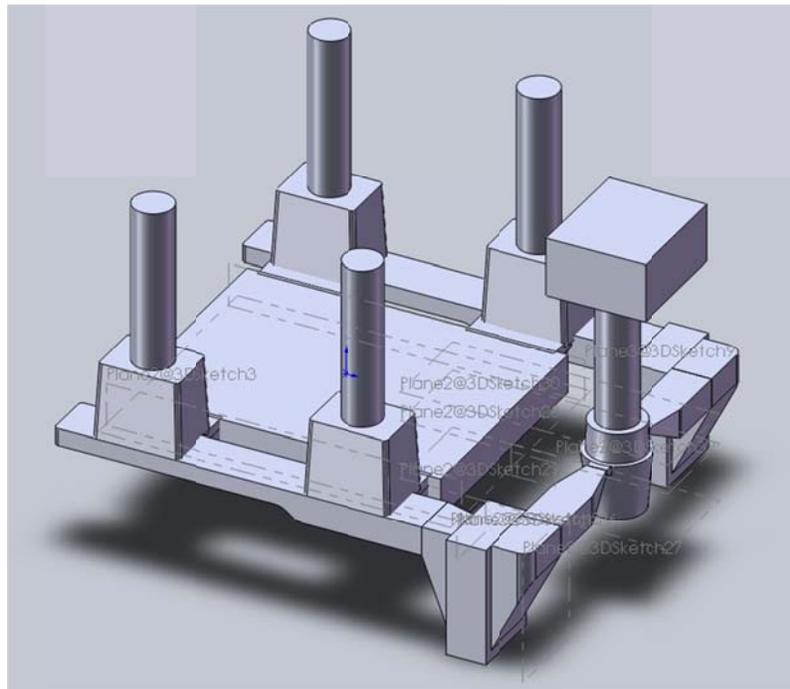

Fig. B-1 CAD model of the plate casting.

Fig. B-2 shows the solidification time for the casting indicating that regions close to the
risers are the last to solidify. Fig. B-3 shows the temperature profile in the plate at the
completion of solidification. Fig. B-4 shows that the plate is completely free of pores,
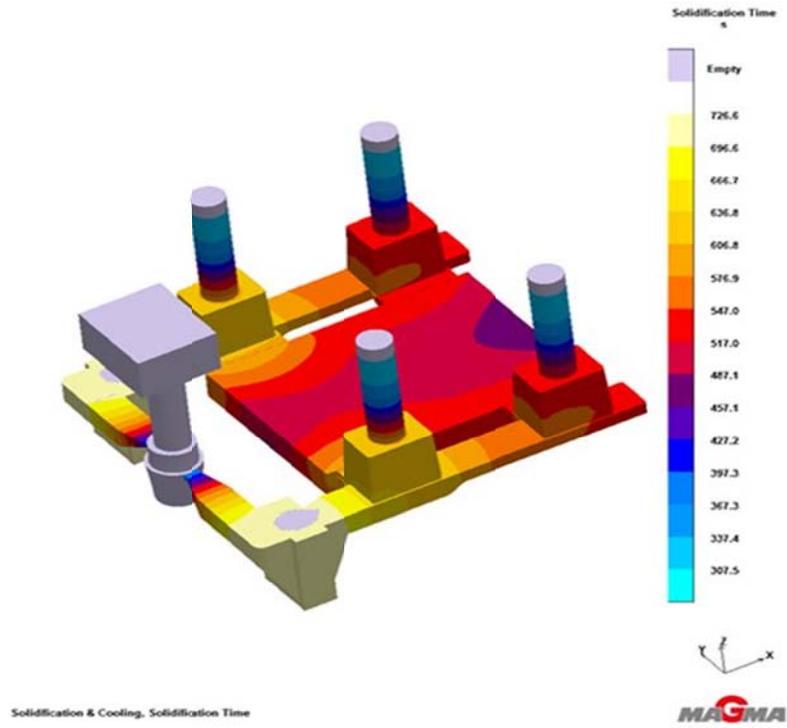and Fig. B-5 shows that the plate is sound.

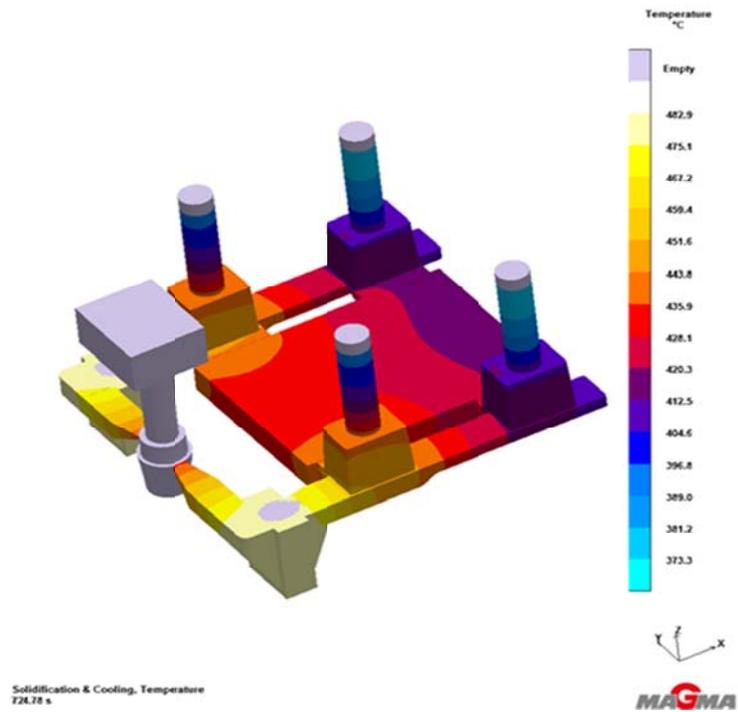**Fig. B-2** Simulation of the plate casting showing solidification time.

Fig. B-3 Simulation of the plate casting showing the temperature distribution in the plate.
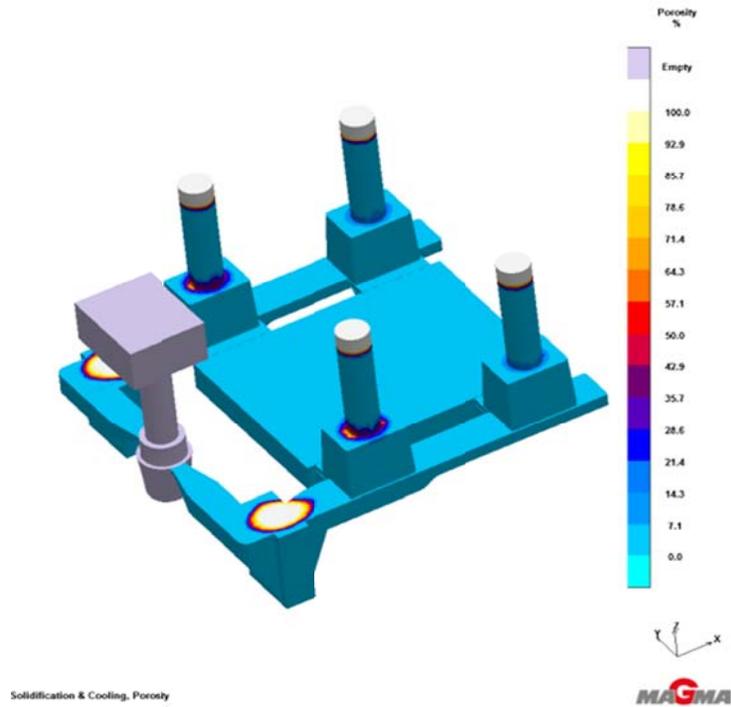
Fig. B-4 Simulation of the plate casting showing the locations where porosity may be present.
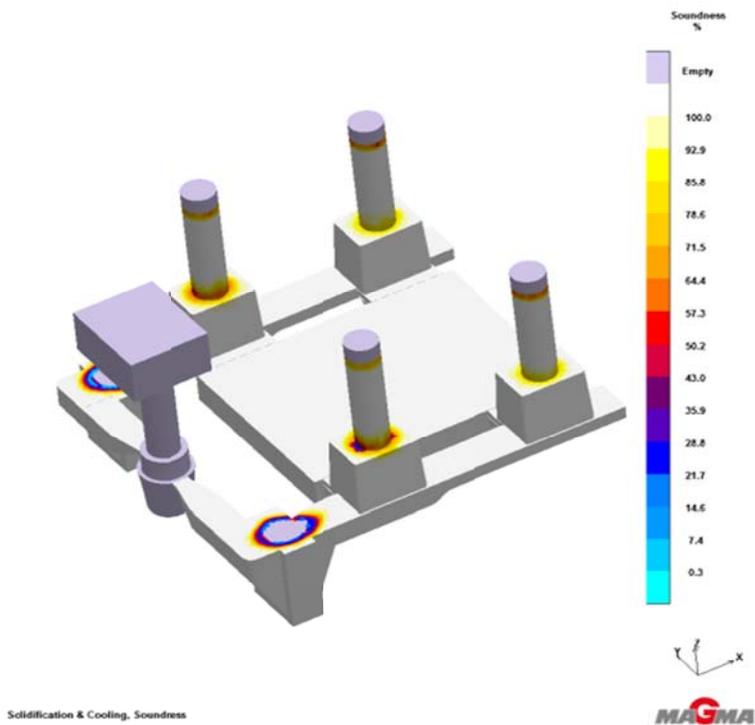

Fig. B-5 Simulation of the plate casting showing soundness.

APPENDIX C

Measurement of the Specific Permeability of the Sand Mold

The specific permeability of the sand mold is determined from the pressure drop measured by two pressure gauges placed upstream and downstream of a 3" x 3" x 3" sample of the mold material as shown in Fig. C-1 and Eq. (C-1) [29].

$$Þ = \frac{V\eta}{\left[\left(\frac{P_2 - P_1}{L}\right) - \rho g\right]}$$
(C-1)

In Eq. (C-1), $Þ$ is the specific permeability, V is the superficial velocity through the porous medium (defined as flow rate/area), $(P_2 - P_1)$ is the pressure drop over the length L of the specimen, ρ and η are the density and dynamic viscosity of air respectively and g is the acceleration due to gravity. At an air flow rate = 23,742 ml/min, the pressure drop is found to be 0.31 Psi. Using η = 1.84 x 10^{-5} kg/m-sec and ρ = 1.18 kg/m^3 [52], in Eq. (C-1) gives $Þ$ = 1.51 x 10^{-11} m^2 at 25°C.

Fig. C-1 Apparatus for measuring specific permeability of sand mold.

Schematics of the Apparatus for Helium-Assisted Sand Casting (Cross Flow mode) in a Partially Encapsulated Mold

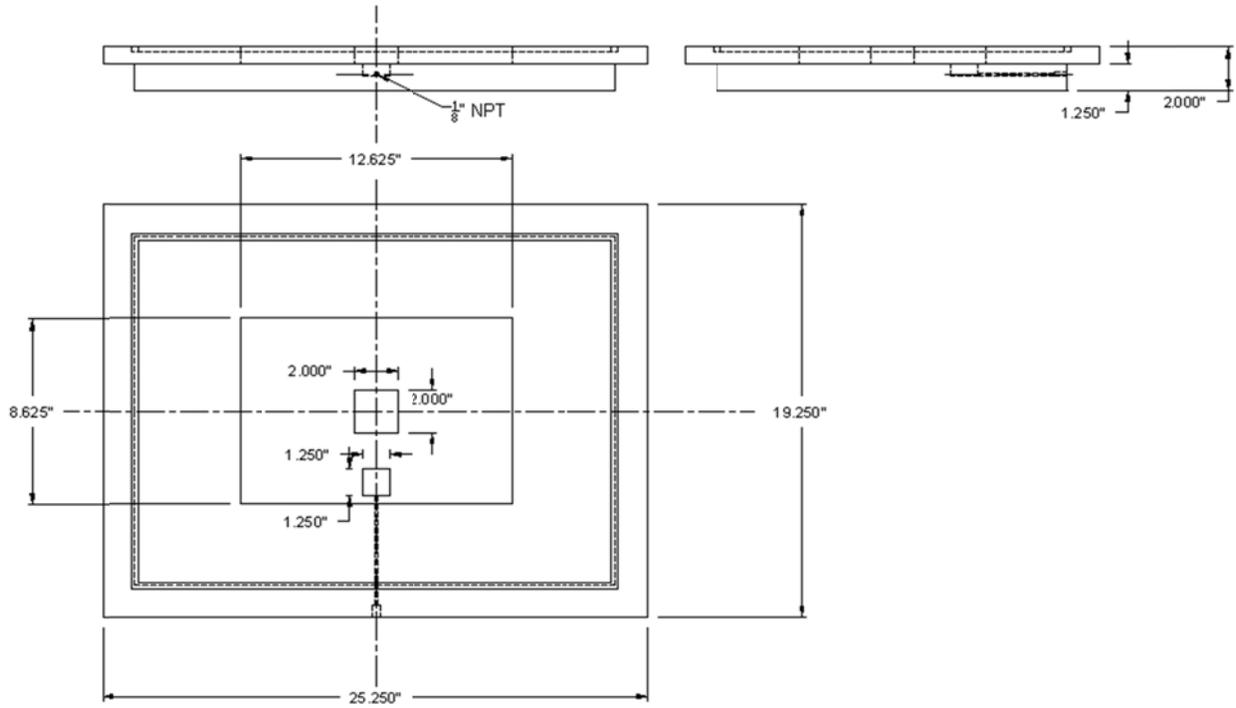**Fig. D-1** Schematic of the base plate.
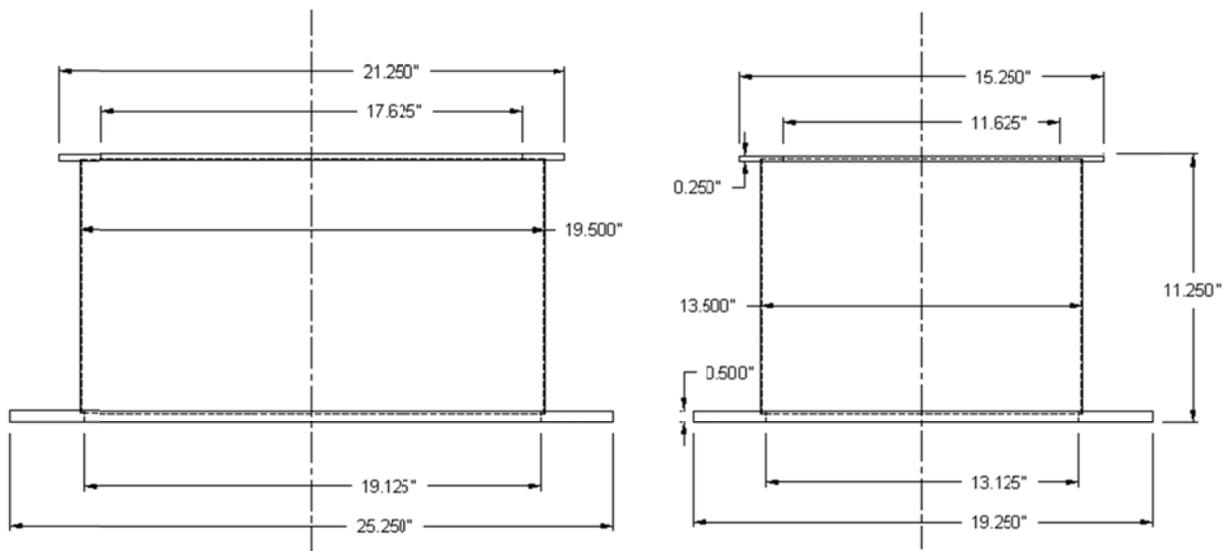
Fig. D-2 Schematic of the encapsulation case.
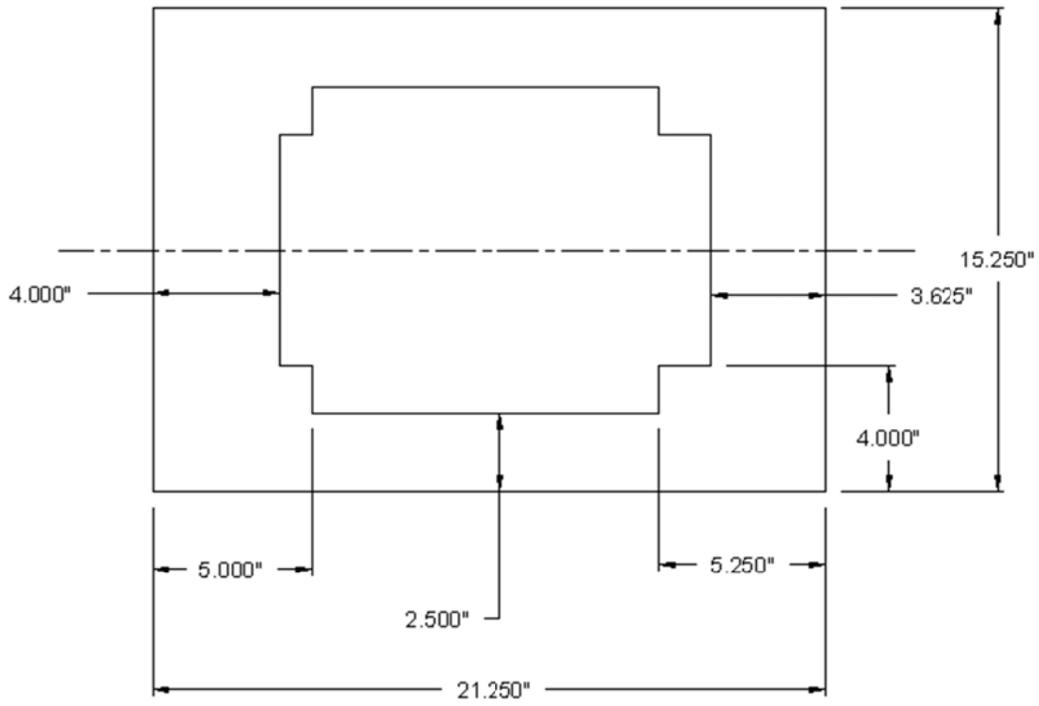
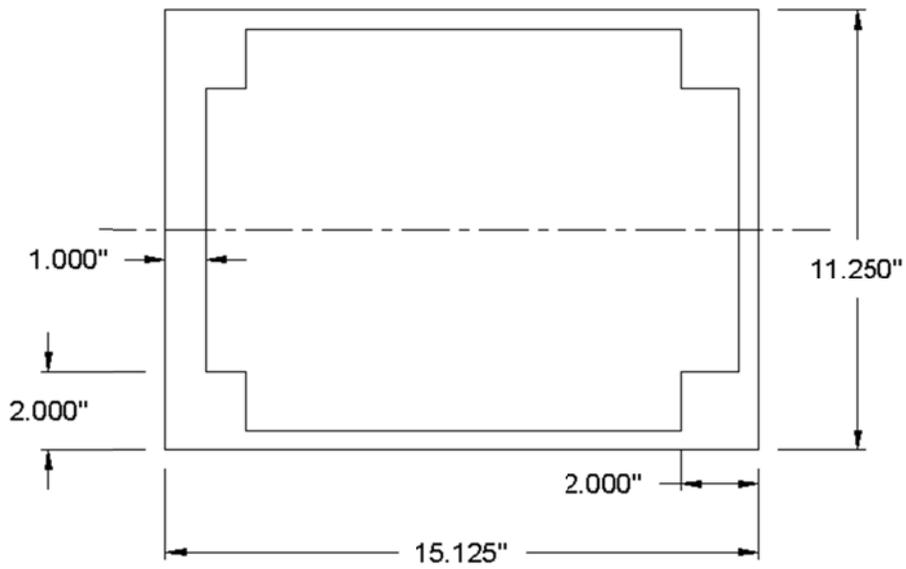**Fig. D-3** Schematic of the gasket.

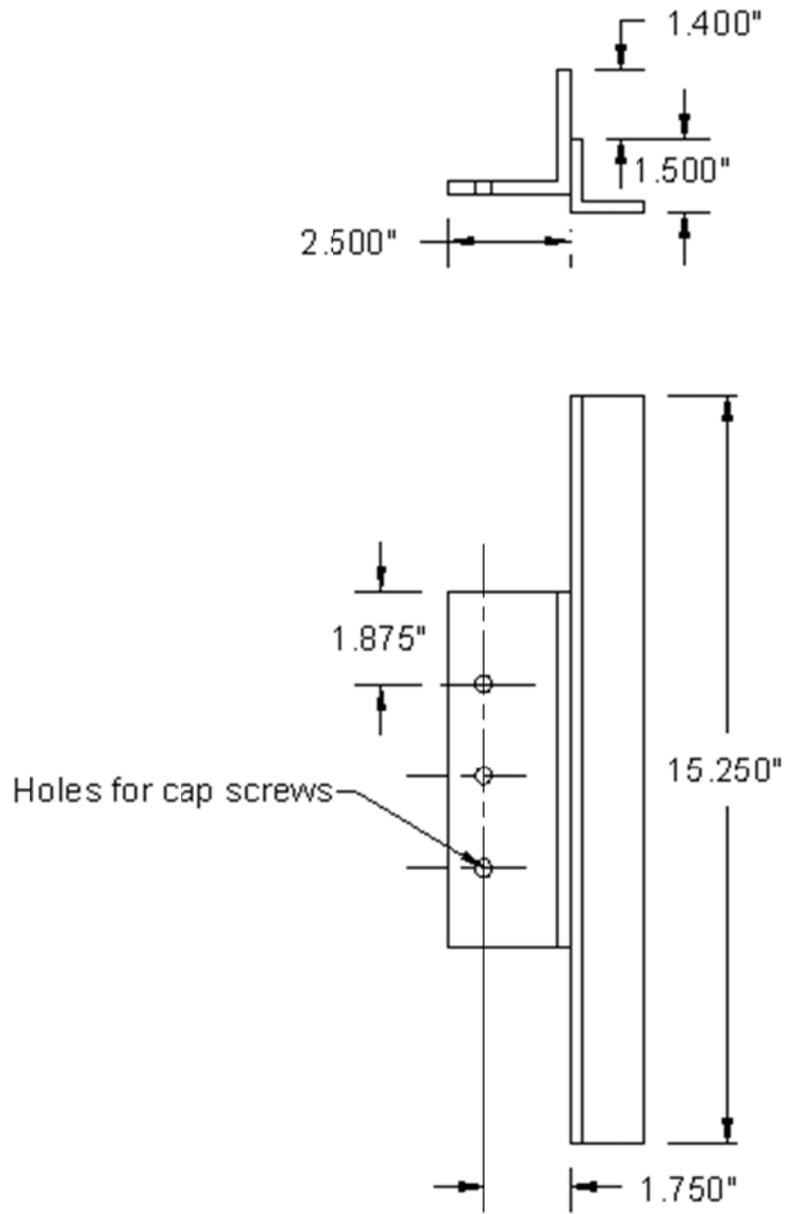**Fig. D-4** Schematic of the top plate.

Fig. D-5 Schematic of the angle assembly 1 (H).
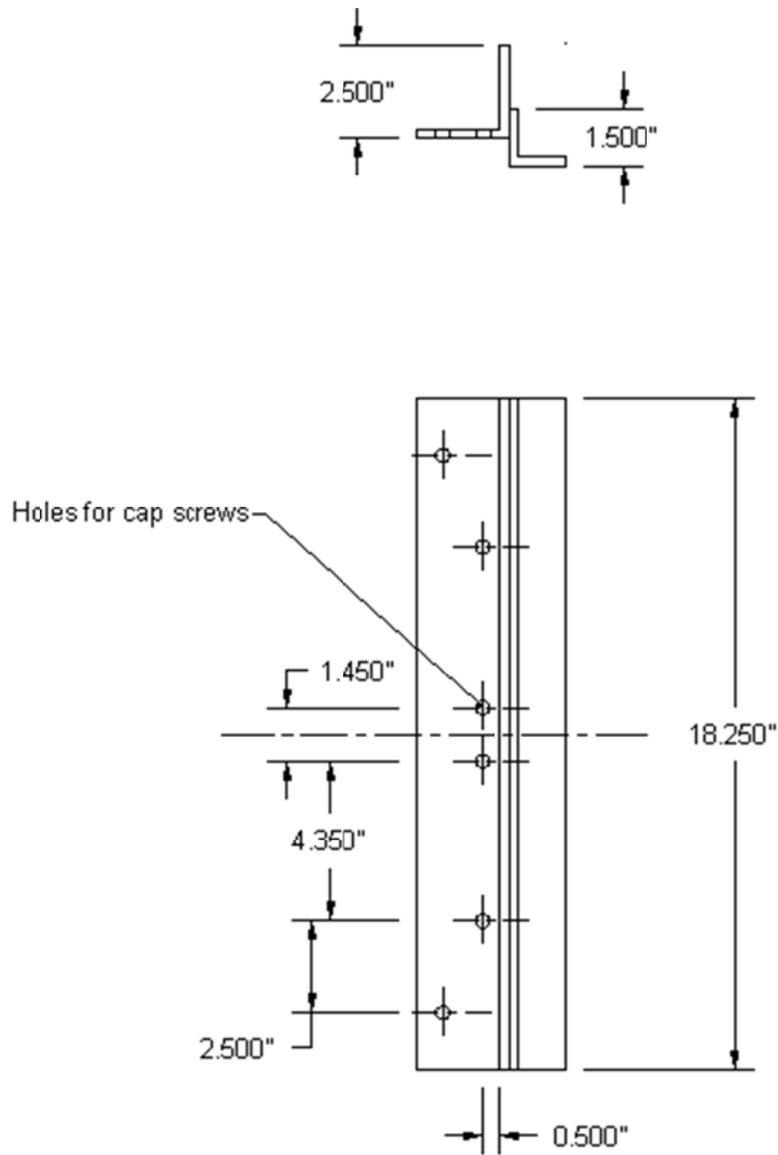
Fig. D-6 Schematic of the angle assembly 2 (I).

Note that "H" covers the width and "I" covers the length of the apparatus.

APPENDIX E

Fixing the Supply Plate to the Mold (Apparatus for Helium-Assisted Sand Casting (Parallel Flow Mode))

For the following reasons, it is not possible to introduce helium directly onto the surface of the casting; instead it has to be introduced at a certain distance from the surfaces.

– The bottom surface of the plate casting coincides with the parting surface of the mold; this parting surface has to be sealed to prevent the liquid metal from leaking out of the mold.

– The top surface of the plate casting has a peripheral web which introduces a default offset for the top surface.

The relative positions of the "supply plates" and mold parts are shown in Figs. E-1 and E-2 for the cope and the drag, respectively.

Fig. E-1 Relative position of the supply plate on the cope.
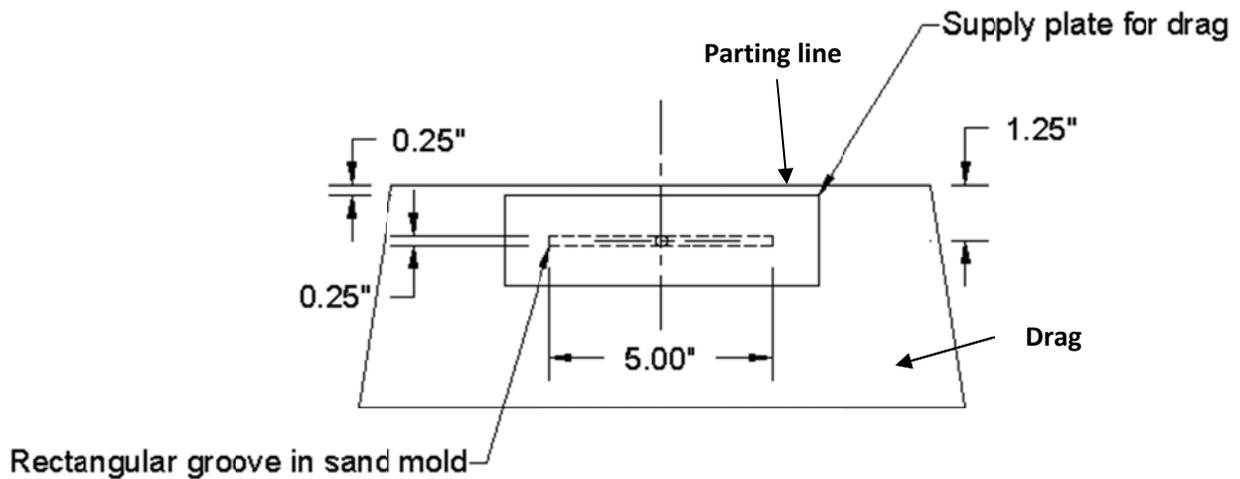
Fig. E-2 Relative position of the supply plate on the drag.
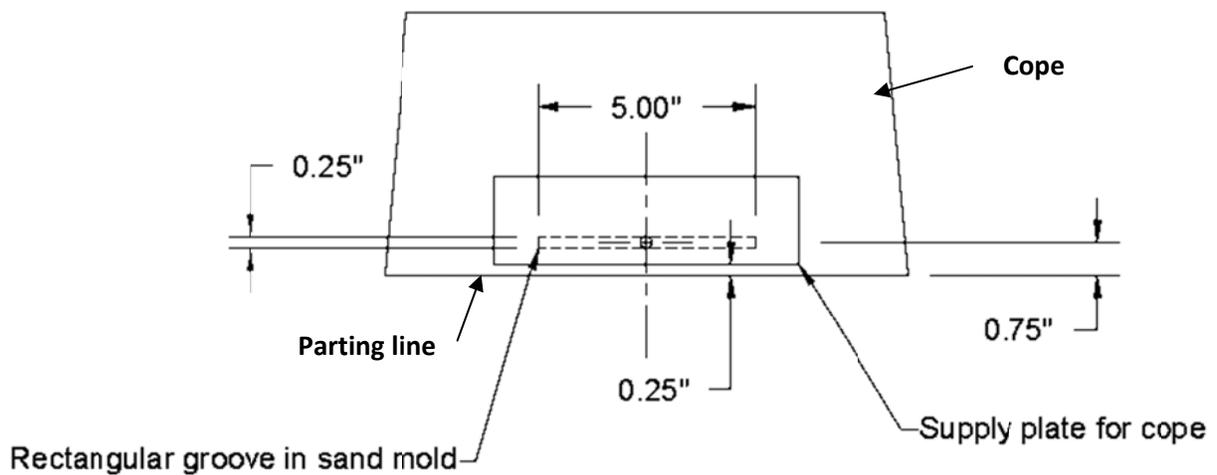
In order to ensure proper flow of helium parallel to the surfaces of the casting, before attaching the "supply plates" the sides of the sand mold are subjected to following:

- The side taper of the mold is removed by means of a saw blade in order to ensure that helium flows parallel to the surface.

- A groove is cut in the side of the mold in order to ensure that helium flows across the whole width of the plate casting. The groove has a width of 5", a height of 0.25" and a depth of 10/32". The supply plate is fixed to the mold so that the point of helium supply is positioned at the middle of the groove.

Fig. E-3 shows the groove and the removed taper of the drag. Fig. E-4 shows a schematic of the clamping assembly. It consists of a fixed angle for supporting the supply plate between itself and mold surface on one side. The adjustable angle can be tightened against the mold surface on the other side to affix the supply plate.

108

Side groove

taper oved

Fig. E-3 The drag for parallel flow helium supply.

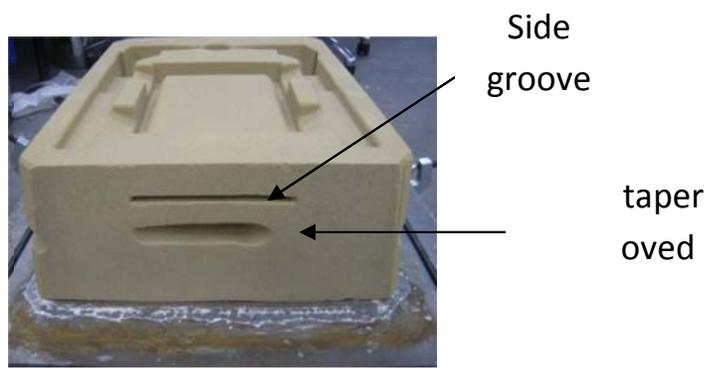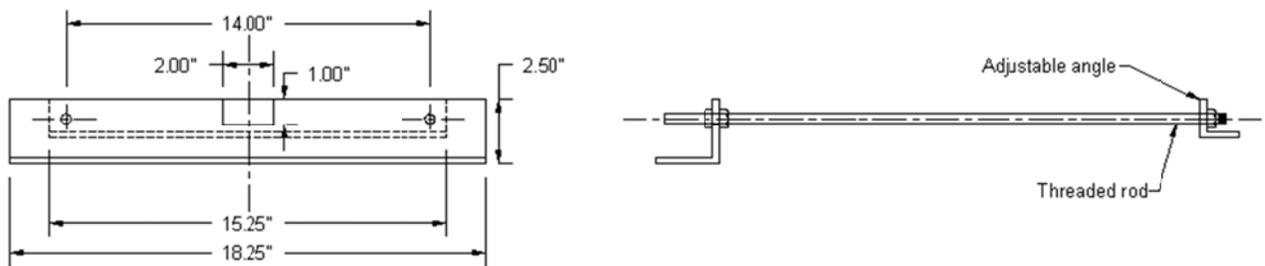**Fig. E-4** Clamping assembly for parallel flow helium supply plates.

APPENDIX **F**

Computation of the Effect of Helium on Solidification Time and on Heat Diffusivity of Sand Mold

The thickness of metal solidified in a sand mold is given by following Eq. (F-1) [15]:

$$M = \frac{2}{\sqrt{\pi}} \frac{(T_M - T_0)}{\rho_s \, \Delta H_s} \sqrt{k_m \, \rho_m \, c_{pm}} \sqrt{t} \qquad \text{(F-1)}$$

For a constant melting temperature and mold temperature, Eq. (F-1) reduces to

$$M \propto \sqrt{k_m \, \rho_m \, c_{pm}} \sqrt{t} \qquad \text{(F-2)}$$

Eq. (F-2) shows that the rate of solidification is determined by the thermal conductivity of, k_m, the heat capacity c_{pm} and the density p_m of the mold material.

For a flat plate of thickness $2L$, solidification is complete when $M = L$; i.e., the solid layers that are growing on the opposite sides of the mold cavity meet at the centerline of the plate; therefore from Eq. (F-1),

$$L = \frac{2}{\sqrt{\pi}} \frac{(T_M - T_0)}{\rho_s \, \Delta H_s} \sqrt{k_m \, \rho_m \, c_{pm}} \sqrt{t_f} \qquad \text{(F-3)}$$

or

$$t_f = \frac{\pi L^2}{k_m \, \rho_m \, c_{pm}} \left(\frac{\rho_s \, \Delta H_s}{2(T_M - T_0)} \right)^2 \qquad \text{(F-4)}$$

Where t_f is the time for complete solidification of the plate.

Therefore,

$$t_f \propto \frac{1}{k_m \, \rho_m \, c_{pm}} \qquad \text{(F-5)}$$

The reciprocal of the term $(k_m \, \rho_m \, C_{pm})$ is known as the heat diffusivity (different from thermal diffusivity) and represents the ability of the mold to absorb heat at a certain rate [15].

An estimation of the density and specific heat can be made with the rule of mixtures as shown in Eqs. (F-6) and (F-7)

$$\rho = \frac{V_{He}\,\rho_{He} + V_{sand}\,\rho_{sand}}{V_{He} + V_{sand}} \tag{F-6}$$

$$c_p = (c_{p_{solid}} \times f_{solid}) + (c_{p_{gas}} \times f_{gas}) \tag{F-7}$$

Using Eq. (F-5) together with Eqs. (F-6) and (F-7) and the data in Table F-1, the following relations are obtained:

For a sand mold with air as the pore gas, $t_f \propto 1.597$

For a sand mold with helium as the pore gas, $t_f \propto 0.823$

Also,

For a sand mold with air as the pore gas, the heat diffusivity = $0.626\,\dfrac{\left(\frac{KJ}{m^2 K}\right)^2}{sec}$

For a sand mold with helium as the pore gas, the heat diffusivity = $1.215\,\dfrac{\left(\frac{KJ}{m^2 K}\right)^2}{sec}$

Table F-1 Dataset used for simulation of helium's benefits on solidification time.

	Helium [53][23]	Air [52]	Sand[24]
Specific heat capacity (C$_p$) kJ/kg K	5.193	1.011	0.830 [54]
Density (ρ) g/cc	14.685 x 10^{-5}	95 x 10^{-5}	1.649
Volume fraction of sand			0.897

---

[23] Values for helium are taken at 373K (100°C) and 1.1234 atm. absolute pressure; i.e. 12.5KPa gauge pressure which is the pressure maintained during the measurements.
[24] C$_p$ value used is for quartz. Archimedes principle is used to determine the density and volume fraction of sand.

APPENDIX G

The Role of Convection

In order to compare the roles played by heat convection and heat conduction in extracting heat during helium-assisted sand casting with parallel flow; the process is visualized as a stream of fluid flowing between two parallel plates. One plate is presented by the surface of the sand mold and the other plate is presented by the surface of the metal plate casting. Fig. G-1 shows a schematic representation of this arrangement.
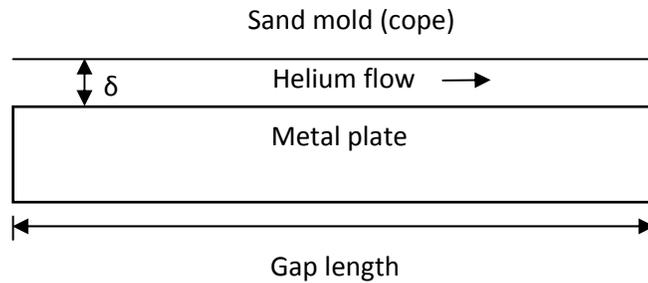
Sand mold (cope)

δ Helium flow $\longrightarrow$

Metal plate

Gap length

Fig. G-1 Schematic representation of fluid flow between two parallel plates.

The steps include determining the hydraulic diameter and the Reynolds number from Eqs. (G-1) and (G-2) [55]. The magnitude of the Reynolds number indicates whether the flow between the parallel plates is turbulent or laminar, and thus it dictates the equation to be used in determining the Nusselt number which will be finally used to calculate the Biot number. The Biot number is a measure of the relative contribution of conduction to convection. Therefore, a Biot number greater than 1 signifies more contribution by convection than by conduction to the process of heat extraction.

$$D_h = \frac{4A_c}{P} \tag{G-1}$$

$$Re_{D_h} = \frac{\left(\frac{m^0}{A_c}\right)D_h}{\mu} \tag{G-2}$$

Where A_c is the area of the gap and P is its perimeter.

The information given in Tables G-1 to G-3 together with A_c = 5.16 x 10^{-4} m^2, P = 0.41 m, and $D_h = 5.03 \times 10^{-3}$ are used in the calculations. Table G-4 shows the Reynolds number calculated for each one of the flow rates.

Table G-1 Dataset used to calculate Biot number.

Metal temp.	850°C
Mold temp.	20°C
Gap height	0.1"
Gap length[25]	8"

Table G-2 Properties of helium at 435°C and 1 atm.[26] [53].

Dynamic viscosity (Pa-sec, kg/m-sec)	3.629 x 10^{-5}
Density (kg/m^3)	0.069
Thermal conductivity (W/m K)	0.283

Table G-3 Properties of the sand mold.

Thermal conductivity[27] (W/m K)	1.033
Mold height[28] (inch)	6

---

[25] Length of the plate.
[26] Average temperature of 850°C and 20°C (435°C) is used for the properties of fluid (helium).
[27] Value of thermal conductivity measured with helium inside the pores at 25°C.
[28] The height of the cope is taken here as we have considered the top surface of the plate for the analysis.

Table G-4 Reynold's number calculated for the various flow rates.

Flow rate	Re$_{Dh}$
1 L/min (1.15 x 10^{-6} kg/sec)	0.31
4 L/min (0.46 x 10^{-5} kg/sec)	1.24
8 L/min (0.92 x 10^{-5} kg/sec)	2.47

Since the Reynolds number for all the flow rates used is less than 2300, then the flow is considered to be laminar and Eq. (G-3) with $Pr = 1.0$ is used to determine the Nusselt number [29] and finally, Eq. (G-4) is used to determine the Biot number.

$$Nu = 0.664Re^{1/2}Pr^{1/3} \tag{G-3}$$

$$Bi = \frac{hL}{K} \qquad (L = Characteristic\ length^{29} = \frac{Volume}{Area}) \tag{G-4}$$

Table G-5 lists the Reynolds and Biot numbers.

Table G-5 Calculation of Biot's number at various flow rates.

Flow rate	Re	Bi
1 L/min (1.15 x 10^{-6} kg/sec)	0.31	3.06
4 L/min (0.46 x 10^{-5} kg/sec)	1.24	6.14
8 L/min (0.92 x 10^{-5} kg/sec)	2.47	8.66

It can be seen that, even at a flow rate of 1 L/min., convection contributes more to the process of heat extraction than conduction; and as the helium flow rate increases, the relative contribution of convection to heat extraction during the casting process increases.

---

[29] Only cope is considered for calculating characteristic length herein.